THE GENERATION OF LANGMUIR WAVES BY THICK TARGET ELECTRON BEAMS IN SOLAR FLARES

by

Kenneth George McClements

Thesis

submitted to the

University of Glasgow

for the Degree of

Ph.D.

Department of Physics and Astronomy
University of Glasgow
Glasgow, G12 8QW.

July 1987

ProQuest LLC.
789 East Eisenhower Parkway
P.O. Box 1346
Ann Arbor, MI 48106 – 1346

To my Father and Elana

Oh, thick target electron beam,

Please go unstable;

Generate those Langmuir waves,

as fast as you are able.

Then give us microwaves

Bremsstrahlung X-rays too

To help the beam relax

To equilibrium.

A.G. Emslie, D. Alexander and K.G. McClements, 1987 (to the tune of 'to be a pilgrim').

ACKNOWLEDGEMENTS

The work presented in this thesis was carried out while I was a research student in the Department of Astronomy (1984-86) and the Department of Physics and Astronomy (1986-87) at the University of Glasgow. Financial support during this period was provided by the University of Glasgow. I would like to thank Professor A.E. Roy (as head of the former Department of Astronomy) and Professor I.S. Hughes (as head of the Department of Physics and Astronomy) for providing the facilities to carry out the research.

I am indebted to many people for providing help and assistance with the work contained herein. In particular I would like to thank my supervisor, Professor John Brown, and Dr. Gordon Emslie (University of Alabama, Huntsville). I would also like to thank Peter Sweet, Alec MacKinnon, Paul McQuillan, David Cromwell, Alan Thompson (all University of Glasgow), Ted LaRosa (University of Alabama, Huntsville) and Bob Bingham (Rutherford Appleton Laboratory) for useful discussions, Mrs. L. Williamson for typing the equations, and Mrs. M. Morris for preparing the figures.

CONTENTS

	Page
ACKNOWLEDGEMENTS	iv
SUMMARY	viii
CHAPTER 1 - REVIEW OF SOLAR FLARE OBSERVATIONS	
1.1 Introduction	1
1.2 Optical Emission	4
1.3 Radio and Microwave Emission	6
1.4 Ultra-Violet Emission	9
1.5 Soft X-Ray Emission	10
1.6 Hard X-Ray Emission	12
1.7 Gamma-Ray Emission	16
1.8 Interplanetary Particles	18
CHAPTER 2 - REVIEW OF RELEVANT THEORY	
2.1 Introduction	20
2.2 Magnetic Reconnection	21
2.3 Acceleration Mechanisms	26
2.4 Models of Hard X-Ray Emission	29
2.5 Models of Microwave Emission	40
CHAPTER 3 - THE STABILITY OF ELECTRON BEAMS IN THE FLARING CORONA	
3.1 Introduction	45
3.2 Wave Growth Rate in a Magnetized Plasma	47
3.3 Stability Boundary in Parameter Space	55
3.4 Discussion	59

Page

CHAPTER 4 - THE QUASI-LINEAR RELAXATION OF THICK TARGET ELECTRON BEAMS - ANALYTICAL MODEL

4.1 Introduction 62

4.2 The One Dimensional Quasi-Linear Equations 64

4.3 Asymptotic Solutions 69

4.4 The Evolution of the Electron Distribution With Depth 76

4.5 Discussion 87

CHAPTER 5 - THE QUASI-LINEAR RELAXATION OF THICK TARGET ELECTRON BEAMS - NUMERICAL MODEL

5.1 Introduction 89

5.2 The Equations 89

5.3 The Electron and Langmuir Wave Distributions 93

5.4 Energy Deposition and Bremsstrahlung Emission 104

5.5 Reverse Current Losses 111

5.6 2nd Harmonic Plasma Radiation 114

CHAPTER 6 - TIME DEPENDENT EFFECTS

6.1 Introduction 121

6.2 The Time Dependent Quasi-Linear Equations 123

6.3 Numerical Results 127

6.4 Discussion 131

CHAPTER 7 - FUTURE WORK

7.1 Introduction 136

7.2 Density Inhomogeneities 137

7.3 Induced and Spontaneous Scattering on Ions 141

APPENDIX A - THE COLLISIONAL ENERGY LOSS RATE OF AN ELECTRON IN A WARM TARGET 144

Page

APPENDIX B - NUMERICAL METHOD

B.1 The Steady State Problem 146

B.2 Reverse Currents 149

B.3 The Time Dependent Problem 149

REFERENCES 152

SUMMARY

Hard X-rays, observed during the impulsive phase of solar flares, are commonly believed to be produced by the bremsstrahlung of collimated beams of electrons, which lose their energy collisionally in the dense chromosphere. This thesis is concerned with the generation of Langmuir waves by such beams.

In Chapter 1 we review observations of solar flares across the electromagnetic spectrum. Particular emphasis is given to the impulsive phase, and to those observations which provide strong evidence for the existence of electron beams. Solar flare theory, insofar as it is pertinent to the original work of this thesis, is reviewed in Chapter 2. After briefly discussing models of primary energy release and particle acceleration, we consider in detail the theoretical interpretation of hard X-ray and microwave observations. Emissions at these wavelengths are believed to contain the most direct information on the electron distribution function in the flaring region.

In Chapter 3 we use the quasi-linear theory to determine the conditions required for the stability of a steady state electron beam propagating in the solar corona. The growth rate for electron plasma waves in a magnetized plasma is evaluated, with the electron distribution being given by an analytic solution of the linearized Fokker-Planck equation. A stability boundary in parameter space is determined, indicating that electron beams must be highly collimated at injection to be Langmuir unstable at any point in space. The implications of this result for

alternative models of hard X-ray emission are discussed and it is argued that Langmuir instability will not occur in either the trap model or the dissipative thermal model. Such models would therefore be refuted by the detection of a large flux of plasma microwave emission associated with hard X-ray emission.

In Chapters 4 and 5 we investigate the quasi-linear dynamics of thick target electron beams, using a combination of analytical and numerical techniques. In Chapter 4, one dimensional quasi-linear equations are derived from the general three dimensional equations for an axisymmetric beam in a magnetized collisional plasma. Asymptotic analytical solutions are discussed, and it is shown that the energy density of Langmuir waves excited by a steady state thick target beam is negligible compared with the beam energy density, although the waves heat the plasma at a rate which is comparable to that of the fast electrons. We also describe an approximate method of incorporating quasi-linear interactions into the collisional treatment of thick target beam evolution, based on the assumption that the asymptotic state is a plateau distribution.

Numerical computations of the thick target electron distribution and the associated Langmuir wavelevel are presented in Chapter 5. It is shown that the energy deposition rate and bremsstrahlung X-ray signature of a thick target beam are essentially unaffected by the presence of Langmuir turbulence. We also show that reverse current energy losses can reduce the wavelevel by as much as a factor of 2, depending on the beam and plasma parameters. Finally, we consider the possible plasma radiation signature of a relaxed beam, and show that an

observable flux of 2nd harmonic radiation will be produced if the Langmuir waves are close to being isotropic.

In Chapter 6 we consider Langmuir wave generation by a time dependent beam. It is shown that the steady state model remains valid if the electrons are injected on a timescale greater than about 1s. If the injection timescale is as short as 100ms, however, the energy density of Langmuir waves produced by a given instantaneous flux of electrons may be amplified by as much as an order of magnitude. We argue that the wavelevel is nevertheless unlikely to exceed the threshold for strong turbulence (i.e. the modulational instability), and that the propagation of thick target beams can therefore be adequately described using the quasi-linear theory.

In Chapter 7 we briefly discuss two possible ways of extending the work described in previous chapters. Specifically, we consider thick target beam relaxation in an inhomogeneous plasma, and the induced scattering of Langmuir waves on thermal ions.

CHAPTER 1

REVIEW OF SOLAR FLARE OBSERVATIONS

1.1 Introduction

Solar flares are transient phenomena in the atmosphere of the Sun which manifest themselves by greatly enhanced radiation across virtually the entire electromagnetic spectrum, and also by energetic particles in the interplanetary medium. The physical processes occuring in flares are common to many other types of astrophysical object, but the relative proximity of the Sun (and the consequent wealth of observational detail) means that a much greater demand is placed on theoretical models. In addition, the physical conditions in flares are similar to those in nuclear fusion devices, and the study of one field can therefore shed light on the other. Despite nearly 130 years of observations, a definitive theoretical model of the solar flare does not yet exist, and it continues to provide a stimulating challenge to the astrophysicist.

Solar flares were first observed in integrated white light by Carrington (1859) and Hodgson (1859). With the advent of optical spectroscopy, radio astronomy and finally space astronomy, a vast quantity of flare observational data has been accumulated. A flare occurs in essentially two stages. First there is the impulsive (or flash) phase, consisting of a rapid rise and fall in radiation flux at microwave, Hα, ultra-violet, hard X-ray and γ-ray wavelengths. This phase lasts for up to a few hundred seconds. Almost invariably, the impulsive phase is followed by a gradual phase, which is observed as a slow rise and fall in

radiation intensity at Hα, ultra-violet and soft X-ray wavelengths. This lasts for between several minutes and several hours. A schematic illustration of flare intensity as a function of time at various wavelengths is shown in Figure 1.1. In a large flare, the total energy released is $\sim 10^{32}$ergs: a large fraction of this appears in the form of bulk plasma motion (e.g. Svestka 1976). The energy is released over a period of about 10^3seconds, and over an area of no more than about 10^{19}cm^2 . Spatially resolved observations of flares on the solar limb indicate that the flaring region has a vertical extent of the order of 10^9cm.

The majority of solar flare theoreticians have concentrated their efforts on modelling large flares (in particular the impulsive phase), since such events place the most severe demands on acceleration mechanisms. There are two fundamental problems associated with solar flares: first, what is the primary energy release mechanism? Secondly, how is energy transported through the atmosphere, thus giving rise to the observed radiation, particle emissions, and mass motion? In particular, observations indicate that a large amount of energy is deposited in the chromosphere, although the primary energy release is believed to occur high in the corona. One possible method of transporting energy from the corona to the chromosphere is by means of high energy electron beams. This thesis is primarily concerned with the generation of Langmuir waves by such beams.

In the following sections of this chapter we review solar flare observations across the electromagnetic spectrum.

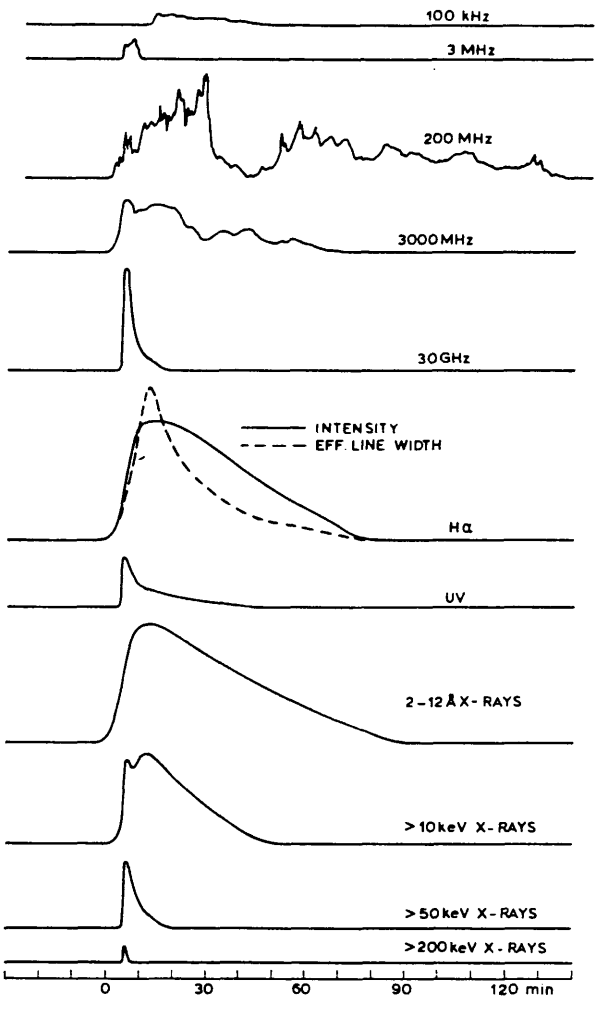

Figure 1.1 Schematic plot of flare intensity as a function of time at various wavlengths (from Svestka 1976).

Particular emphasis is given to the impulsive phase, and to those observations which provide evidence for the existence of electron beams. Theories of the primary energy release, and of hard X-ray and microwave emission, are reviewed in Chapter 2.

1.2 Optical Emission

With the exception of a few rare events, flares cannot be observed in integrated white light, thus implying that the flaring process occurs well above the photosphere. In the majority of cases, optical flare radiation consists of enhanced line emission from the chromosphere. The most important lines are those of the hydrogen Balmer series (particularly Hα), and the singly ionized calcium H and K lines. Flares are classified in importance according to the area of the solar disk which shows a brightening in Hα emission (cf. Svestka 1976), although this scheme is somewhat anachronistic since the total energy radiated in a flare is only poorly correlated with Hα brightening.

In the course of a large flare, the Hα line develops an emission profile, which is both broadened and slightly redshifted. The broadening is almost certainly due to the Stark effect, and this allows an estimate of the chromospheric electron density to be made (Svestka 1972). The cause of the redshift is less certain, but it may be due to the impact of an electron beam on the chromosphere (Zirin and Tanaka 1973; Ichimoto and Kurokawa 1984). The electron beam interpretation is supported by theoretical modelling of impulsive Hα profiles, using parameters inferred from simultaneous hard X-ray

observations (Canfield et al. 1984; Canfield and Gunkler 1985).

Hα observations are useful as indicators of flare geometry. During the impulsive phase, two or more bright localized regions of Hα emission called 'kernels' are observed. They are closely correlated with impulsive emission at other wavelengths. In large disk flares, the region of Hα brightening consists of two ribbons, expanding and moving apart, on either side of a magnetic neutral line (revealed by Zeeman splitting of photospheric spectral lines). From Skylab soft X-ray observations (Cheng and Widing 1975), it has been established that Hα ribbons are the 'footpoints' of an arcade of loops, each loop being a magnetic flux tube. This conclusion is confirmed by the observation of Hα flares on the solar limb, which often have a loop structure (Bruzek 1964; Zirin 1978). Such loops are of course confined to the chromosphere, but EUV and soft X-ray observations indicate that flaring loops extend into the corona to a height of typically 10^9cm (e.g. Vorpahl et al. 1975). Hα observations of limb flares also provide direct evidence of high velocity mass ejections (e.g. Svestka 1976).

Observations of the CaII H and K lines can be used to infer the temperature and density structure of the flaring chromosphere (e.g. Ayres and Linsky 1976). In particular, Machado et al. (1978) used CaII K line observations to show that there is a considerable temperature enhancement during a flare even at photospheric depths. In a few events, this enhancement may be enough to produce optical continuum emission, i.e. a white light flare. However, the mechanism for white light events remains uncertain. Their observed properties have recently been

reviewed by Canfield et al. (1986).

1.3 Radio and Microwave Emission

Radio emission from flares extends from the metric down to the millimetric range. Early observations indicated that metric radio bursts from the Sun can be divided into five types, according to their 'dynamic spectra' (a dynamic spectrum is a plot of radiation intensity contours on the frequency-time plane). Metric radiation from flares has been discussed in detail in the book edited by McLean and Labrum (1985): we shall concentrate on bursts of type III, which are most closely associated with the impulsive phase.

A type III burst is observed as an intense, narrow band of emission, drifting to lower frequency at a rate of typically 100MHzs^{-1}. Such bursts frequently have a 2:1 harmonic structure, and are closely correlated with impulsive hard X-ray emission (e.g. Benz and Kane 1986). The emission mechanism is generally accepted to be plasma radiation (at the fundamental and second harmonic), produced by electron streams as they propagate out through the corona along open magnetic field lines. The electron stream develops a 'gentle-bump' instability (due to fast electrons overtaking slow ones), and consequently generates Langmuir waves which are then converted to plasma radiation. The exact mechanism of the conversion process is, however, controversial (see e.g. Melrose 1985). The plasma physics involved in the propagation of type III streams is of central importance for the subject matter of this thesis: this will become clear in later chapters.

Impulsive microwave bursts in flares are closely associated with hard X-ray emission and are of crucial importance for inferring the physical conditions in the flaring region: this will be discussed in detail in Chapter 2. A typical microwave spectrum in a large flare is shown in Figure 1.2. The peak intensity of a microwave burst generally lies in the range $1\text{-}10^4$ solar flux units, 1 solar flux unit (s.f.u.) being 10^{-19} ergs cm^{-2} s^{-1} Hz^{-1}. The spectrum turns over at a frequency which is typically 10GHz: recently, however, a burst was observed by Kaufmann et al. (1985a) with a peak frequency in excess of 90GHz. Microwave bursts very often exhibit extremely fast time structures: spikes of duration $\lesssim$10ms have been detected (Slottje 1978; Benz 1986; Stähli and Magun 1986), indicating brightness temperatures as high as 10^{15}K. In general, the time profiles of microwave bursts are closely correlated with those of hard X-ray bursts, although there is some evidence for time delays between the two (e.g. Kaufmann et al. 1983).

Recently, evidence has emerged of a new class of microwave burst in the range (3-5)GHz which is qualitatively similar to the metric type III burst in duration, bandwidth and polarization, but which drifts towards <u>higher</u> frequencies with time (Stähli and Benz 1987). These are (somewhat confusingly) referred to as 'reverse drift' events. Similar phenomena have been detected at decimetric wavelengths, again closely associated with hard X-ray emission, showing both positive and negative frequency drift rates (Benz et al. 1983). The significance if these observations will be discussed in later chapters.

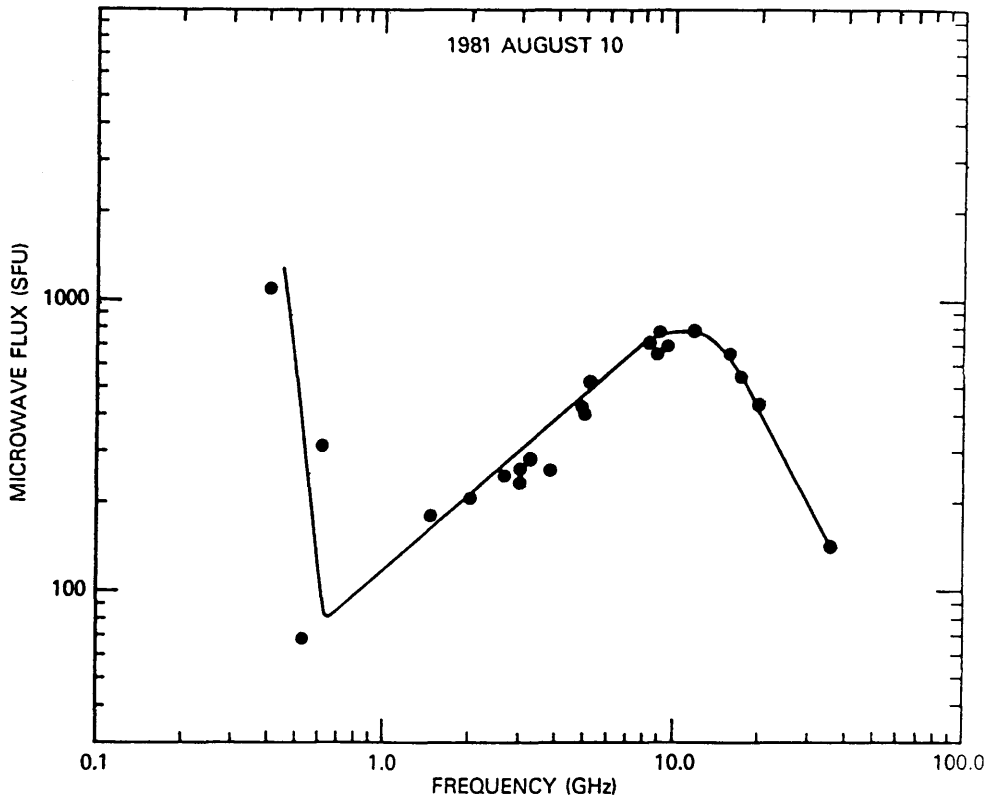

Figure 1.2 Typical microwave spectrum in a large flare (from Wiehl et al. 1985)

1.4 Ultra-Violet Emission

Ultra-violet emission from flares has been observed in the range 1150-3600Å by the UVSP instrument on the Solar Maximum Mission (SMM) satellite (Woodgate et al. 1980), and in the EUV range (10-1000Å) by the OSO satellites and the ATM instrument on Skylab (Widing and Cheng 1974). Flares are observed to produce both continuum and line UV emission, in both the impulsive and the gradual phase. EUV bursts are closely correlated with hard X-ray emission, although as with the microwave emission there is a time delay between the two (e.g. Emslie et al. 1978).

UV lines such as those of OV (1371Å) are extremely useful because they can only be formed in the transition region ($T \sim 10^5$K), and can thus be used to provide sensitive diagnostics of the temperature and density structure of that part of the atmosphere during the impulsive phase of a flare. The flaring transition region lies deeper in the atmosphere than the quiet Sun transition region, because of chromospheric heating. The OV intensity depends on both the plasma density and the temperature gradient, and Emslie and Nagai (1985), on the basis of a hydrodynamic model, have argued that the observed time profiles of UV lines and hard X-rays are consistent with electron beam heating, but not conductive heating. This conclusion is supported by Mariska and Poland (1985).

As indicated previously, spatially resolved ultra-violet observations confirm the existence of loop structures. Poland et al. (1982) used the FeXXI line (1354Å) to study the morphology of a limb flare as a function of time, and showed that

transition region line emission is strongly concentrated at the footpoints of the loop.

1.5 Soft X-Ray Emission

Soft X-ray emission from flares (photon energies in the range 1-10keV) is associated with the gradual rather than the impulsive phase. Soft X-ray continuum is generally assumed to be thermal bremsstrahlung emission from the flaring corona - this enables the temperature T and emission measure n^2V (where n is the plasma density, and V the volume) of the emitting region to be inferred (assuming the region to be homogeneous). V can be estimated from spatially resolved observations, such as those made with the Hard X-Ray Imaging Spectrometer (HXIS) instrument on SMM (Van Beek et al. 1980), thus yielding values for n. The plasma density can also be inferred directly from soft X-ray line ratios, particularly those of high ionization states of iron (see Svestka 1981). Using these methods, it has been shown that the plasma density in the flaring corona lies in the range 10^{10} - 10^{12} cm^{-3} (e.g. Hudson and Ohki 1972; Wolfson et al. 1983), while the temperature rises from $1\text{-}4\times10^6$K before the flare to greater than 10^7K during the impulsive phase (Moore et al. 1980). The thermal energy in the flare plasma is a significant fraction of the total energy released in the flare.

In reality, of course, the emitting region is inhomogeneous and the observed soft X-ray spectrum is a convolution of the temperature and density structure of the source. In principle, one can use spectral data to determine an emission measure differential in temperature $\xi(T)$, which may yield information on

the physics of the flaring plasma (Craig 1981). It can be shown, however, that the problem of inferring $\xi(T)$ from soft X-ray spectra is mathematically ill-posed, in the sense that $\xi(T)$ is extremely sensitive to small perturbations in the data (Craig and Brown 1976, 1986). The spatial information contained in the (spatially unresolved) soft X-ray spectrum is therefore extremely limited.

Soft X-ray imaging has revealed a great deal of information about the morphology of flaring loops, particularly in the highest temperature ($T \gtrsim 10^7$K) region of the flare. For a review of the different kinds of structure observed, see Svestka (1981).

Soft X-ray observations raise several theoretical problems. There is some controversy regarding the mechanism whereby the coronal plasma is heated to a temperature in excess of 10^7K. One proposal is that coronal heating occurs as the direct result of Ohmic dissipation in the primary energy release region (e.g. Spicer 1977). Another scenario involves nonthermal electron beams, which impact on the chromosphere and heat the footpoints of the loop. This results in hot material 'evaporating' from the chromosphere, filling the loop and giving rise to the observed temperature and emission measure (Antiochos and Sturrock 1978). Chromospheric evaporation is certainly observed to take place, and there is evidence that, during the impulsive phase at least, it is indeed produced by electron beams (Acton et al. 1982; Antonucci and Dennis 1983). The cooling of the coronal plasma, as revealed by the decay phase of the soft X-ray flare, is believed to take place due to a combination of thermal

conduction and radiation (Moore et al. 1980).

1.6 Hard X-Ray Emission

The wealth and quality of hard X-ray observations of flares have improved dramatically in the past few years with the launch of SMM and the Astro-A (Hinotori) satellite. In particular, the Hard X-Ray Burst Spectrometer (HXRBS) instrument on SMM has been used to obtain observations of several thousand flares, with a time resolution of 128ms. The instrument can also be used to obtain total flux measurements with a time resolution of 10ms (Orwig et al. 1980). SMM results have been reviewed recently by Dennis (1985). Only a brief review of hard X-ray burst observations will be given in this section: their theoretical interpretation will be discussed in Chapter 2.

As photon energy is increased, the impulsive phase increasingly dominates over the gradual phase, the transition occuring at an energy typically lying in the range (10-20)keV. Prior to the launch of SMM, it was known that an impulsive hard X-ray burst consists of a series of spikes, typically of a few seconds duration and certainly longer than one second in duration (Hoyng et al. 1976; de Jager and de Jonge 1978). The apparent non-existence of faster variations was almost certainly due to the rather poor time resolution (>1s) of the observations available at that time. Using HXRBS results, Kiplinger et al. (1983a) claimed to have detected individual spikes with e-folding times of the order of 20ms. Brown et al. (1985) showed that these features may in fact be due to Poisson noise in the data, and concluded that only spikes with timescales in excess

of about 100ms have yet been shown to be statistically significant. In any case, a majority ($\sim$90%) of the events analysed by Kiplinger et al. (1983a) did not exhibit fluctuations on timescales of less than a second. This conclusion has important implications for models of hard X-ray burst emission (see Chapter 2), and also for the level of Langmuir waves produced by a hard X-ray-emitting electron beam (see Chapter 6 and McClements 1987a).

Hard X-ray burst spectra are generally parametrized using a power law representation

$$I(\varepsilon) = I_o \varepsilon^{-\gamma} \qquad (1.1)$$

where $I(\varepsilon)$ is the observed radiation flux (photons cm^{-2} s^{-1} keV^{-1}) and ε is photon energy. Spectra with high resolution have been obtained using balloon-borne detectors (e.g. Lin et al. 1981a) and HXRBS, which has fifteen photon counting channels in the range (20-260)keV. The value of the spectral index γ, averaged over the spectrum, varies between 3 and 10, although the majority of events have spectral indices in the range 3-5 (see Figure 4 of Dennis 1985). Several authors (e.g. Hoyng et al. 1976) have reported a steepening ('softening') of the spectrum towards higher photon energy, the break occuring around 50-60keV, γ increasing by between 1 and 2. This may be regarded as evidence in favour of a thermal interpretation. Kiplinger et al. (1983b) and Wiehl et al. (1985) have found that some hard X-ray spectra can be fitted more accurately by an isothermal bremsstrahlung curve

$$I(\varepsilon) = I_o \exp (- \varepsilon/k_B T) / \varepsilon \qquad (1.2)$$

than by a power law (in (1.2) T is the source temperature and k_B is Boltzmann's constant). Brown (1974) has shown that a multi-thermal interpretation may be valid for any hard X-ray spectrum. The qualitative behaviour of γ as a function of time seems to vary between different events, but in the majority of impulsive bursts the spectrum hardens (i.e. γ decreases) during the rise phase, and softens during the decay phase (Hoyng et al. 1976; Dennis 1985). Figure 1.3 shows the flux time profile in various energy bands, together with the time dependence of γ, of a typical large hard X-ray burst.

Hard X-ray polarization measurements have been confined, for technical reasons, to comparitively low photon energies (ε<20keV). Tindo et al. (1976) found degrees of polarization in the range 0-5%, at a photon energy of 15keV. More recently, Tramiel et al. (1984), using an instrument on the space shuttle Columbia, obtained similar results for photon energies in the range 5-20keV. The significance of these results will be discussed in Chapter 2. Related to polarization observations are those of directivity, i.e. the systematic variation of hard X-ray emission across the solar disk. There are theoretical grounds for believing that the observed directivity of hard X-ray emission will be rather small (Henoux 1975), and in fact no statistically significant centre-to-limb variation has yet been detected (e.g. Datlowe et al. 1977).

The HXIS instrument on SMM enables hard X-ray images to be obtained up to an energy of 30keV. HXIS images typically consist

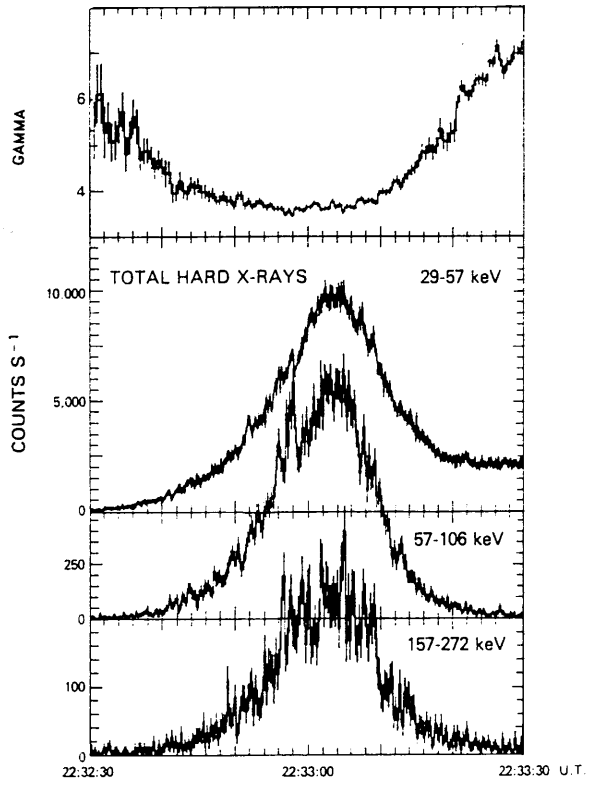

Figure 1.3 Time profile of hard X-ray spectral index and radiation intensity in three energy bands, during the flare of 1980 November 5, 22:33UT (from Dennis 1985).

of 2 or 3 bright patches, coincident with Hα kernels, which brighten simultaneously to within a few seconds of each other (e.g. Duijveman et al. 1982). These areas can be identified as the footpoints of magnetic loops. MacKinnon et al. (1985) have shown, however, that the hard X-ray flux at HXIS energies is much less localized than was previously thought, and in fact only a small fraction of the X-rays are produced by the footpoints. This conclusion is supported by the fact that the footpoint X-ray flux is much less than would be expected from an extrapolation to energies less than 30keV of HXRBS data.

HXIS observations of limb flares have also been used to infer the height structure of hard X-ray emission. Haug and Elwert (1985) claim to have detected a systematic softening of the X-ray spectrum with increasing height during the flare of 1980 November 18, 14:51UT. It appears doubtful, however, that the data justify such a conclusion. Height structure observations have also been made using two spacecraft widely separated in heliocentric longitude (Kane 1983). Results indicate a decrease in X-ray brightness with increasing height above the photosphere.

1.7 Gamma-Ray Emission

Both γ-ray continuum and nuclear line emission are observed in solar flares. The theory of gamma-ray emission has been treated in detail by Ramaty et al. (1975): more recently, nuclear line production has been reviewed by Hudson (1985) and Ramaty (1986).

Gamma-ray continuum from flares was first observed by

Peterson and Winckler (1959), below 1MeV. This is generally believed to be relativistic electron bremsstrahlung: there are, however, alternative mechanisms for continuum emission at both X-ray and γ-ray energies which will be discussed in Chapter 2. In many events there seems to be a hardening of the spectrum at $\varepsilon \sim 500$keV, above which the spectral index is typically $\gamma \sim 2$ (Ramaty et al. 1975).

The fact that γ-ray line emission is observed during the impulsive phase indicates the presence of energetic nuclei. The most intense γ-ray lines are those of neutron capture by protons (2.223MeV) and positron annihilation (0.511MeV). Many other lines are produced by the deexcitation of nuclear levels of elements such as C, N and O (e.g. Chupp et al. 1973). In the range 4-7MeV the Doppler broadening of these lines creates a quasi-continuum. The theory of line production is fairly well established, and this has made it possible for the number of energetic protons accelerated in a flare to be measured. The total energy in protons with energies greater than 30MeV in a large flare is typically of the order of 10^{28}ergs, a small fraction of the total flare energy (Hudson 1985).

Significant time delays have been found between γ-ray line emission and X-ray emission in the tens of keV range (e.g. Bai 1982), suggesting that there is a second stage of acceleration occuring after the impulsive phase (Bai and Ramaty 1976).

Using simultaneous Hα observations, γ-ray flares can be located on the solar disk, and Rieger et al. (1983) determined the spatial distribution of fourteen flares observed at $\varepsilon > 10$MeV (presumably electron bremsstrahlung continuum). It appears that

such events can only be observed close to the limb, implying that the relativistic electrons are highly anisotropic (Dermer and Ramaty 1986).

1.8 Interplanetary Particles

Electrons, protons, heavier nuclei and neutrons associated with solar flares have been detected in the interplanetary medium. Observations of such particles can in principle yield direct information on the acceleration mechanisms operating in flares, but this requires an accurate knowledge of the physical conditions in the interplanetary medium (i.e. density, temperature and magnetic field). Such knowledge is lacking, especially in the case of large flares which eject a substantial quantity of matter from the Sun and thereby affect the propagation properties of the medium.

Observations of flare-produced electrons using the ISEE-3 spacecraft have been reviewed recently by Lin (1985) (see also the review papers by Lin (1974) and Simnett (1974)). Non-relativistic electrons are the most commonly observed particles from the Sun: they are impulsive in character, and exhibit a velocity dispersion which implies simultaneous acceleration. They have a power law energy spectrum up to about 100keV, with a spectral index of typically 3-4. At higher energies, the spectrum either steeper sharply or continues as a power law with the same spectral index up to highly relativistic energies (at least 10MeV). The latter only occurs if protons are also observed, which is comparatively rare. In such a mixed event, the total number of electrons with energies above 20keV

may be as high as 10^{36}: this represents only a small fraction of the total flare energy, and implies a low escape probability (about 0.1-1%).

Interplanetary protons are associated with large flares, and have been observed up to relativistic ($\gtrsim$1GeV) energies. The escape probability of protons in an impulsive event is of the order of 0.1% (cf. Table 1 of Hudson 1985). Like electrons, the protons accelerated in a large flare constitute a significant fraction of the total flare energy. Both relativistic electrons and protons are believed to be associated with the second stage acceleration referred to in the previous section. Support for this hypothesis lies in the fact that proton events are associated with type II radio bursts, which indicate the presence of a shock wave propagating out through the corona (cf. Svestka 1981).

Turning now to nuclei heavier than hydrogen, there is an anomalous abundance of ^{3}He (compared with ^{4}He) associated with small flares. ^{3}He and electron events are closely correlated in time and have a similar spectrum, implying a common acceleration mechanism (Reames et al. 1985). Other heavy nuclei enhancements have been observed, in particular that of Fe (e.g. Dietrich and Simpson 1978). The preferential acceleration of heavy nuclei is discussed by Ramaty et al. (1980).

Neutrons produced by nuclear reactions in flares were first detected by Chupp et al. (1982) using the Gamma Ray Spectrometer instrument on SMM. The energy spectrum and total number of accelerated protons implied by these events are consistent with those inferred from gamma-ray observations (Ramaty et al. 1983).

CHAPTER 2

REVIEW OF RELEVANT THEORY

2.1 Introduction

In this chapter we consider those aspects of solar flare theory which have the most direct bearing on the original work of this thesis. The problem of primary energy release is fundamental, and must be discussed for that reason. We will, however, concentrate on the theoretical interpretation of those impulsive phase observations which give the most direct information on the distribution function of the radiating particles and on the physical conditions in the flaring atmosphere. Such information is believed to be contained in hard X-ray and microwave data.

It is virtually certain that the energy released in a flare originates in the magnetic field. Nuclear processes (responsible for the overall radiative output of the Sun) are not a viable energy source since the density in the solar atmosphere is far too low, and it can be easily shown that gravitational and thermal sources are also inadequate (Brown and Smith 1980). The magnetic field in the low corona, where the primary energy release is believed to take place, cannot be measured directly, but the observed photospheric field can be extrapolated to the corona using various physical models. The simplest of these is the potential field approximation, in which the current is prescribed to be zero and the magnetic field is obtained as the solution of Laplace's equation. The magnetic field energy above an active region inferred by this method is comparable to or

greater than the energy required to power a flare (e.g. Sakurai and Uchida 1977). More sophisticated models employ the force-free approximation, which involves a nonzero current flowing parallel to the magnetic field (so that the Lorentz force is zero). Using this model, Gold and Hoyle (1960) showed that a single, suitably twisted magnetic flux tube can store the energy released in an average-sized flare. Tanaka and Nakagawa (1973) showed that as much as 6×10^{32} ergs can be stored in a twisted force-free field over an area of 3×10^{18} cm^2. However, potential fields and linear force-free fields (such as those invoked by Tanaka and Nakagawa) represent a minimum energy state of the plasma (Woltjer 1958), and therefore cannot yield the energy required to power a flare. Nevertheless, it appears that even a small departure from the equilibrium configuration should be enough to provide the necessary free energy. It may be mentioned in passing that models of coronal arcades have been developed which generalize the force-free assumption, including pressure gradient and gravity terms in the magnetohydrostatic force equation (e.g. Zweibel and Hundhausen 1982).

There is compelling evidence, therefore, that flare energy is released via some form of magnetic reconnection (i.e. a change in magnetic field topology). In the next section we briefly review the various reconnection theories which have been proposed.

2.2 Magnetic Reconnection

Models of energy release in flares have been based on the interaction of two (or more) flux tubes, or on MHD instabilities

of a single flux tube. Theories of the former type postulate the creation of a current sheet at a magnetic neutral line in which field dissipation can take place. The evolution of the magnetic field in this process is described by the induction equation

$$\frac{\partial \underline{B}}{\partial t} = \underline{\nabla} \times (\underline{v} \times \underline{B}) + \frac{\eta c^2}{4\pi} \underline{\nabla}^2 \underline{B} \qquad (2.1)$$

where $\underline{B}$ is the magnetic field, η is the plasma resistivity and c is the speed of light (throughout this thesis cgs Gaussian units are used). Under normal circumstances, the diffusion term can be neglected since the corona is highly conducting (more specifically, it has a very high magnetic Reynolds number), so that the magnetic field is 'frozen' into the plasma. Thus, for example, motions of the photosphere can bring about the approach of two bipolar sunspot groups, and the creation of an X-type neutral point in the corona, as shown in Figure 2.1.

This idea forms the basis of the current sheet flare model proposed by Sweet (1958) and Parker (1963). In the vicinity of a neutral point the diffusion (i.e. dissipative) term in (2.1) can dominate, thus converting field energy into plasma kinetic energy. The rate of energy release in the Sweet-Parker model is, however, extremely slow, the physical reason for this being that the accelerated plasma is constrained to flow along a very narrow current sheet. One possible solution to this problem was suggested by Petschek (1964), whose model forms the basis of most subsequent work on steady-state current sheet reconnection. Petschek proposed that there is a small central diffusion region which bifurcates into 2 standing MHD shock waves, across which most of the inflowing plasma is accelerated. Fast reconnection,

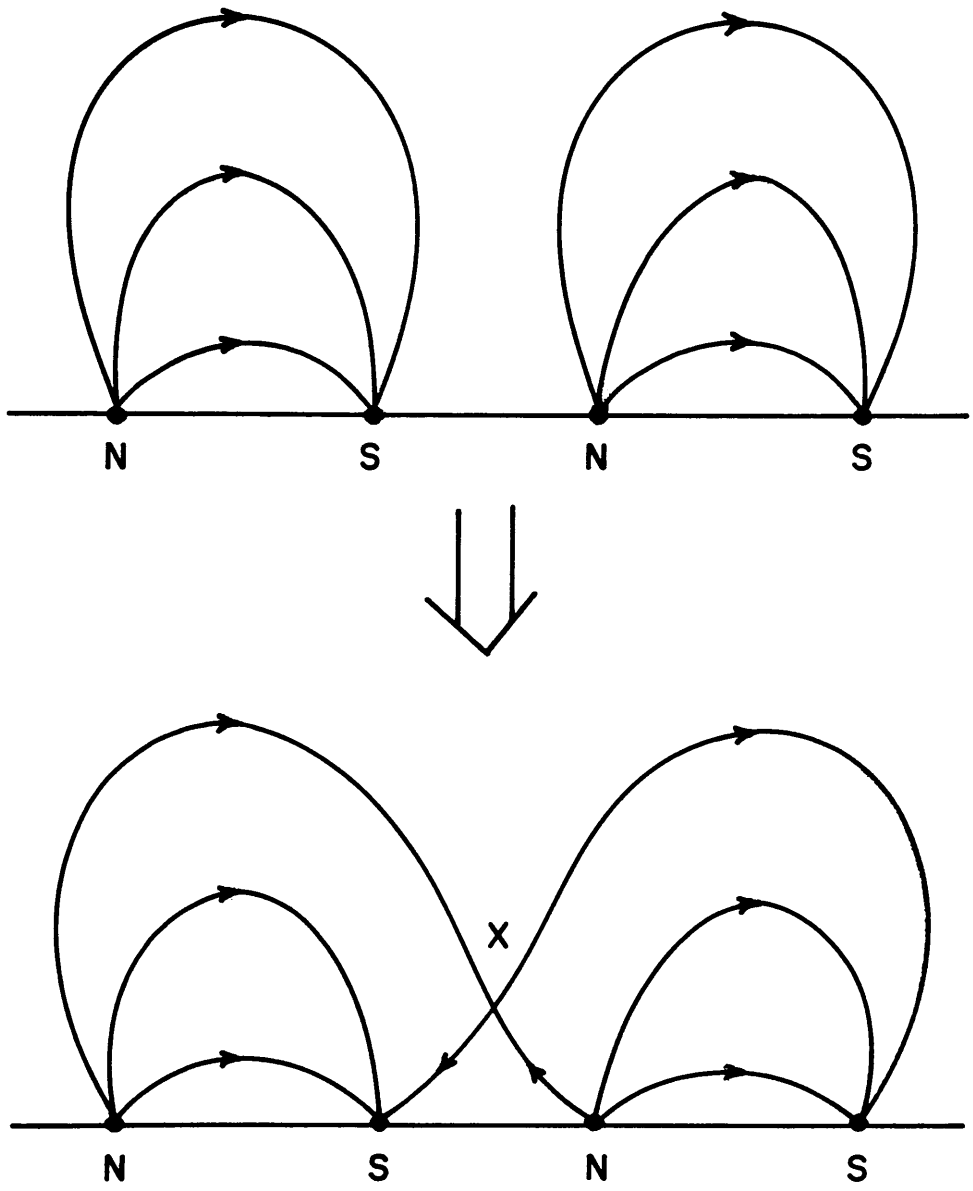

Figure 2.1 The formation of an X-type neutral point due to the interaction of 2 bipolar magnetic fields.

consistent with the observed energy release timescale of $\lesssim 10^3$s, is then possible.

Petschek's original analysis was not mathematically rigorous, and was criticised by several authors (e.g. Green and Sweet 1966). The basic mechanism has, however, been placed on a sound mathematical basis by Soward and Priest (1977), and has been generalized to compressible plasmas (Soward and Priest 1982). The model is also supported by the results of numerical simulations (Ugai and Uchida 1977).

Comprehensive flare models which invoke Petschek reconnection include those of Sturrock (1968) and Heyvaerts et al. (1977). In the Sturrock model, a Y-type neutral point is formed due to the presence of both open and closed field lines above a bipolar magnetic region. In the model of Heyvaerts et al., magnetic flux tubes emerge from below the photosphere and reconnect with the overlying field. Microinstabilities in the resulting current sheet cause it to expand, inducing an electric field which accelerates electrons towards the chromosphere (giving rise to a hard X-ray burst) and along open magnetic field lines (producing a type III burst). The model also attempts to explain the gradual phase by invoking marginal stability in the current sheet.

In contrast to current sheet models are those which invoke ideal or resistive MHD instabilities of a single loop. The first detailed model of this type was proposed by Spicer (1977). In this case reconnection results from the cylindrical tearing (or resistive kink) instability of a twisted flux tube. One advantage of such a mechanism is that field dissipation can

occur at every point in the loop, whereas in a current sheet the field dissipation region is necessarily small (Brown and Smith 1980).

Recent work on reconnection has been mostly numerical, and has linked up the Petschek mechanism with the tearing mode instability. Van Hoven et al. (1983) and Steinolfson and Van Hoven (1984a, 1984b) included the effects of optically thin radiation in a time-dependent calculation, and identified a previously unknown radiative mode which, for typical coronal parameters, is 10^2 times faster than the tearing mode. Other numerical simulations of time-dependent reconnection have revealed the limitations of the Petschek model. In particular, Forbes and Priest (1982) and Biskamp (1982) have shown that when the speed of the plasma flowing into the diffusion region exceedes a critical value, the current sheet grows and eventually becomes unstable to secondary tearing and coalescence, as magnetic islands are created and destroyed, giving an enhanced rate of energy release. In fact Biskamp (1986) has claimed that there is no regime in which the Petschek mechanism is valid, and that fast reconnection in 2 dimensions will invariably give rise to the secondary instabilities identified by Forbes and Priest.

We may conclude by saying that there exist plausible modes of reconnection which are capable of accounting for the total energy released in a flare, and the rate at which it is released. The process whereby individual particles are accelerated to high energies will be considered in the next section: clearly the nature of the acceleration mechanism will

depend on the mode of reconnection.

A concise review of the physics of reconnection has been given by Cowley (1985). Recent developments in this field have been reviewed by Priest (1986) and Priest et al. (1986).

2.3 Acceleration Mechanisms

The first point to note is that particles in flares can only be accelerated by electric fields: magnetic fields do no work on charged particles, and the solar gravitational field is completely inadequate as a particle accelerator. Essentially 2 kinds of electric field have been invoked in theories of particle acceleration: DC and stochastic. We will deal with each of these in turn. The requirements of acceleration mechanisms are that they account for the total number and velocity distribution of particles inferred from hard X-ray and type III bursts, and observed directly in the interplanetary medium. There are several competing models of hard X-ray emission which will be discussed in detail in the next section, and which place very different requirements on acceleration mechanisms.

The creation of an electric field $\underline{E}$ in a reconnecting plasma follows from the Maxwell equation

$$\underline{\nabla} \times \underline{E} = - \frac{1}{c} \frac{\partial \underline{B}}{\partial t} \qquad (2.2)$$

If we now consider the simplest case of a steady $\underline{E}$-field parallel to the $\underline{B}$-field (the perpendicular component of $\underline{E}$ merely causes a drift of the guiding centre of the particle's Larmor orbit), the behaviour of a given electron depends on the competing effects of the DC field and Coulomb collisions. Since

the collision frequency varies inversely as the cube of the electron velocity (e.g. Trubnikov 1965), electrons of sufficiently high initial energy can be freely accelerated out of the thermal distribution. An electron at the thermal speed v_e can escape if E exceedes the Dreicer field

$$E_D = \frac{e \ln \Lambda_o}{\lambda_D^2} \qquad (2.3)$$

where e is the electronic charge, λ_D is the electron Debye length and $\ln \Lambda_o$ is the Coulomb logarithm for a thermal plasma (Spitzer 1962). For an arbitrary field E, the fraction of escaping particles is given by (Norman and Smith 1978)

$$f = \frac{1}{2} \exp \left[- \frac{1}{2} \left(\left(\frac{E_D}{E} \right)^{\frac{1}{2}} - \frac{E}{E_D} \right)^2 \right] \qquad (2.4)$$

and therefore depends critically on the ratio E/E_D. Order of magnitude calculations indicate that $E \gtrsim E_D$ can result from the tearing mode instability (Van Hoven 1979, Heyvaerts 1981). However, such calculations neglect the role of microinstabilities, many of which have thresholds at currents corresponding to $E \ll E_D$, and which may greatly increase the effective collision frequency of the plasma (thus rendering the acceleration process ineffective).

A systematic study of particle acceleration and the associated Ohmic heating in the presence of a prescribed DC electric field has been carried out by Holman (1985). This author pointed out that the nonthermal interpretation of hard X-ray emission implies a current with a corresponding induced magnetic field $\gtrsim 10^6$G, compared with a known coronal field

$\sim 10^2$G. Holman concluded from this that DC field acceleration is only consistent with a nonthermal hard X-ray model if there exist at least 10^4 separate counterflowing current channels in the acceleration region. The heating and acceleration required by a thermal hard X-ray model, on the other hand, can be acheived with a single current sheet and a comparitively modest electric field, $0.02 \lesssim E/E_D \lesssim 0.1$. Holman also found, in agreement with previous authors (e.g. Smith 1980), that DC field acceleration results in more energy going into heating than anisotropic fast particles.

Moghaddam-Taaheri et al. (1985) have studied DC field acceleration using the quasi-linear theory, allowing for Coulomb collisions. They find that for $E/E_D \gtrsim 0.2$, electrons accelerated along the field are rapidly isotropized due to the Cerenkov and anomalous Doppler resonance instabilities, and therefore conclude that effective electron acceleration can only be acheived with $E/E_D \lesssim 0.2$. This conclusion depends, however, on the assumption that the gyrofrequency is appreciably greater than the plasma frequency, which may not be true in the energy release region (see Chapter 3).

Stochastic (or Fermi) acceleration is a generic term for any process in which a charged particle interacts with a randomly varying field, and gains energy on average. One way of acheiving this is by means of a turbulent spectrum of Langmuir waves: electrons with speeds in excess of the phase velocity of the waves may be accelerated, depending on the particle distribution function (e.g. Melrose 1980a). The basic problem with such a mechanism is that it is difficult to produce a Langmuir wave

spectrum which is capable of particle acceleration. The most obvious way of generating Langmuir waves is by means of a pre-existing distribution of anisotropic fast particles, so that one is faced with a 'bootstrapping' problem. One solution, proposed by Tsytovich et al. (1975), is that electrons emit Langmuir waves as the result of scattering on ion-acoustic waves, excited by some current-driven instability. There are several arguments against the feasibility of this mechanism (see e.g. Heyvaerts 1981). Indeed, Kuijpers and Melrose (1985) have argued, on the basis of a quantum electrodynamic calculation, that the scattering process does not even exist, although this claim has been challenged by Nambu (1986).

Other kinds of stochastic mechanism have been proposed to explain the 2nd phase acceleration of relativistic electrons and protons, involving resonant scattering on Alfvén waves (e.g. Barbosa 1979) and magnetosonic waves (e.g. Achterberg 1981), and hydrodynamic shock waves (e.g. Ellison and Ramaty 1985). Decker and Vlahos (1986) have shown that shock acceleration of ions (to energies of around 50MeV) can occur on a timescale as short as 10ms, and it is therefore possible that shocks play an important role in impulsive phase acceleration as well. Reviews of recent work in this field have been given by Forman et al. (1986) and Vlahos et al. (1986).

2.4 Models of Hard X-Ray Emission

The three basic mechanisms which have been invoked to account for the production of cosmic X-ray continuum are bremsstrahlung, synchrotron radiation and inverse Compton radiation. Korchak

(1967, 1971) concluded that electron-proton bremsstrahlung is likely to be the dominant process in the case of solar hard X-ray bursts: the synchrotron interpretation places prohibitive demands on electron acceleration mechanisms, while the inverse Compton process (i.e. scattering of relativistic electrons on thermal photons) would require a density lower than that generally found in the flaring atmosphere in order to be dominant over bremsstrahlung. Kaufmann et al. (1986) proposed that hard X-ray bursts and microwave bursts with very high turnover frequencies (such as those observed by Kaufmann et al., 1985a) may be explained by a single mechanism involving the inverse Compton scattering of relativistic electrons on synchrotron microwave photons. McClements and Brown (1986) showed that both the thermal/inverse Compton and synchrotron/inverse Compton models require exceptional source parameters, and are not any more attractive than the conventional bremsstrahlung model in terms of efficiency. It appears, therefore, that some form of bremsstrahlung is the most promising candidate for impulsive hard X-ray emission, although the contribution of inverse Compton emission may be non-negligible.

Bremsstrahlung models of hard X-ray emission fall into two broad categories, depending on the distribution function of the emitting electrons: thermal and nonthermal. Essentially three kinds of nonthermal model have been proposed: the thin target model, the thick target model and the trap model.

In the thin target model (Datlowe and Lin 1973), electrons are accelerated continuously and injected upwards along open

field lines, as shown in Figure 2.2a. The X-ray emission is then proportional to the column depth of plasma traversed by the electrons (Brown 1975). The model was originally proposed by Datlowe and Lin to account for the appearance of X-ray bursts behind the solar limb. However, Brown and McClymont (1974) showed that a thin target interpretation of such events would imply an extremely low radiative efficiency and would place unacceptable constraints on the number and total energy of accelerated electrons. In addition, the thin target picture is inconsistent with the observed synchronism of hard X-ray bursts with emissions which could only have originated from the chromosphere, such as UV and Hα.

The thick target model postulates that electrons are injected from the low corona into the chromosphere where they lose essentially all their energy through Coulomb collisions with ambient electrons, and where most of the hard X-rays are produced (Brown 1971). The rate of injection may be either 'impulsive', meaning that the duration of the X-ray burst is determined by the collisional lifetime of the electrons, or 'continuous', meaning that the collisional lifetime is much less than the burst duration, and the X-ray time profile is therefore determined by the acceleration process. The latter case is sometimes referred to as <u>the</u> thick target model, and enables one to treat the electron distribution as if it were in a steady state. In such circumstances the integral equation relating the injection rate of electrons per unit energy $\mathcal{J}(E)$ to the observed photon spectrum $I(\varepsilon)$ can be solved analytically (Brown 1971). In the case of a power law photon spectrum (equation (1.1)) one

(a) Thin Target Model

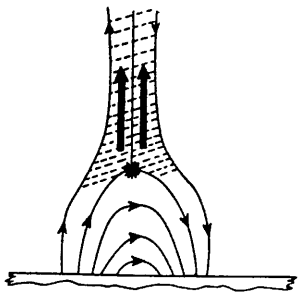

(b) Thick Target Model

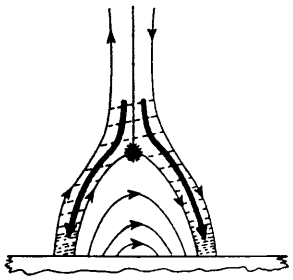

(c) Trap Model

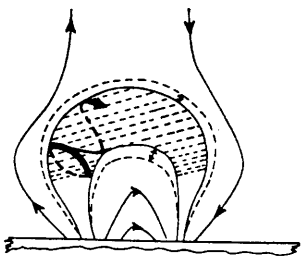

Figure 2.2 Alternative nonthermal models of hard X-ray emission. The spatial distribution of emission is indicated by the shading. Electron trajectories are indicated by heavy arrows, and in (a) and (b) the acceleration region is denoted by a star (from Brown 1976).

obtains the result

$$\mathcal{J}(E) = 4{\cdot}15 \times 10^{33} \gamma(\gamma-1)^2 B(\gamma-\tfrac{1}{2},\tfrac{1}{2}) I_o E^{-\gamma-1} \qquad (2.5)$$

where B is the beta function, E is in keV and $\mathcal{J}(E)$ is in electrons s^{-1} keV^{-1} (for a given injected electron flux, the X-ray spectrum is independent of the density of the source). Taking a lower cutoff of (20-30)keV in the observed photon spectrum, (2.5) implies that at least a large fraction of the total energy released in a flare lies in nonthermal electrons (Hoyng et al. 1976). The thick target interpretation therefore implies an improbably high acceleration efficiency, particularly in view of the problems associated with both DC and stochastic acceleration mechanisms described in the previous section (see Smith 1980). The situation is aggravated when one considers that the thick target calculation neglects energy losses due to collective processes, and therefore (2.5) represents a minimum electron flux requirement for a given X-ray yield.

Notwithstanding the acceleration problem, the thick target model has attracted a great deal of theoretical interest. The predicted spatial distribution of thick target hard X-ray emission was computed by Brown and McClymont (1975), Emslie (1981a) and Leach and Petrosian (1983). The latter authors used the results of a numerical Fokker-Planck calculation, allowing for dispersion in pitch angle scattering and a converging magnetic field (Leach and Petrosian 1981). They found that, with plausible source parameters, they could get good agreement with the stereoscopic observations of Kane et al. (1979, 1982). Thick target polarization calculations have been carried out by Brown

(1972), Leach and Petrosian (1983) and Kel'ner and Skrynnikov (1985). Brown (1972), using a mean scattering rate treatment, estimated degrees of polarization as high as 30% at 15keV, contrary to the observations of Tindo et al. (1976) and Tramiel et al. (1984). Leach et al. (1985), using the more physically realistic numerical calculations of Leach and Petrosian (1983), showed that the observed degrees of polarization are consistent with thick target electron beams injected with a hard energy spectrum. This result is independent of the degree of collimation of the electron beam at the point of injection. In the case of an initially highly collimated beam, the effect of a converging magnetic field is to reduce even further the predicted polarization.

The assumption of a steady state in the standard thick target model requires reevaluation in the light of high time resolution HXRBS observations. The important quantity in this respect is the collisional decay time of a fast electron, given by (Trubnikov 1965)

$$\tau_{coll} \simeq 10^{-4} \frac{E^{3/2}}{n_{12}} \text{ s} \qquad (2.6)$$

where E is the electron energy in keV and n_{12} is the plasma density in units of 10^{12} cm^{-3}. As previously stated, most of the thick target X-rays are produced in the flaring chromosphere where $n \gtrsim 10^{12}$ cm^{-3}. Putting E=30keV in (2.6) then gives $\tau_{coll} \lesssim 20$ms, which implies that even the shortest time structures detected by HXRBS ($\tau \simeq 100$ms) are consistent with the continuous injection model. Emslie (1983) has pointed out that time-of-flight effects alone can smear out the X-ray time

profile, even in the case of instantaneous injection. For the majority of events, however, with e-folding times in excess of 1s, the steady-state assumption is certainly justified.

Perhaps surprisingly, it is only in the past few years that the electrodynamics of electron beams in flares has been studied in detail. Kane and Anderson (1970) noted that the magnetic self-energy of an unneutralized thick target beam is several orders of magnitude greater than the total energy released in a typical flare. Knight and Sturrock (1977) therefore proposed that the beam current is compensated by a reverse current carried by thermal electrons. Due to the finite resistivity of the plasma, the reverse current gives rise to an enhanced rate of dissipation of beam energy. Such energy losses may be greatly enhanced if the resistivity is anomalous. The importance of reverse current energy losses has been assessed by Emslie (1980, 1981b) and Brown and Hayward (1982). These authors assumed a steady state in which the electric field driving the reverse current is purely electrostatic. Spicer and Sudan (1984) pointed out that this assumption is unphysical since it neglects inductive effects. Brown and Bingham (1984) agreed that inductive processes must take place, but showed that they occur on a sufficiently long timescale that the steady state treatment is essentially valid. Even in the absence of anomalous resistivity, reverse current energy losses may be greater than collisional losses near the point of injection, in the case of high beam flux and low plasma density. The thick target energy requirement is considerably increased in such cases. McQuillan et al. (1987) have considered the problem of ion-acoustic wave

generation by an unstable reverse current, and the consequent anomalous heating of the plasma. They show that rapid heating to $T \gtrsim 10^8$K can occur, and that the resulting thermal hard X-ray emission can exceed the thick target emission due to the beam.

Thick target beams may also be unstable to the generation of Langmuir waves. Hoyng et al. (1979) studied numerically the combined evolution of beam electrons and Langmuir waves using a Legendre series expansion method developed previously by Hoyng and Melrose (1977). Hoyng et al. found that Langmuir wave generation had a negligible effect on the thick target hard X-ray signature. Emslie and Smith (1984) pointed out that the inverse cubic velocity dependence of the Coulomb collision frequency means that a positive gradient can be produced in electron beam distributions which are monotonic decreasing functions of velocity at injection. Such distributions may be unstable, and a high level of Langmuir waves may therefore be produced. Emslie and Smith did not consider, however, the effect of such wave generation on the propagation of the beam. Vlahos and Rowland (1984) and Rowland and Vlahos (1985) claim that the Langmuir waves excited by an unstable thick target beam will be strongly turbulent, giving rise to a number of nonlinear processes (notably soliton formation) which take the waves out of resonance with the beam electrons and thereby allow the beam to propagate without significant energy loss, except through Coulomb collisions. The problem of electron beam stability in three dimensions in a magnetized plasma has been investigated by McClements (1987b): the quasi-linear relaxation of a one dimensional beam has been studied by McClements et al. (1986)

and McClements (1987a, 1987c). These papers contain the bulk of the original work of this thesis.

We now turn to the nonthermal trap model. The basic picture, as depicted in Figure 2.2c, is that magnetic field lines converge rapidly towards the chromosphere, thereby confining nonthermal electrons in a coronal magnetic bottle. Takakura and Kai (1966) proposed that electrons are accelerated up to the maximum of the hard X-ray burst, and then decay collisionally on the same timescale as the burst itself. Since slow electrons lose energy first, one would expect the X-ray spectrum to harden with time, contrary to observations (cf. Figure 1.3). This problem may be overcome by invoking a time-dependent magnetic field (e.g. Brown and Hoyng 1975), so that acceleration continues after the burst maximum. Hudson (1972) pointed out that some initially confined electrons are scattered into the loss cone by Coulomb collisions, and consequently escape from the trap. The rate at which this occurs may be greatly enhanced by the presence of waves excited by the loss cone instability (Wentzel 1976). This led Melrose and Brown (1976) to develop the trap-plus-precipitation model, in which escaping electrons produce thick target X-ray emission in the chromosphere. Melrose and Brown estimated that collisional scattering results in about one third of the initially trapped particles escaping. The model has the advantage over the original trap model of explaining the heating of the chromosphere revealed, for example, by Hα observations. The analysis of Melrose and Brown has been challenged, however, by MacKinnon (1987) on the grounds that the collisional energy loss associated with scattering into the loss

cone was neglected. The flux of precipitating electrons may therefore have been grossly overestimated, depending on the energy distribution of electrons in the trap.

Before leaving nonthermal models we briefly discuss proton beams. Boldt and Serlemitsos (1969) proposed that solar hard X-ray emission might be produced by the interaction of fast protons with thermal electrons, rather than fast electrons with thermal protons ('inverse bremsstrahlung'). Protons are certainly accelerated in flares, as observations of γ-rays and interplanetary particles indicate. Emslie and Brown (1985) showed that, for a given X-ray yield, thick target proton beams are slightly more efficient than thick target electron beams, and carry a much smaller current. It appears, however, that the proton beam model is inconsistent with both γ-ray line observations and hard X-ray height structure observations.

We finally consider thermal models. The basic attraction of a purely thermal hard X-ray interpretation is energetic efficiency: essentially all the available energy goes into radiation, as opposed to $\lesssim 0.01\%$ in the case of the thick target or trap model. In addition, bulk heating is easier to acheive than acceleration (cf. previous section), and on general thermodynamic grounds thermal models are more credible than nonthermal models.

Fitting (1.2) to hard X-ray burst spectra generally yields temperatures in the range 10^8 - 10^9 K and emission measures in the range 10^{44} - 10^{46} cm^{-3} (e.g. Wiehl et al. 1985). Kahler (1971) pointed out that these parameters, combined with a coronal density $n \gtrsim 10^8$ cm^{-3}, imply a conductive cooling time of

a fraction of a second. Kahler concluded from this that impulsive hard X-rays are unlikely to be thermal. The thermal model was consequently ignored for several years, but was revived by Brown et al. (1979) who showed that free streaming of thermal electrons may generate a conduction front of ion-acoustic turbulence, which propagates at the ion sound speed. This model was subsequently developed by Smith and Lilliequist (1979) and Vlahos and Papadopoulos (1979). The latter authors showed that electrons with speeds in excess of about 3 times the thermal speed are not confined by the conduction fronts, so that about 1% of the particles escape. These precipitate towards the chromosphere, producing thick target hard X-ray emission, as in the trap-plus-precipitation model.

The energy requirement of the thermal model, as proposed by the above authors, is typically a few per cent of that of nonthermal models. There are difficulties reconciling it with observations, however. For example, conservation of energy requires that the temperature should fall as the emission measure increases, thus producing a spectral softening during the rise of the impulsive phase. In fact the opposite is generally observed to take place (cf. Figure 1.3). To overcome this shortcoming, Brown et al. (1980) proposed the multiple kernel thermal model, in which the energy release occurs in a large number of sources with sizes and lifetimes below current instrumental resolution. Such a scenario enables the thermal model to be reconciled with most observations, although it cannot explain the hardest observed spectra and is energetically

more efficient than the thick target model.

2.5 Models of Microwave Emission

The close correlation of microwave and hard X-ray time profiles suggests that a common population of particles is responsible for both emissions. The broad bandwidth of microwave bursts such as the one depicted in Figure 1.2 further suggests an incoherent radiation mechanism. The two candidates for such a mechanism are thermal bremsstrahlung and gyrosynchrotron radiation. A thermal interpretation may be applicable to some gradual microwave bursts (e.g. Shimabukuro 1972), but there are several compelling reasons for rejecting it in the case of impulsive events. In the first place, an optically thin thermal bremsstrahlung spectrum is essentially flat whereas impulsive microwave bursts fall off rapidly at high frequency, with a spectral index of typically between 1 and 4 (e.g. Wiehl et al. 1985). In addition, a thermal interpretation of simultaneous hard X-ray emission would imply a temperature so high that the source would be optically thin at microwave frequencies, for any reasonable source size (e.g. McClements and Brown 1986). Finally, a thermal source would be unpolarized whereas microwave bursts have a high degree of circular polarization (e.g. Kaufmann et al. 1985b).

The only viable continuum emission mechanism is therefore gyrosynchrotron radiation. The electrons producing this radiation are mildly relativistic ($E \sim 100keV$), and the theory of the emission process is considerably more complicated than it is at extremely relativistic energies (see e.g. Ramaty 1969). As a

result of this, several authors have developed simplified expressions for the gyrosynchrotron emission and absorption coefficients, valid in a limited parameter regime (Petrosian 1981; Dulk and Marsh 1982; Klein 1987). Gyrosynchrotron emission in flares is complicated by a number of essentially unknown source parameters (such as the structure of the magnetic field), and therefore microwave observations place less unambiguous constraints on flare models than hard X-ray observations.

Holt and Cline (1968) estimated that the number of electrons inferred from a nonthermal interpretation of hard X-ray emission ought to produce a gyrosynchrotron flux several orders of magnitude in excess of that observed. A large part of the discrepancy may be accounted for, however, when one takes into account gyrosynchrotron self-absorption (Takakura 1972), Razin suppression, gyroresonance absorption, free-free absorption (Ramaty and Petrosian 1972) and inhomogeneities in the magnetic field (Klein et al. 1986). In addition, the gyrosynchrotron emission is produced by electrons with higher energies than those producing the bulk of the hard X-ray emission, and one might therefore expect some discrepency if the two populations of electrons have different energy spectra (MacKinnon et al. 1986). Gyrosynchrotron radiation is produced by electrons with large pitch angles, whereas thick target beams are collimated in the direction of the magnetic field. Holman et al. (1982) have suggested that a highly anisotropic electron beam will be isotropized on a collisionless timescale due to the anomalous Doppler resonance instability. Those electrons with sufficiently large pitch angles are trapped in the corona, thus giving rise

to the observed spatial structure of microwave emission (e.g. Marsh and Hurford 1980). This would require, however, a rather strong coronal magnetic field (see Chapter 3).

Analysis of simultaneous microwave and hard X-ray bursts indicates electron densities in the range 10^8 - 10^{10} cm^{-3} and magnetic fields in the range 100-500G (Crannell et al. 1978; Wiehl et al. 1985). Microwave observations do not unambiguously discriminate between thermal and nonthermal models of hard X-ray emission. MacKinnon and Brown (1984), for example, show that the gyrosynchrotron interpretation is consistent with the multiple kernel thermal model of Brown et al. (1980).

We now consider coherent emission mechanisms. Coherent processes must be involved to account for the detection of brightness temperatures as high as 10^{15}K. Melrose and Dulk (1982) proposed that narrowband microwave bursts of short duration ($\lesssim$100ms) could be produced by the electron cyclotron maser instability (e.g. Melrose 1986). The instability is driven by an anisotropy in the electron distribution, such as a loss cone anisotropy. The growth rate for the process is extremely fast, and it rapidly saturates due to the radiation-induced diffusion of electrons into the loss cone. The model can thus account for the very short duration of microwave spikes. It also predicts very high degrees of circular polarization (as observed, for example, by Slottje, 1978), and brightness temperatures as high as 10^{16} - 10^{17}K. Maser emission is produced at harmonics of the gyrofrequency: low harmonics are gyroresonance absorbed, resulting in heating of the corona (Melrose and Dulk 1984), while higher harmonics escape to

produce the observed radiation. The theory of cyclotron maser emission has been further developed by Winglee (1985) and Winglee and Dulk (1986).

The other coherent mechanism which has been proposed for impulsive microwave emission is plasma radiation. Smith and Spicer (1979) suggested that observable fluxes of fundamental and 2nd harmonic plasma radiation may be produced in the primary energy release region if the acceleration process involves Langmuir turbulence. Fundamental emission is produced due to the scattering of Langmuir waves by ion-acoustic waves or thermal ions, while 2nd harmonic emission results from the coalescence of two Langmuir wave quanta. Emslie and Smith (1984) estimated the flux density of 2nd harmonic radiation produced by a thick target electron beam to be several orders of magnitude greater than the microwave flux observed in a typical event. There are several reasons for doubting the accuracy of this estimate, however, which will become clear in later chapters. The reverse drift microwave bursts described in Section 1.3 have been interpreted by Stähli and Benz (1987) as 2nd harmonic radiation, produced by a beam of downward propagating electrons. However, the flux densities involved ($\sim$ 50sfu) are very much less than those predicted by Emslie and Smith. Plasma radiation generated by electron beams in the low corona also appears to be the most likely explanation of the decimetric bursts observed by Benz et al. (1983). The majority of these bursts drift towards lower frequency with time, and therefore cannot be due to downward propagating electrons. A few events could, however, be the plasma radiation signature of thick target beams. We will

discuss this further in Chapter 5. Benz (1986) has argued that the microwave spikes observed by, for example, Stähli and Magun (1986) are probably not plasma radiation, on the grounds that the observed brightness temperature is too high and the observed bandwidth is too small. He concludes that cyclotron maser emission is the more likely mechanism.

CHAPTER 3

THE STABILITY OF ELECTRON BEAMS IN THE FLARING CORONA

3.1 Introduction

In this chapter we examine the possibility that electron beams producing hard X-ray burst emission are unstable to the generation of Langmuir waves. Emslie and Smith (1984) pointed out that the temperature and density in the flaring chromosphere are such that, for any reasonable beam density, the collisional damping rate of Langmuir waves is much larger than the quasi-linear growth rate. We shall therefore be concerned only with the propagation of fast electrons through the (hot and tenuous) flaring corona, where the collisional damping rate is much smaller than it is in the chromosphere.

Emslie and Smith claimed that the collisional degradation of a thick target beam will inevitably result in instability, and consequently a high level of Langmuir turbulence. An electron beam distribution is only two-stream unstable, however, if it is sufficiently well-collimated. Since collisional pitch angle scattering occurs on a comparable timescale to collisional energy loss (Trubnikov 1965), it is by no means clear that the collisional degradation of an electron beam will necessarily give rise to Langmuir instability. Emslie and Smith only considered Langmuir waves propagating along the magnetic field, and neglected the possible role of the field in destabilizing the beam (cf. Holman et al. 1982).

In general, a necessary condition for Langmuir instability is that the quasi-linear growth rate γ is positive. Although

collisional wave damping plays a crucial role in the dynamics of the Langmuir waves (see Chapters 4 and 5), the condition $\gamma > 0$ is in practice both necessary and sufficient for instability. The growth rate in a magnetized plasma depends on the electron distribution function, the evolution of which is in turn determined partly by the level of plasma waves. Unless instability occurs, however, wave-particle interactions have a negligible effect on the electron distribution compared with Coulomb interactions (see Chapter 5). For the purpose of determining a stability boundary in parameter space (corresponding to $\gamma = 0$) it is therefore sufficient to prescribe an electron distribution whose spatial and temporal evolution is determined by collisions alone, provided one neglects any other forces, such as those arising from a converging magnetic field and the electric field required to drive a beam-neutralizing reverse current. In practice both of these will tend to reduce the degree of anisotropy of the distribution, thereby stabilizing it.

In this chapter we will consider the stability of a steady state electron beam: this precludes the possibility of a positive slope developing in the electron distribution as the result of velocity dispersion, which is unlikely to be important provided the injection timescale is greater than the time of flight across the propagation region (see Chapter 6). The transit time of a fast electron from the acceleration region to the chromosphere is $\lesssim 0.3$s, compared with an e-folding time of $\gtrsim 1$s in the majority of hard X-ray events. Leach and Petrosian (1981) obtained an analytic solution of the time-independent

Fokker-Planck equation describing the collisional interaction of a dilute electron beam (axisymmetric about a uniform magnetic field) with a hydrogen plasma, in the limit of small pitch angle. Leach and Petrosian showed that their analytic solution is in good agreement with the results of a numerical calculation, even for large pitch angles.

In Section 3.2 we use the Leach and Petrosian solution to evaluate numerically the electron plasma wave growth rate as a function of wave pitch angle for prescribed beam and plasma parameters. The normal and anomalous Doppler resonances are taken into account. In Section 3.3 the conditions required for the stability of an electron beam are established, under the assumption that the maximum growth rate occurs along the magnetic field. The results are applied to the trap-plus-precipitation model and the dissipative thermal model in Section 3.4.

3.2 Wave Growth Rate in a Magnetized Plasma

The growth rate (s^{-1}) of electron plasma waves ('generalized Langmuir waves') in a magnetized plasma is given by (e.g. Harris 1969)

$$\gamma = \omega \sum_{s=-\infty}^{+\infty} \frac{8\pi^3 e^2}{m k^2 |k_{\parallel}|} \int_0^{\infty} dv_{\perp}\, v_{\perp}\, J_s^2 \left(\frac{k_{\perp} v_{\perp}}{\omega_H}\right) \times \left[\frac{s\omega_H}{v_{\perp}} \frac{\partial f}{\partial v_{\perp}} + k_{\parallel} \frac{\partial f}{\partial v_{\parallel}}\right]\Bigg|_{v_{\parallel} = \frac{\omega - s\omega_H}{k_{\parallel}}} \qquad (3.1)$$

where $f(\underline{x},\underline{v},t)$ is the electron distribution function, J_s is the Bessel function of the first kind of order s, ω is the wave

frequency, $\underline{k}$ is the wavevector and ω_H is the electron gyrofrequency. The parallel direction is that of the magnetic field (f is assumed to be axisymmetric with respect to the field line). m denotes the mass of the electron. f is normalized such that

$$\int f(\underline{x}, \underline{v}, t)\, d^3 \underline{v} = n \qquad (3.2)$$

where n is the plasma density. To first order in the thermal correction, the wave frequency is given by (Melrose 1980b, Section 12.1)

$$\omega^2 = \omega_\pm^2 \pm \frac{\omega_p^2 (\omega_\pm^2 - \omega_H^2)}{\omega_+^2 \omega_-^2} \frac{k^2 v_e^2}{\omega_\pm^2} g\left(\frac{\omega_H}{\omega_\pm}, \theta\right) \qquad (3.3)$$

where

$$\omega_\pm^2 = \frac{1}{2}\left[\omega_p^2 + \omega_H^2 \pm ((\omega_p^2 + \omega_H^2)^2 - 4\, \omega_p^2\, \omega_H^2 \cos^2\theta)^{\frac{1}{2}}\right] \qquad (3.4)$$

and

$$g(x,\theta) = 3\cos^4\theta - \frac{\cos^2\theta \sin^2\theta}{x^2} - \frac{\sin^4\theta}{x^2(1 - x^2)} + \frac{(1+3x^2)\sin^2\theta\cos^2\theta}{x^2(1 - x^2)^3} + \frac{\sin^4\theta}{x^2(1 - 4x^2)} \qquad (3.5)$$

Here ω_p is the plasma frequency, v_e is the electron thermal speed and $\theta = \cos^{-1}(k_\parallel/k)$ is the wave pitch angle. The upper sign is taken in (3.3) and (3.4) if $\omega_p > \omega_H$, and the lower sign if $\omega_p < \omega_H$. The thermal correction term in (3.3) is only valid if $\omega_\pm$ is not close to ω_H or $2\omega_H$ (cf. Melrose 1980b): specifically, we require that

$$(\omega_\pm - s\,\omega_H)^2 >> 2k_\parallel^2 v_e^2 \qquad (3.6)$$

where s = 1 or 2. The parameters used in this chapter are such that (3.6) is not always satisfied. However, in all cases the thermal correction is small and it therefore appears unlikely that the use of (3.3) will lead to grossly erroneous results.

At a given point in space f consists of a collisionally evolved nonthermal distribution plus a thermal background: the thermal damping rate may be evaluated analytically, yielding

$$\gamma_T = -\omega^2 \frac{(2\pi)^{3/2} e^2}{mk^2 |k_{\parallel}| v_e^3} \; n \sum_{s=-\infty}^{+\infty} I_s \left[\left(\frac{k_\perp v_e}{\omega_H} \right)^2 \right] \exp\left[- \frac{\omega_D^2}{2k_{\parallel}^2 v_e^2} - \frac{k^2 v_e^2}{\omega_H^2} \right] \tag{3.7}$$

where $\omega_D = \omega - s\omega_H$ is the Doppler shifted frequency and I_s is the modified Bessel function of the first kind of order s (Gradshteyn and Ryzhik 1980).

To evaluate the nonthermal part of γ it is convenient to change the variable of integration in (3.1) to $v=(v_{\parallel}^2+v_\perp^2)^{\frac{1}{2}}$. This yields

$$\gamma_{NT} = \frac{8\pi^3 e^2 \omega}{mk^2} \frac{k_{\parallel}}{|k_{\parallel}|} \sum_{s=-\infty}^{+\infty} \int_{\left|\frac{\omega_D}{k_{\parallel}}\right|}^{\infty} dv \; J_s^2 \left[\frac{k_\perp v (1-\mu^2)^{\frac{1}{2}}}{\omega_H} \right]$$

$$\times \left[\frac{\omega}{k_{\parallel}} \frac{\partial f}{\partial v} + \left(1 - \frac{\omega \omega_D}{k_{\parallel}^2 v^2}\right) \frac{\partial f}{\partial \mu} \right] \Bigg|_{\mu = \frac{\omega_D}{k_{\parallel} v}} \tag{3.8}$$

where $\mu = v_{\parallel}/v$. We take f to be given by the solution of the appropriate nonrelativistic Fokker-Planck equation, with only Coulomb interactions being taken into account. In the small pitch angle limit, the solution may be written in the form (Leach and Petrosian 1981)

$$f(x,v,\alpha) = f_o \left[(v^4+v_c^4)^{\frac{1}{4}} \right] \frac{2}{\alpha_o^2 + \ell n\left(1+\frac{v_c^4}{v^4}\right)} \exp\left[- \frac{\alpha^2}{\alpha_o^2 + \ell n\left(1+\frac{v_c^4}{v^4}\right)} \right] \tag{3.9}$$

where $v_c^4 = 16\pi e^4 \ln\Lambda\, nx/m^2$ ($\ln\Lambda$ being the Coulomb logarithm of the fast electrons), x is the distance along the field line from the point of injection, α is the electron pitch angle and α_o is a constant. Λ is given explicitly by (Ginzburg and Syrovatskii 1964)

$$\Lambda = \left(\frac{m}{\pi \hbar^2 e^2}\right)^{\frac{1}{2}} \frac{mv^2}{n^{\frac{1}{2}}} \qquad (3.10)$$

where $2\pi\hbar$ is Planck's constant. In practice it is sufficiently accurate to take a constant value $\ln\Lambda=22$. f and f_0 in (3.9) have the same dimensions and normalization as f in (3.1), so that $2\pi f(x,v,\alpha)v^2 dv\alpha d\alpha$ is the number of particles per unit volume with velocities in the range v to v+dv and pitch angles in the range α to $\alpha+d\alpha$. The injected distribution function is assumed to be of the form

$$f(o,v,\alpha) = f_o(v)\,\frac{2}{\alpha_o^2}\, e^{-\alpha^2/\alpha_o^2} \qquad (3.11)$$

A Gaussian pitch angle distribution was chosen by Leach and Petrosian for analytical convenience: it may be shown that the solution as $x \to \infty$ is insensitive to the choice of injection profile, although the stability of the distribution depends quite critically on the value of the collimation parameter α_o. For example, suppose instead of (3.11) we take a step function pitch angle profile

$$\begin{aligned} f(o,v,\alpha) &= f_o(v)\,\frac{2}{\alpha_o^2}, \quad \alpha < \alpha_o \\ &= 0, \quad \alpha > \alpha_o \end{aligned} \qquad (3.12)$$

Then, repeating the analysis of Leach and Petrosian, we obtain the result

$$f(x,v,\alpha) = f_o[(v^4+v_c^4)^{\frac{1}{4}}] \frac{2}{\alpha_o} \int_0^\infty [1 + \frac{v_c^4}{v^4}]^{-\omega^2/4} J_1(\alpha_o \omega)\, J_o(\alpha\omega) d\omega \quad (3.13)$$

which, for $\alpha_o << 1$, tends to the solution (3.9) in the limit $v_c^4 >> v^4$. The fact that very different injection profiles can give rise to identical asymptotic solutions may be attributed to the diffusive (i.e. entropy-increasing) character of collisional pitch angle scattering.

It is convenient to express $f_0(v)$ in terms of the total injected flux of electrons (since this is one of the beam parameters inferred from hard X-ray observations). Following Knight and Sturrock (1977), we take the electrons to have an injected energy flux spectrum of the form (electrons cm^{-2} s^{-1} keV^{-1})

$$F(E) = (\delta-1)\, F_o\, E_o^{\delta-1}\, (E_o + E)^{-\delta} \quad (3.14)$$

where F_0, E_0 and δ are constants. F_0 is the total injected flux of electrons and E_0 is a characteristic energy above which F(E) becomes essentially a power law. At photon energies $\varepsilon >> E_0$ such electron beams injected into a thick target produce hard X-ray spectra with spectral index $\gamma = \delta - 1$ (cf. (2.5)). Assuming that $\alpha_o << 1$, it then follows from (3.11) and (3.14) that

$$f_o(v) = \frac{m}{2\pi v^2}(\delta-1)\, F_o\, E_o^{\delta-1}\, (E_o + E)^{-\delta} \quad (3.15)$$

It is now possible to compute $\partial f/\partial v$ and $\partial f/\partial \mu$, using the small angle approximation $\alpha^2 \simeq 2(1-\mu)$ in (3.9). The integrals in (3.8) may then be evaluated numerically. An assumption

frequently made (e.g. Emslie and Vlahos 1980; Holman et al.1982) is that $\omega_H >> \omega_p$. This means that only one or two resonances ever contribute to the summation in (3.8), and also means that the small argument expansion of the Bessel functions can be used. Although analytically convenient, this assumption is of questionable validity, even in the low corona. The ratio of gyro to plasma frequency is given by

$$\frac{\omega_H}{\omega_p} = 3 \times 10^2 \, B/n^{\frac{1}{2}} \qquad (3.16)$$

and observations suggest that this parameter could lie anywhere in the range 0.1 to about 10 (cf. Section 2.5). It is therefore of interest to investigate the dependence of the growth rate on the magnetic field, and in particular to explore the weak field regime.

Figure 3.1 shows the maximum growth rate (in k-space) as a function of wave pitch angle for various magnetic fields, and for typical beam and plasma parameters. The beam parameters used here were $F_0 = 10^{19}$ cm^{-2} s^{-1}, E_0 = 20keV, δ =4 and α_o =5°. The contribution of thermal damping is taken into account, with T=10^7K and n=10^{10}cm^{-3}. For definiteness, the column depth was taken to be 2x10^{19}cm^{-2} in Figure 3.1a and 4x10^{19}cm^{-2} in Figure 3.1b, although it should be emphasized that the following remarks are valid throughout the unstable region of the corona. The growth rate along the field is independent of the field strength, since only the Cerenkov resonance (s=0) can make a nonzero contribution. For $\omega_H < \omega_p$ the growth rate falls monotonically with pitch angle, the angular range of the instability in wave vector space having a minimum value when

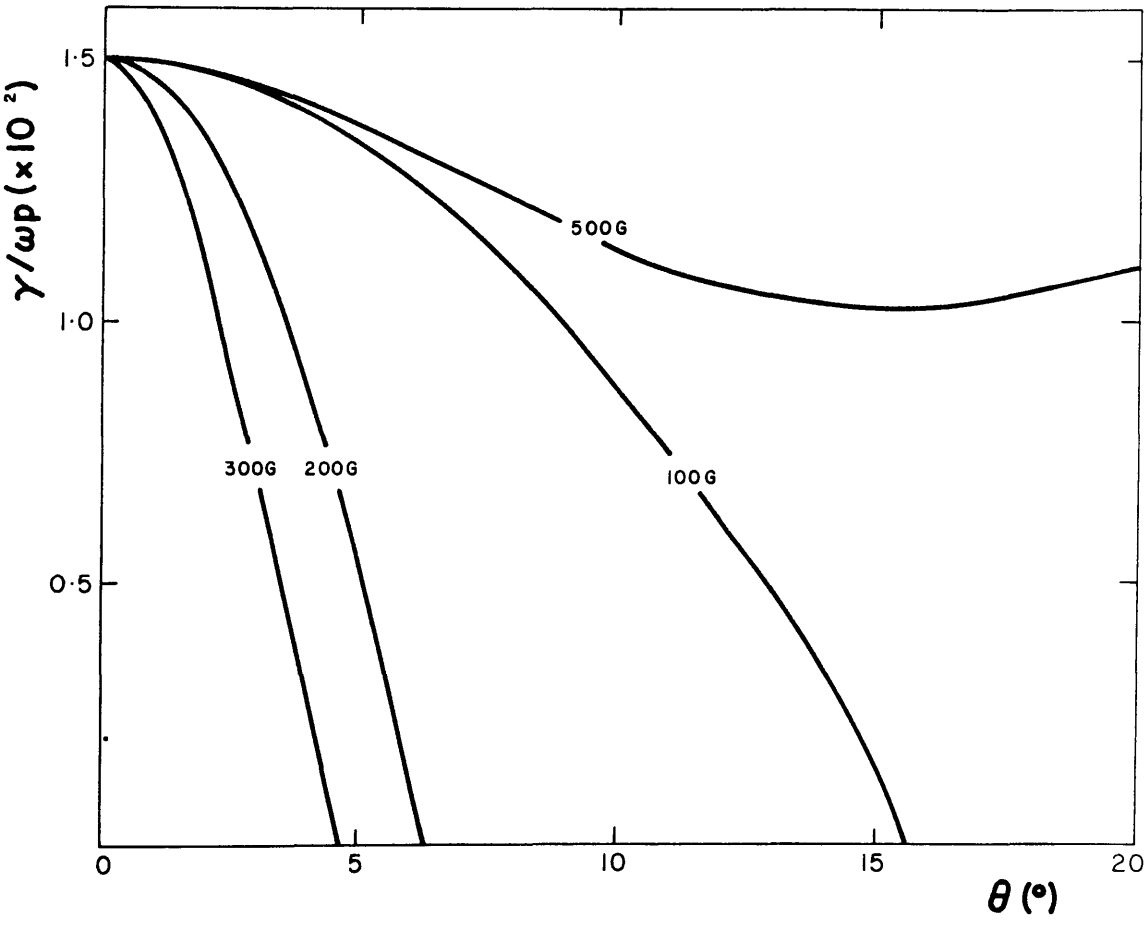

Figure 3.1(a) Growth rate of electron plasma waves (in units of the plasma frequency) as a function of wave pitch angle, for various magnetic fields in the range (100-500)G , at a column depth of 2×10^{19} cm^{-2}. The beam and plasma parameters are given in the text.

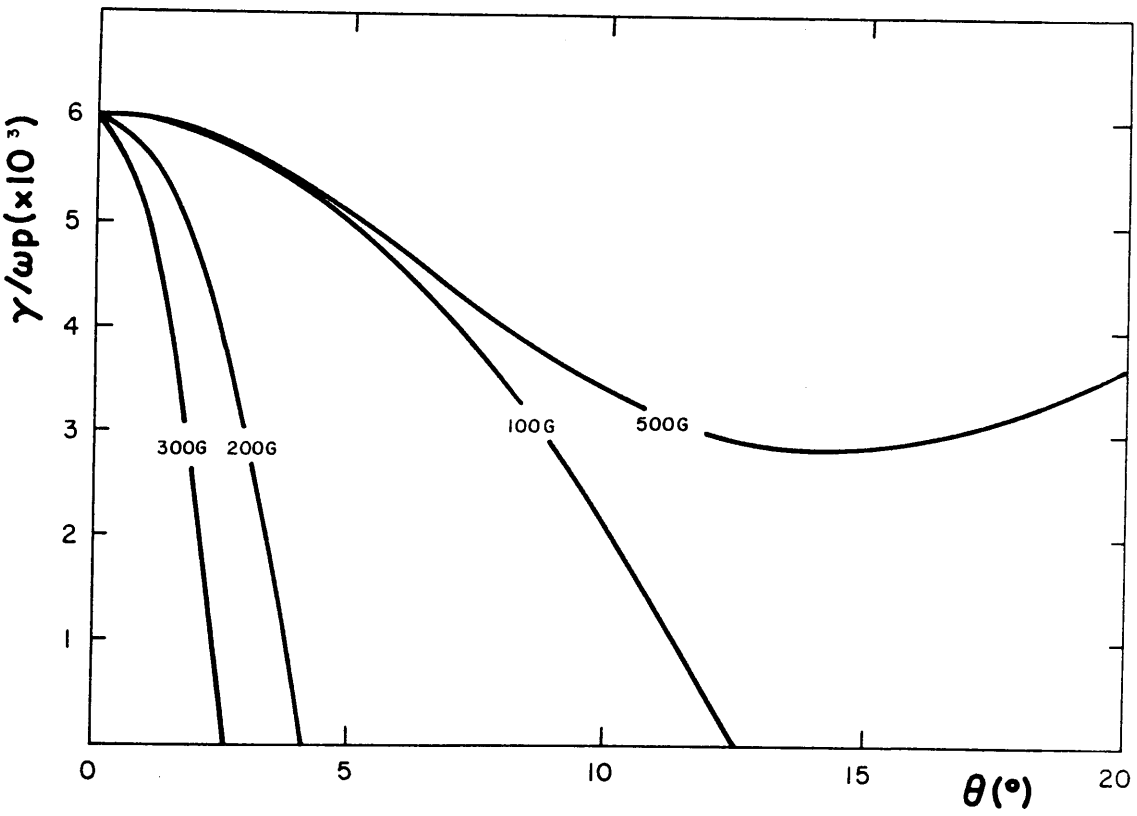

Figure 3.1(b) As Figure 3.1(a) except at a column depth of 4×10^{19} cm^{-2}.

$\omega_H \simeq \omega_p$. This may be attributed to the normal Doppler resonance s=+1, which corresponds to a resonant velocity $v \lesssim v_e$. Waves propagating at a finite angle to the field are consequently heavily damped by the thermal electrons. When α_o is increased the growth rate actually falls off more rapidly with pitch angle. Both the maximum growth rate and the angular range of the instability rise rapidly at the onset of instability, but then fall with increasing column depth, since the electron beam is isotropized as it propagates down the corona. When $\omega_H >> \omega_p$, the growth rate is almost isotropic and is non-monotonic. The curves corresponding to B=500G reach a local maximum at $\theta \simeq 30$, and thereafter fall monotonically. In this regime, only the Cerenkov resonance makes an appreciable contribution to the growth rate, since the distribution function is negligible at the velocities corresponding to all the other resonances.

The above calculation neglects the effect of quasi-linear interactions on the electron distribution when $\gamma > 0$. This will, however, tend to reduce both the growth rate and the angular range of the instability, and it may be concluded that, whenever $\omega_H < \omega_p$, the Langmuir waves produced by an electron beam are always highly collimated (unless some additional nonlinear process is involved, such as induced scattering on ions).

3.3 Stability Boundary in Parameter Space

Figure 3.1 implies that a sufficient condition for instability in the limit $\omega_H < \omega_p$ is that $\gamma>0$ when $\theta=0$. Even in the case $\omega_H > \omega_p$, it appears that the maximum growth rate occurs along the field direction, at least for a wide range of

parameters. From (3.8) it can be seen that the growth rate along the field is

$$\gamma_{NT} = \frac{8\pi^3 e^2 \omega}{mk^2} \int_{\omega/k}^{\infty} dv \left[\frac{\omega}{k} \frac{\partial f}{\partial v} + (1 - \mu^2) \frac{\partial f}{\partial \mu} \right]_{\mu = \frac{\omega}{kv}} \qquad (3.17)$$

where $\omega = (\omega_p^2 + 3k^2 v_e^2)^{\frac{1}{2}}$. The nonthermal contribution to γ must be evaluated numerically as before, while (3.7) indicates that the thermal contribution is given by

$$\gamma_T = -\omega^2 \frac{(2\pi)^{3/2} e^2}{mk^3 v_e^3} n \exp\left(-\frac{\omega^2}{2k^2 v_e^2}\right) \qquad (3.18)$$

i.e. the classic Landau damping result (Landau 1946).

The stability of our electron beam depends on six parameters - the plasma temperature T and density n, the beam flux F_0, the beam energy E_0, the injection angle α_o and the spectral index δ. For the sake of definiteness we concentrate on the three parameters which appear to be most critical for stability - n, α_o and F_0. Figure 3.2 shows the stability boundary in (n, α_o) space for two different values of F_0 when, as before, $T=10^7$K, E_0=20keV and δ=4. The total length of corona from the point of injection was taken to be 3×10^9cm in every case. Beyond a certain density ($n \gtrsim 3\times10^{10}$cm^{-3}) the maximum unstable value of α_o increases with n. The reason for this is that instability arises because of a positive slope in f(v) at $v \simeq v_c$: when the column depth is sufficiently large, $v_c >> v_e$ so that thermal damping is small and instability is more likely to occur. The main conclusion to be drawn from these results is that the stability of the electron distribution depends crucially on the

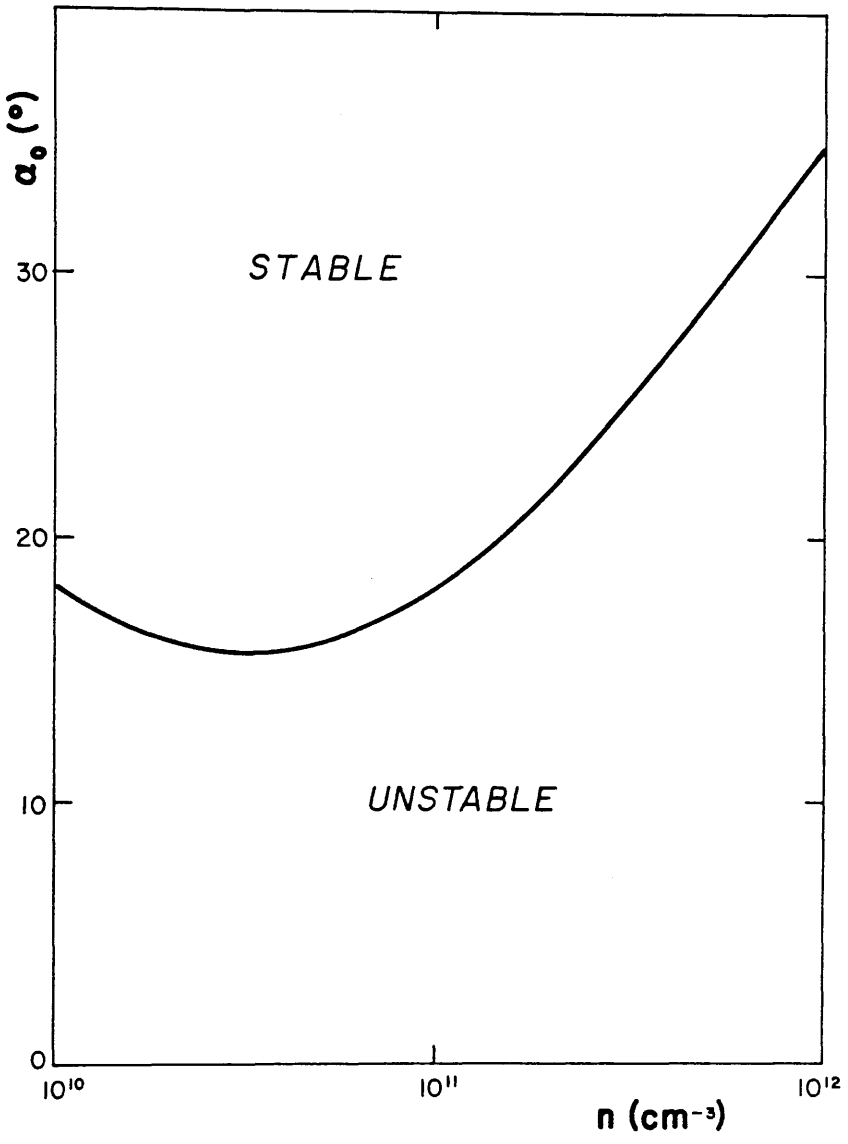

Figure 3.2(a) Stability boundary in (n,α_o) space with a total injected flux of 10^{19} electrons cm^{-2} s^{-1}.

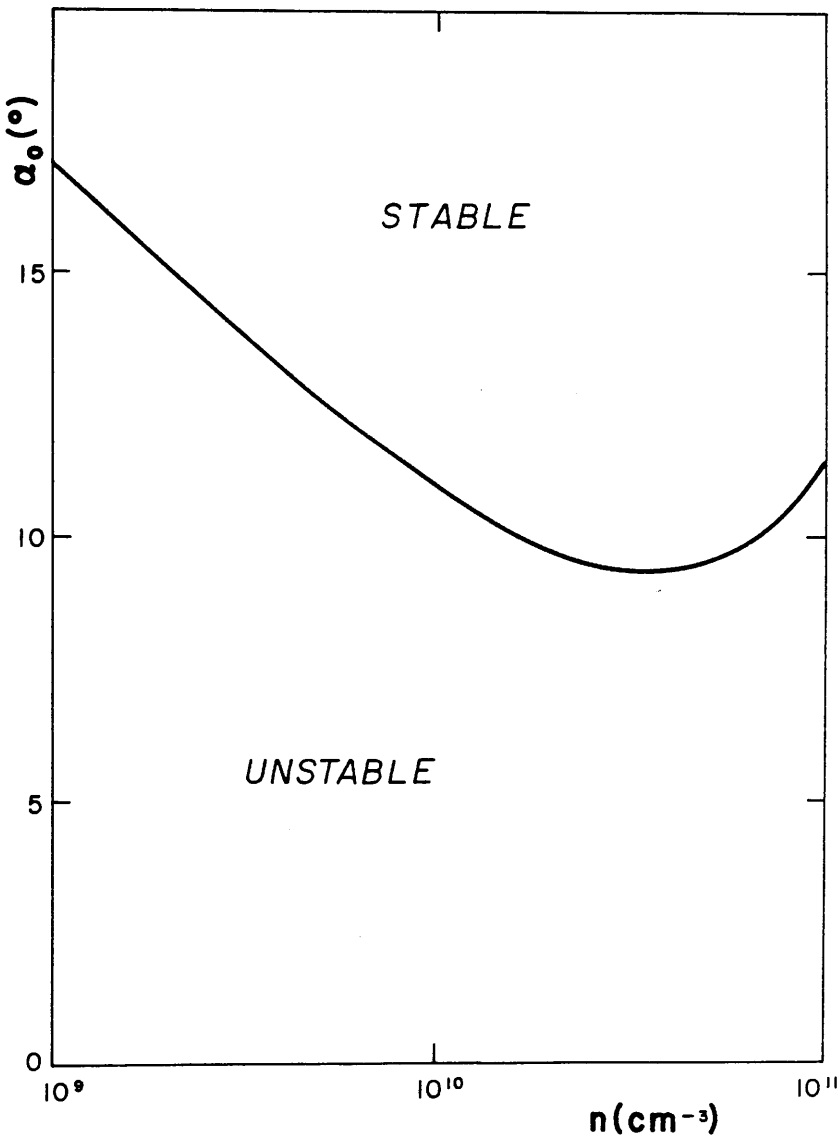

Figure 3.2(b) Stability boundary in (n, α_0) space with a total injected flux of 10^{18} electrons cm^{-2} s^{-1}.

value of α_o . We require that $\alpha_o \lesssim 20^o$ for significant wave generation to occur, unless the coronal density is extremely high.

3.4 Discussion

The results described above emphasize the fact that electron beam stability is an essentially three-dimensional problem. The apparently widely held assumption, that in practice a sufficient condition for Langmuir instability is the formation of a positive slope in $f(\underline{v})$ along the streaming direction in velocity space, is incorrect. Whether electron distributions in the solar corona are in fact sufficiently collimated at injection to be Langmuir unstable is not clear. Leach and Petrosian (1983) and Leach et al. (1985) have shown that hard X-ray polarization and height structure observations are consistent with electron beams injected with a narrow pitch angle profile ($\alpha_o \gtrsim 5^o$). The existing data is, however, ambiguous, and it would be very useful to obtain, for example, more detailed height structure observations, such as those planned for the payload of MAX'91 (Dennis et al.1986). From the theoretical point of view, it is not easy to see how a highly collimated electron beam could be produced (cf. comments in Section 2.3). Our ignorance of the nature of the acceleration process is, however, such that high degrees of collimation cannot be ruled out. A conclusive indicator of the presence of unstable electron beams would be second harmonic plasma radiation, some evidence for which does indeed exist (see Section 2.5).

There are specific models of hard X-ray emission in which

definite statements can be made regarding the stability of the electron distribution. In the trap-plus-precipitation model, described in Chapter 2, electrons initially confined in a coronal magnetic bottle are pitch angle scattered into the loss cone and escape, thus forming a 'beam' (Melrose and Brown 1976; MacKinnon 1987). But if the electron distribution inside the trap is isotropic, the escaping component will also be isotropic out to $\alpha = 90^{\circ}$ (Leach and Petrosian 1981) and, contrary to Emslie and Smith (1984), will therefore be stable. The observation of second harmonic plasma emission simultaneously with hard X-ray emission would therefore rule out such a model. In general, a downward-propagating electron beam will encounter a converging magnetic field which will tend to broaden the pitch angle distribution of electrons, thus making instability less likely to occur. Unfortunately, however, the analytic solution of the Fokker-Planck equation obtained by Leach and Petrosian cannot be generalized to allow for a magnetic field gradient, even in the perturbative limit of a slowly converging field.

In the dissipative thermal model proposed, inter alia, by Vlahos and Papadopoulos (1979) the primary energy release leads to impulsive heating of the upper part of a coronal loop, the hot electrons being confined between regions of ion-acoustic turbulence. Electrons with $v_{\parallel} \gtrsim 3v_e$ escape to produce thick-target hard X-ray emission at the footpoints of the loop. Emslie and Vlahos (1980) parametrised the beam distribution injected into the lower part of the loop by

$$f(v_{\parallel},v_{\perp}) \sim e^{-v_{\perp}^2/2v_e'^2} v_{\parallel}^{-\delta} \qquad (3.19)$$

where $v_e' \simeq 3v_e$ is the thermal speed in the upper part of the loop ($T \simeq 10^8$K). In the small pitch angle limit ($v_\perp \simeq v\alpha$, $v_\parallel \simeq v$), the boundary condition given by (3.19) again allows us to solve the Fokker-Planck equation using the method of Leach and Petrosian. The result is identical to (3.9) except that α_o is now velocity dependent:

$$\alpha_o^2 = \frac{2v_e'^2}{(v^4 + v_c^4)^{\frac{1}{2}}} \simeq \frac{18v_e^2}{(v^4 + v_c^4)^{\frac{1}{2}}} \qquad (3.20)$$

Now, with the beam and plasma parameters assumed in Section 3.2, a positive slope first appears in the combined distribution at $v \simeq v_c \simeq 5v_e$, which implies that $\alpha_o \sim 1$. Although our numerical results are not strictly valid in this case (because of the velocity dependence of α_o), it does appear from this argument that the injected distribution given by (3.19) is unlikely to satisfy the criteria for Langmuir instability. As with the trap model, one would therefore be inclined to reject the thermal model if a large flux of plasma microwave radiation were to be observed.

In conclusion, the requirements for an electron beam in the flaring solar corona to become Langmuir unstable are more stringent than appears to be generally realized. If thick-target hard X-ray emission is produced as the result of electron precipitation from either a coronal trap or a confined thermally-emitting region, Langmuir wave generation and hence plasma radiation are unlikely to occur.

CHAPTER 4

THE QUASI-LINEAR RELAXATION OF THICK TARGET ELECTRON BEAMS - ANALYTICAL MODEL

4.1 Introduction

Having discussed the conditions required for the Langmuir instability of an electron beam in the corona, we now consider the non-collisional evolution of such a beam and the associated growth of Langmuir waves. The quasi-linear equations, describing the coupled evolution of particles and waves, are in general very much more complicated than the Fokker-Planck equation describing the collisional degradation of a dilute beam. Even if one reduces the number of velocity dimensions to 2 (by assuming symmetry about the magnetic field), the equations are completely intractable analytically and in practice can only be solved numerically under rather restrictive conditions. For example, Hoyng et al. (1979) truncated their Legendre series expansion of the pitch angle distributions of the particles and waves at $\ell \geq 2$, and thereby effectively decomposed each distribution into 2 one dimensional streams. Such a model is only appropriate when the electrons and Langmuir waves are close to isotropy, and would be expected to break down in the case of a highly anisotropic beam. Hoyng et al. neglected the magnetic field, which may play an important role in the quasi-linear dynamics of electron beams in the low corona, depending on the value of ω_H / ω_p (cf. Figure 3.1). Moghaddam-Taaheri et al. (1985) included the magnetic field, but were only able to construct a tractable set of equations by assuming $\omega_H >> \omega_p$.

In order to progress both analytically and numerically (without incurring very large computing costs), it is necessary to construct a one dimensional model of the beam-plasma system. Such a model has been developed by Grognard (1985) to describe the propagation of a collisionless electron beam through an unmagnetized plasma. Like Grognard, we will impose the condition that electrons and Langmuir waves propagate along a given direction (in our case the magnetic field direction) with no pitch angle scattering. In general, such an assumption is of course unphysical since electrons are scattered by both Coulomb collisions and quasi-linear interactions. We have shown, in Chapter 3, that an electron beam which is sufficiently collimated at injection will become Langmuir unstable as Coulomb collisions deplete the low velocity part of the distribution. If instability occurs at all, it first appears at a point in space where the electron distribution is still highly anisotropic. In such cases, one would expect the one dimensional model to be a reasonably accurate representation of the system, especially if $\omega_H \lesssim \omega_p$ so that the Langmuir instability has a narrow angular range.

In Section 4.2 we derive the equations of our one dimensional model from the general three dimensional equations for a magnetized plasma, including both quasi-linear and Coulomb interaction terms. Asymptotic analytical solutions are discussed in Section 4.3. In Section 4.4 we use an approximate method of incorporating quasi-linear relaxation into the collisional treatment of thick target beam evolution, in order to ascertain the effect of Langmuir wave generation on the form of the

electron distribution. The significance of the results obtained, and the limitations of the analytical approach, are discussed in Section 4.5.

4.2 The One Dimensional Quasi-Linear Equations

The evolution equations for the electrons and Langmuir waves may be written in the form

$$\frac{df}{dt} = \left(\frac{\partial f}{\partial t}\right)_w + \left(\frac{\partial f}{\partial t}\right)_c \qquad (4.1)$$

$$\frac{dP}{dt} = \left(\frac{\partial P}{\partial t}\right)_w + \left(\frac{\partial P}{\partial t}\right)_c \qquad (4.2)$$

where $f(\underline{x},\underline{v},t)$, as before, is the electron distribution and $P(\underline{x},\underline{k},t)$ is the Langmuir wave spectrum. 'w' and 'c' denote quasi-linear and Coulomb interactions respectively. P is normalized such that

$$\int P(\underline{x},\underline{k},t)\,\frac{d^3\underline{k}}{(2\pi)^3} = W_p\,(\underline{x},t) \qquad (4.3)$$

where W_p is the energy density in Langmuir waves. The normalization of f is given by (3.2). In general, d/dt denotes the total (i.e. advective) time derivative, which is given in the case of (4.2) by (e.g. Davidson 1972)

$$\frac{d}{dt} = \frac{\partial}{\partial t} + \frac{\partial\omega}{\partial\underline{k}} \cdot \frac{\partial}{\partial\underline{x}} - \frac{\partial\omega}{\partial\underline{x}} \cdot \frac{\partial}{\partial\underline{k}} \qquad (4.4)$$

We shall only be considering waves propagating along the magnetic field, in which case $\omega = (\omega_p^2 + 3k^2v_e^2)^{\frac{1}{2}}$ and therefore

$$\frac{\partial\omega}{\partial\underline{k}} = \frac{3v_e^2}{\omega}\,\underline{k} \simeq \frac{3v_e^2}{\omega_p}\,\underline{k} \qquad (4.5)$$

$$\frac{\partial \omega}{\partial \underline{x}} \simeq \frac{\partial \omega_p}{\partial \underline{x}} = \frac{1}{2}\ \omega_p \frac{\partial\ \ell n\ n}{\partial \underline{x}} \qquad (4.6)$$

In this chapter we will consider, for simplicity, the case of a homogeneous atmosphere, in which n and T are independent of x, and therefore the wave refraction term (4.6) is identically zero. The presence of a density gradient may have important consequences for the level of langmuir waves: specifically, Langmuir waves may be taken out of resonance and subsequently Landau damped. This effect is discussed quantitatively in Chapter 7.

The rates of change of f and P due to quasi-linear interactions may be written in the form (Walters and Harris 1968; Harris 1969)

$$\left(\frac{\partial f}{\partial t}\right)_w = 4\pi^2 e^2 \sum_{s=-\infty}^{+\infty} \int \frac{d^3\underline{k}}{(2\pi)^3} \cdot \frac{1}{k^2} \left(\frac{s\omega_H}{v_\perp} \cdot \frac{\partial}{\partial v_\perp} + k_{\shortparallel} \frac{\partial}{\partial v_{\shortparallel}}\right)$$

$$\times J_s^2 \left(\frac{k_\perp v_\perp}{\omega_H}\right) \delta\ (\omega - s\omega_H - k_{\shortparallel} v_{\shortparallel})$$

$$\times \left[P(\underline{k})\left(\frac{s\omega_H}{v_\perp} \cdot \frac{\partial}{\partial v_\perp} + k_{\shortparallel} \frac{\partial}{\partial v_{\shortparallel}}\right) f(\underline{v}) + m\omega f(\underline{v})\right] \qquad (4.7)$$

$$\left(\frac{\partial P}{\partial t}\right)_w = \alpha + \gamma P \qquad (4.8)$$

where

$$\alpha = \frac{4\pi^2 e^2 \omega^2}{k^2} \sum_{s=-\infty}^{+\infty} \int d^3\underline{v}\ J_s^2 \left(\frac{k_\perp v_\perp}{\omega_H}\right) \delta\ (\omega - s\omega_H - k_{\shortparallel} v_{\shortparallel}) f(\underline{v}) \qquad (4.9)$$

$$\gamma = \frac{4\pi^2 e^2 \omega}{mk^2} \sum_{s=-\infty}^{+\infty} \int d^3\underline{v}\ J_s^2 \left(\frac{k_\perp v_\perp}{\omega_H}\right) \delta\ (\omega - s\omega_H - k_{\shortparallel} v_{\shortparallel})$$

$$\times \left[\frac{s\omega_H}{v_\perp} \frac{\partial f}{\partial v_\perp} + k_{\shortparallel} \frac{\partial f}{\partial v_{\shortparallel}}\right] \qquad (4.10)$$

We have assumed plane-parallel geometry in coordinate space, with the magnetic field normal to the plane of stratification, so that there are no guiding centre drift terms. The parameters of our problem are such that instability occurs at comparitively low electron energies ($E \lesssim 100$keV), and therefore the nonrelativistic equations are valid. Langmuir waves only exist with wave vectors $k \lesssim k_D = 1/\lambda_D$. (4.8) therefore only applies for wave vectors in that range, and the volume of integration in (4.7) is the interior of the sphere of radius k_D. α and γ describe the spontaneous and stimulated emission of Langmuir waves respectively. Note that (4.10) is simply an alternative form of (3.1). In (4.7)-(4.10) we will assume $\omega = \omega_p$, which is only strictly valid for $\omega_p >> \omega_H$ and $(k\lambda_D)^2 << 1$ (cf. (3.3)-3.5)).

The Fokker-Planck equation describing the effects of Coulomb interactions on the electron distribution may be written in the form

$$\left(\frac{\partial f}{\partial t}\right)_c = \frac{\partial}{\partial \underline{v}} \cdot \left(\underline{A} + \underline{\underline{D}} \cdot \frac{\partial f}{\partial \underline{v}}\right) \qquad (4.11)$$

Summing over electron and proton species one obtains, in the limit of a highly dilute suprathermal electron beam (Montgomery and Tidman 1964, Section 7.4),

$$\underline{A} = \frac{2 K n}{m^2} \cdot \frac{\hat{\underline{v}}}{v^2} \qquad (4.12)$$

$$\underline{\underline{D}} = \frac{Kn}{m^2} \left[2 \left(\underline{\underline{I}} - \hat{\underline{v}}\,\hat{\underline{v}}\right) \frac{1}{v} - \left(\underline{\underline{I}} - 3\,\hat{\underline{v}}\,\hat{\underline{v}}\right) \frac{v_e^2}{v^3} \right] \qquad (4.13)$$

where $\underline{\underline{I}}$ is the unit tensor and $K = 2\pi e^4 \ell n \Lambda$. Only the dominant terms (i.e. those terms factored by $\ell n \Lambda$) have been retained. A circumflex is used to denote a unit vector. In the case of an

azimuthally symmetric f, (4.11) reduces to the Fokker-Planck equation used by Leach and Petrosian (1981) in the cold target limit $v>>v_e$. We impose the condition that there is no pitch angle scattering resulting from Coulomb collisions by setting all the friction and diffusion coefficients equal to zero except for $A_{\parallel}$ and $D_{\parallel\parallel}$.

To complete the system of equations, we must also consider the collisional damping of Langmuir waves: this was neglected by Hoyng et al. (1979). It will be shown in this chapter and in Chapter 5 that collisional damping is fundamentally important, because it limits the growth of Langmuir waves at the onset of instability. Assuming the electron distribution to be predominantly thermal (i.e. assuming the beam to be sufficiently dilute) we can write

$$\left(\frac{\partial P}{\partial t}\right)_c = - \gamma_c P \qquad (4.14)$$

where the collisional damping rate γ_c is given by (Ginzburg 1961)

$$\gamma_c = \frac{2}{3} \left(\frac{8\pi}{m}\right)^{\frac{1}{2}} \frac{n}{(k_B T)^{3/2}} e^4 \ell n \Lambda_o \qquad (4.15)$$

where

$$\Lambda_o = \left(\frac{m}{\hbar^2 e^2}\right)^{\frac{1}{2}} \frac{k_B T}{n^{\frac{1}{2}}} \qquad (4.16)$$

For coronal values of T and n, $\ell n \Lambda_o$ lies in the range 17-20.

Following Grognard (1985) we now impose the condition that

$$f = \delta(v_x)\, \delta(v_y)\, f_{\parallel}(v_{\parallel}) \qquad (4.17)$$

$$P = (2\pi)^2\, \delta(k_x)\, \delta(k_y)\, P_{\parallel}(k_{\parallel}) \qquad (4.18)$$

where the parallel (i.e. magnetic field) direction is normal to the (x,y) plane. It is also convenient to introduce a new variable $W(\omega_p/k_{\parallel})$, differential in the phase velocity $v_\phi = \omega_p/k_{\parallel}$, such that

$$P_{\parallel}(k_{\parallel}) \frac{d k_{\parallel}}{2\pi} = W(v_\phi)\, dv_\phi$$

i.e.

$$P_{\parallel}\left(\frac{\omega_p}{v_\phi}\right) = \frac{2\pi v_\phi^2}{\omega_p} W(v_\phi) \qquad (4.19)$$

W is normalized such that

$$\int_{v_e}^{\infty} W(v_\phi)\, dv_\phi = W_p \qquad (4.20)$$

Integrating (4.1) over v_x and v_y, and (4.2) over k_x and k_y then yields (using (4.7)-(4.15), and omitting the subscripts on f and v)

$$\frac{\partial f}{\partial t} + v\frac{\partial f}{\partial x} = \frac{e^2\omega_p^2}{m} \cdot \frac{\partial}{\partial v}\left(\frac{\ell n\, v/v_e}{v^2} f\right) + \frac{\pi\omega_p}{mn} \cdot \frac{\partial}{\partial v}\left(v\, W \frac{\partial f}{\partial v}\right) + \frac{2\,Kn}{m^2} \cdot \frac{\partial}{\partial v}\left(\frac{f}{v^2} + \frac{v_e^2}{v^3} \cdot \frac{\partial f}{\partial v}\right) \qquad (4.21)$$

$$\frac{\partial \omega}{\partial t} + \frac{3\, v_e^2}{v} \cdot \frac{\partial \omega}{\partial x} = e^2\omega_p^2 \frac{\ell n\, v/v_e}{v} f + \frac{\pi\omega_p}{n} v^2 W \frac{\partial f}{\partial v} - \gamma_c W \qquad (4.22)$$

Neglecting collisional damping, (4.22) implies that wave growth will occur if $\partial f/\partial v > 0$. This is in fact a necessary but insufficient condition for instability. In practice, a sufficient condition is that the beam velocity is large enough for the Penrose criterion to be satisfied (Penrose 1960; Krall and Trivelpiece 1973). In our case, a positive slope appears in f(v) at $v \gtrsim 4v_e$, and under those conditions the distribution is certainly Penrose unstable. In general, there is a force term on

the left hand side of (4.21), which may arise due to the electric field required to drive a reverse current. We will consider the importance of reverse current energy losses in Chapter 5. In the three dimensional case, there is also a force term arising from the convergence of the magnetic field. This results in pitch angle scattering with no energy loss, and therefore cannot be represented in a one dimensional model.

Neglecting collisional wave damping, one can easily show that (4.21) and (4.22) have thermal equilibrium solutions in a homogeneous plasma

$$f(v) = \frac{n}{(2\pi)^{\frac{1}{2}} v_e} e^{-v^2/2v_e^2} \qquad (4.23)$$

$$W(v) = \frac{e^2\omega_p v_e^2 n}{\pi} \cdot \frac{\ell n\, v/v_e}{v^4} \qquad (4.24)$$

4.3 Asymptotic Solutions

The quasi-linear equations for a collisionless plasma have been studied extensively by many authors, and have been used to describe the propagation of electron streams producing type III bursts. Only in a few, highly idealized cases can analytical results be obtained, even in the one dimensional model. The asymptotic state of the electron distribution is generally assumed to be a plateau in velocity space, i.e. $\partial f/\partial v=0$ over some finite range of v. Shapiro (1963) showed that a homogeneous, initially mono-energetic beam eventually loses two thirds of its energy to Langmuir waves. Grognard (1975) obtained self-similar asymptotic solutions of the inhomogeneous

quasi-linear equations, and found that no more than one third of the particle energy could be transferred to waves. The discrepancy between these two results is hardly surprising since the assumption of self-similarity is only valid for certain special kinds of initial and boundary condition. In any event, it appears physically plausible for there to be an approximate equipartition of energy between electrons and Langmuir waves in the asymptotic state, provided Coulomb collisions can be neglected.

If thick target electron beams were to undergo quasi-linear relaxation on a collisionless timescale, a large fraction of the beam energy would therefore be dissipated in the form of Langmuir waves, and the efficiency of the thick target model would be further reduced. Vlahos and Papadopoulos (1979) claim that a beam with a large positive slope will be formed due to the precipitation of fast electrons from a thermally-emitting source region (cf. Sections 2.4 and 3.4). Such a beam would relax to a plateau distribution on a timescale determined by the linear growth rate (e.g. Tsytovich 1970a)

$$\gamma_W \approx \left(\frac{n_b}{n}\right) \left(\frac{v_b}{\Delta v_b}\right)^2 \omega_p \qquad (4.25)$$

where n_b is the beam density, v_b is a typical beam velocity and Δv_b is the spread in v_b. Assuming a typical thick target value of n_b (10^6 - 10^9 cm^{-3}) and $\Delta v_b \sim v_b$, we find that γ_ω is several orders of magnitude greater than the collisional damping rate in the flaring corona, and quasi-linear relaxation would then proceed on a collisionless timescale. Vlahos and Papadopoulos

state that the resulting asymptotic wavelevel is

$$\frac{W_p}{n\, k_B\, T} \approx \frac{1}{15} \left(\frac{n_b}{n}\right) \left(\frac{v_b}{v_e}\right)^4 \qquad (4.26)$$

For sufficiently large v_b, this implies that the energy density of Langmuir waves is greater than the kinetic energy density in the beam ($\sim\frac{1}{2} m n_b v_b^2$). On the other hand, if we assume equipartition of energy between electrons and waves, the appropriate expression for a homogeneous beam is

$$\frac{W_p}{n\, k_B\, T} \approx \left(\frac{n_b}{n}\right) \left(\frac{v_b}{v_e}\right)^2 \qquad (4.27)$$

which is typically rather less than the wavelevel given by (4.26). Whichever expression is correct, it appears certain that the energy density of Langmuir waves produced by the collisionless relaxation of a thick target beam will be a substantial fraction of the thermal energy density. Vlahos and Papadopoulos use this conclusion to argue that the relaxed plasma will be strongly turbulent, and invoke nonlinear stabilization mechanisms which allow the beam to reach the chromosphere without giving up most of its energy to plasma waves (see also Rowland and Vlahos 1984; Vlahos and Rowland 1985).

We will discuss strong turbulence quantitatively in Chapter 6. In the meantime, we consider the question of whether or not wave generation is indeed likely to occur on a collisionless timescale. In the specific context of the dissipative thermal model, Smith and Brown (1980) pointed out that electrons

escaping from the source region are decelerated by a thermoelectric field resulting from the turbulent conduction fronts which confine the bulk of the distribution. Consequently, the streaming electrons have an initially monotonic decreasing velocity distribution and can only become Langmuir unstable due to the effect of Coulomb collisions or (perhaps) velocity dispersion. We have already shown in Chapter 3 that collisional losses are unlikely to produce instability in the case of precipitation from a thermal source. Regardless of how a thick target beam is produced, it is reasonable to expect the electron distribution to be rapidly stabilized by quasi-linear interactions in the acceleration region (cf. Moghaddam-Taaheri et al. 1985).

If an electron beam is injected with a stable velocity distribution, the situation is fundamentally different from the one envisaged by Vlahos and Papadopoulos. Neglecting velocity dispersion, instability can only occur on a collisional timescale, and collisions therefore determine the subsequent evolution of the beam. The collisionless quasi-linear equations are consequently invalid, and the expression for the saturation wavelevel given by (4.27) is incorrect. Our problem is therefore qualitatively different from the type III problem, which involves the propagation of electron streams through a collisionless plasma.

If W(v) is much greater than the thermal level, we can to a first approximation neglect the spontaneous emission term in (4.22). For the same reason, we can neglect the first term on the right hand side of (4.21), and also the diffusive term

provided $v>>v_e$. In a steady state, the equations then reduce to

$$v \frac{\partial f}{\partial x} = \frac{\partial}{\partial v} \left(\frac{\pi \omega_p}{mn} v W \frac{\partial f}{\partial v} + \frac{2 Kn}{m^2} \cdot \frac{f}{v^2}\right) \tag{4.28}$$

$$\frac{3 v_e^2}{v} \cdot \frac{\partial W}{\partial x} = \frac{\pi \omega_p}{n} v^2 W \frac{\partial f}{\partial v} - \gamma_c W \tag{4.29}$$

If collisions produce $\partial f/\partial v>0$ for some finite range of v, the Langmuir waves will react back on the electron distribution in such a way as to stabilize it. The terms on the right hand sides of (4.28) and (4.29) suggest that a quasi-homogeneous steady state might exist, in which a positive slope in f(v) is continously created by collisions, and continuously flattened by quasi-linear interactions. At the same time, the Langmuir waves are driven by the positive $\partial f/\partial v$, and damped by collisions. Setting $\partial f/\partial x=\partial W/\partial x=0$ in (4.28) and (4.29), we obtain the equilibrium solutions

$$f(v) = f_p - \frac{\gamma_c n}{\pi \omega_p} \cdot \frac{1}{v} \tag{4.30}$$

$$W(v) = \frac{2 Kn}{\gamma_c m} f_p \frac{v}{v_1^2} \left(1 - \left(\frac{v_1}{v}\right)^2\right) \tag{4.31}$$

where f_p and v_1 are constants. The electron distribution is a plateau, modified by a small correction term. Note that

$$\frac{\partial \ell n f}{\partial \ell n v} = \frac{\gamma_c n}{\pi \omega_p} \cdot \frac{1}{vf} \sim \frac{\gamma_c}{\omega_p} \left(\frac{n}{n_b}\right) \tag{4.32}$$

which is typically $\lesssim 10^{-4}$. v_1 can be identified as the velocity at the lower edge of the plateau. Taking the velocity at the upper edge to be v_2, the energy density in Langmuir waves is

given by

$$W_p = \int_{v_1}^{v_2} W(v)\, dv$$

$$W_p = \frac{K n f_p}{\gamma_c m} \left[\left(\frac{v_2}{v_1}\right)^2 - 1 - \ell n \left(\frac{v_2}{v_1}\right) \right] \qquad (4.33)$$

It should be emphasized that this result is only accurate to at best an order of magnitude, and is an overestimate. We can justify setting the left hand side of (4.29) equal to zero on the grounds that the wave group velocity $v_{gr} = 3v_e^2/v$ is very small compared with the beam velocity v. The solution (4.30), which is determined only by (4.29), is therefore an accurate representation of the electron distribution. On the other hand, the neglect of $\partial f/\partial x$ in (4.28) is only justified for electron energies $E \lesssim (KN)^{\frac{1}{2}}$, where N is the column depth traversed by the beam. This is approximately the energy at which a positive slope forms in f(v) due to collisional losses, and therefore (4.31) is not valid throughout the plateau region in velocity space. We would expect the true solution to reach a maximum, and then fall off to zero at the upper edge of the plateau.

Nevertheless, (4.33) can be used to illustrate the qualitative difference between wave generation by a thick target beam and wave generation in a collisionless plasma. Putting $f_p \simeq n_b/v$ and assuming the factor in brackets is of order unity, we obtain

$$\frac{W_p}{n k_B T} \approx \left(\frac{n_b}{n}\right) \left(\frac{v_e}{v_b}\right) \qquad (4.34)$$

This result was obtained by Zaitsev and Kaplan (1968) using a rather different argument. It differs from (4.27) by a factor $(v_e/v_b)^3$, and in practice we find that instability occurs at $v_b \simeq (4\text{-}10)v_e$. (4.27) therefore overestimates the wavelevel by between 2 and 3 orders of magnitude, which means that only a very small fraction of the beam energy is transferred to Langmuir waves.

Having derived an approximate expression for the asymptotic wavelevel, we can now estimate the rate at which Langmuir waves heat the plasma. The rate of energy deposition is given simply by

$$I_W = \gamma_c W_p$$

$$= \frac{Kn\, f_p}{m} \left[\left(\frac{v_2}{v_1}\right)^2 - 1 - \ell n \left(\frac{v_2}{v_1}\right) \right] \qquad (4.35)$$

We can compare this with the collisional energy deposition rate due to the beam itself, which is given by

$$I_B = \int_o^\infty f_b(v) \left| \left(\frac{dE}{dt}\right)_c \right| dv \qquad (4.36)$$

where f_b is the beam component of the electron distribution and $(dE/dt)_c$ is the mean energy loss rate resulting from Coulomb collisions. For the purposes of the present discussion, it is sufficiently accurate to use the expression for $(dE/dt)_c$ which is applicable to a fast electron in a cold, fully ionized hydrogen plasma (Trubnikov 1965)

$$\left(\frac{dE}{dt}\right)_c = - \frac{Kn\, v}{E} \qquad (4.37)$$

(if we set W=0, this is simply the equation for the

characteristics of (4.28)). If we now crudely approximate the beam distribution by

$$f_b(v) = f_p , \quad v_1 < v < v_2$$
$$= 0 , \quad \text{otherwise} \qquad (4.38)$$

then we obtain from (4.36) the result

$$I_B = \frac{2\,Kn\,f_p}{m} \ln\left(\frac{v_2}{v_1}\right) \qquad (4.39)$$

which, apart from a factor of order unity, is the same as (4.35). Thus, although Langmuir waves contain a negligible fraction of the original beam energy, they heat the plasma at a rate which is comparable to that of the fast electrons. The reason for this is that waves are damped collisionally almost as fast as they are amplified by a positive slope in f(v). We will consider more quantitatively the relative contributions of beam and wave heating in Chapter 5.

4.4 The Evolution of the Electron Distribution With Depth

According to our one dimensional model, Langmuir instability occurs if there is a region of positive slope in the combined electron distribution, which is given by

$$f(x,v) = f_o(v) + f_b(x,v) \qquad (4.40)$$

where f_0 is the (Maxwellian) distribution function of the background plasma, which we assume to be homogeneous and in a steady state. f_0 is given explicitly by (4.23). The assumption of a steady state requires that the electron and ion temperatures are equal, that the corona is in hydrostatic

equilibrium, that heat is conducted away from the source region as rapidly as it is deposited by the beam (either directly, due to Coulomb collisions, or indirectly, via Langmuir wave damping or the ohmic dissipation of reverse currents), and that the beam itself is in a steady state (cf. Section 3.1). If the beam energy losses are predominantly collisional, the temperature is a very insensitive function of the injected electron flux ($T \sim F_0^{2/7}$), and changes by no more than a factor of 2 along the length of a coronal loop (cf. Emslie 1985; Emslie and Smith 1984). The fall in temperature towards the chromosphere may destabilize the beam (due to the beam component of f dominating over the background component at lower velocities), but this will be partly offset by the increasing density.

We use a mean collisional energy loss rate treatment to determine $f_b(x,v)$. Neglecting pitch angle scattering, the steady state electron flux distribution G(E) is given by the continuity equation

$$G(E)\, dE = F(E_1) dE_1 \qquad (4.41)$$

where F is the injected flux spectrum and E_1 is the initial energy of an electron of energy E. We take the same form for F as in Chapter 3, viz (3.14). The beam velocity distribution is given in terms of G by

$$v\, f_b(v)\, dv = G(E) dE \qquad (4.42)$$

i.e.

$$f_b(v) = m\, G(E)$$

$$f_b(v) = m\, F(E_1) \frac{dE_1}{dE} \qquad (4.43)$$

To determine E_1 from a prescribed E we require the mean collisional energy loss rate. In our case, $f_b(v)$ is not negligible close to the thermal speed, and it is therefore necessary to evaluate $(dE/dt)_c$ for a warm (finite temperature) plasma. For an electron beam in a fully ionized hydrogen plasma the appropriate expression is (see Appendix A)

$$\left(\frac{dE}{dt}\right)_c = - \frac{Kn\ v}{E} \left(\Phi(y) - 2y\ \Phi'(y)\right) \qquad (4.44)$$

where Φ is the error function and $y=(E/k_BT)^{\frac{1}{2}}$. For $E>>k_BT$, (4.44) gives the cold target result (4.37), while for $E \to k_BT$, $(dE/dt)_c \to 0$. It should be emphasized that (4.44) cannot describe the relaxation towards thermal equilibrium of a nonthermal distribution, since it does not include the effect of diffusion in velocity space (cf. (4.21)). It is, however, germane to the present discussion since the effect of a finite temperature is to inhibit the formation of a positive slope in f(v) close to the thermal speed.

Changing the independent variable in (4.44) from t to column depth N, and writing $\psi(y) = \Phi(y) - 2y\Phi'(y)$, we obtain

$$\frac{dE}{dN} = - \frac{K}{E}\ \psi(y) \qquad (4.45)$$

i.e.

$$KN = \int_E^{E_1} \frac{E\ dE}{\psi[(E/k_BT)^{\frac{1}{2}}]} \qquad (4.46)$$

The problem is then to determine E_1, given E and N. In the cold target limit, (4.46) yields

$$E_1 = (E^2 + 2\ KN)^{\frac{1}{2}} \qquad (4.47)$$

In general, (4.46) may be solved for E_1 by iteration, using (4.47) as an initial estimate. To evaluate $f_b(v)$ we also require dE_1/dE, which can be obtained by differentiating (4.46):

$$\frac{dE_1}{dE} = \frac{E}{E_1} \cdot \frac{\psi(y_1)}{\psi(y)} \qquad (4.48)$$

where $y_1 = (E_1/k_B T)^{\frac{1}{2}}$.

Using the above equations we can evaluate f(v), neglecting quasi-linear interactions, for any prescribed set of parameters (F_0, E_0, δ, T and n). Quasi-linear relaxation can be incorporated in the scheme in the following way: if a region of positive slope is produced in the combined distribution, it is immediately replaced by a plateau which conserves particle number. The three parameters which define the plateau are, as indicated schematically in Figure 4.1, v_1, v_2 and f_p. These are (uniquely) defined by the condition that

$$\int_{v_1}^{v_2} (f(v) - f_p)\, dv = 0 \qquad (4.49)$$

although there are three unknown parameters, only one of these is independent: they may all be readily determined numerically. The smoothed-out distribution function minus the background Maxwellian can then be taken to be the new $F(E_1)$, and the distribution function G(E) corresponding to the subsequent N-step can be evaluated as before. E_1-E is thus the energy lost by an electron in a single N-step. If E_1 lies in the plateau region then

$$m\, F(E_1) = f_p - f_o\, [\, v(E_1)\,] \qquad (4.50)$$

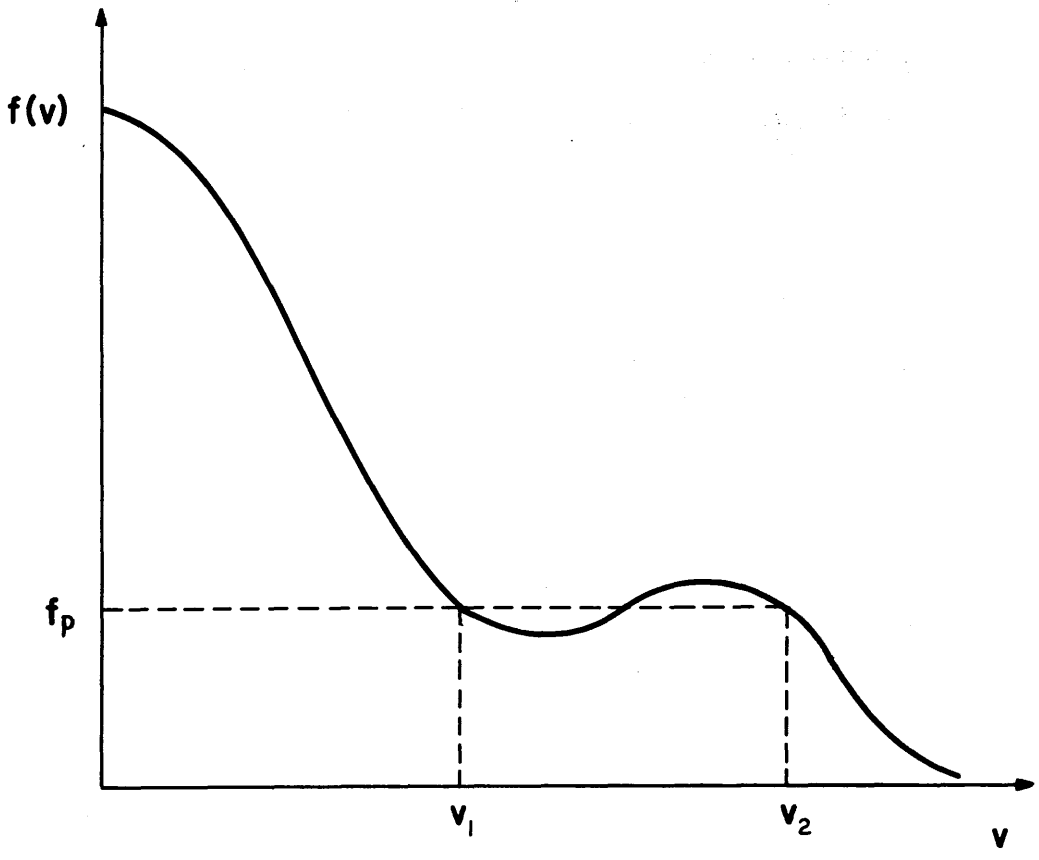

Figure 4.1 The form of the combined electron distribution giving rise to Langmuir instability. The plateau of the relaxed distribution is defined by the three parameters v_1, v_2 and f_p.

Otherwise, $F(E_1)$ is given by the function $G(E)$ as evaluated in the previous step.

We can justify setting $f(v)=f_p$ in the above procedure on the grounds that the velocity-dependent correction term in (4.30) is negligibly small. Once instability has occured, the distribution evolves collisionally in a single N-step to a state in which $\partial f/\partial v$ is sufficiently large for quasi-linear interactions to dominate, and we can then replace $f(v)$ with the appropriate asymptotic solution. It should be noted that the collisional evolution described by (4.43) does not conserve particle number: beam electrons are lost from the system, because the (constant density) background plasma acts as a particle sink. The rate at which electrons are lost in this way depends on the form of $f(v)$: the relaxation process transfers electrons to lower velocities, where they decay collisionally more rapidly. In order to realistically model the evolution of the beam it is therefore necessary to ensure that the step size δN is much less than a collisional stopping distance: only then could the results be expected to converge. This was found to be indeed the case. In fact convergence occured for $\delta N \lesssim 0.01E^2/2K$. In practice it is also necessary to use a small step size in energy space, so that v_1 and v_2 can be accurately determined.

In Figures 4.2 and 4.3 we present numerical computations of $f(v)$ at two different points in the atmosphere, for two different values of the plasma density. The basic feature to note is that the quasi-linear plateau falls below the collisionally-evolved distribution as the beam propagates down the corona. This may be compared with an analytical result

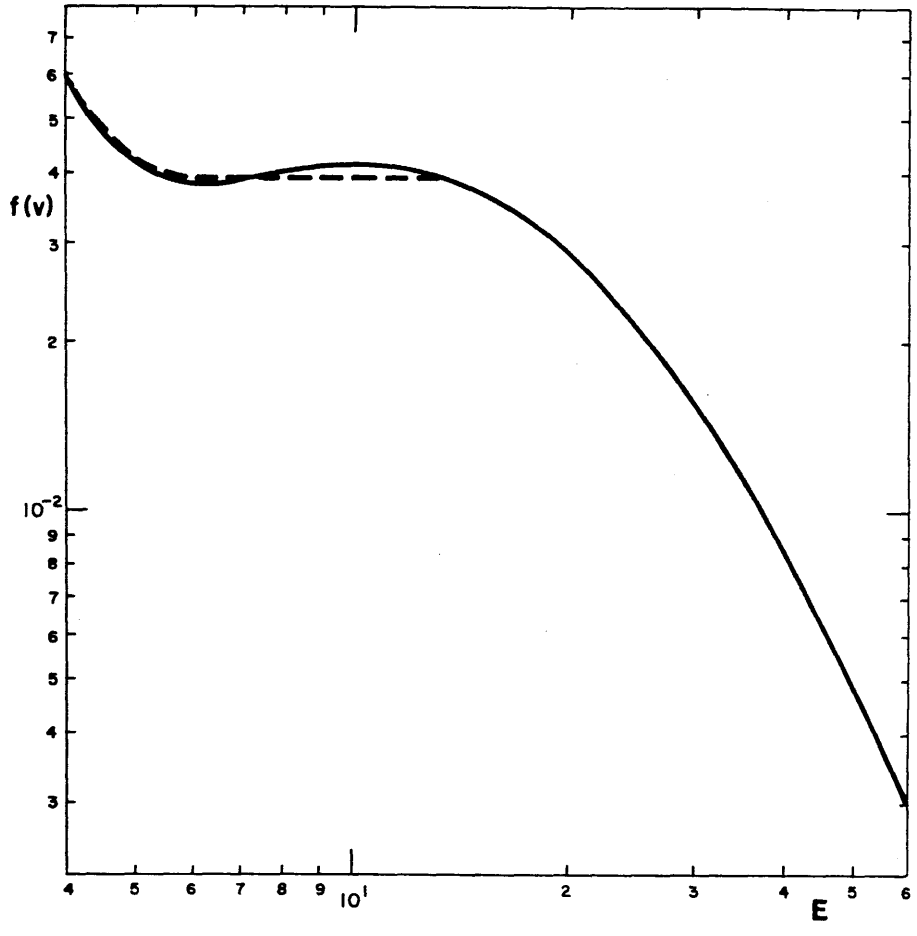

Figure 4.2(a) Electron distribution function for the model parameters $F_0 = 10^{19}$ electrons cm^{-2} s^{-1}, $E_0 = 20keV$, $\delta = 4$, $T = 10^7 K$ and $n = 10^{10}$ cm^{-3}, at a column depth of $3x10^{19}$ cm^{-2}. The dotted line shows the plateau formed by quasi-linear relaxation (f is measured in electrons cm^{-3} $(cms^{-1})^{-1}$ and E is measured in keV).

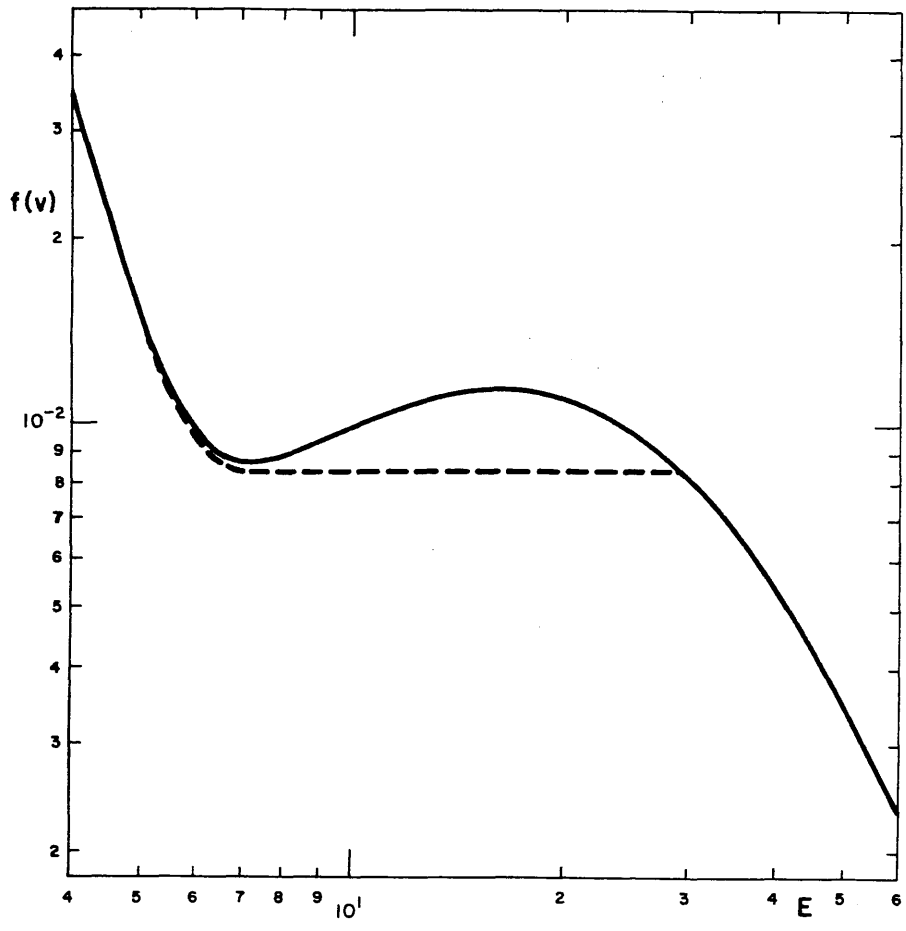

Figure 4.2(b) As Figure 4.2(a) except at a column depth of 10^{20} cm^{-2}.

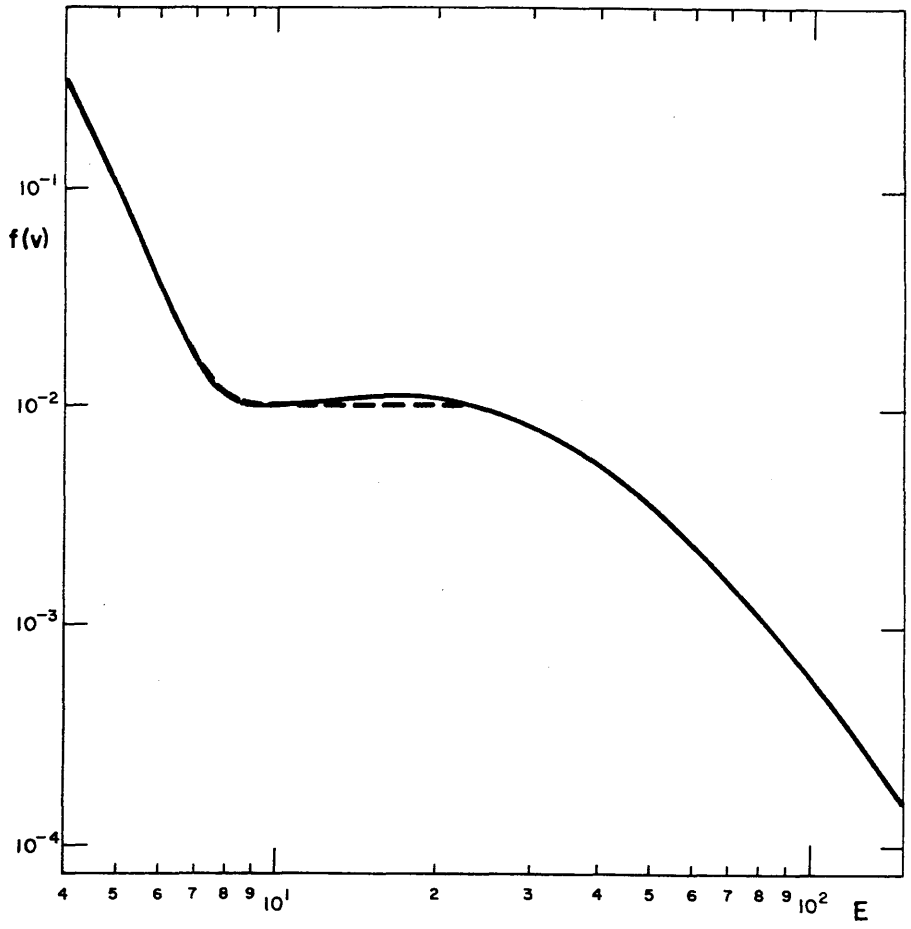

Figure 4.3(a) As Figure 4.2(a) except with n = 10^{11} cm^{-3}, at a column depth of 10^{20} cm^{-2}.

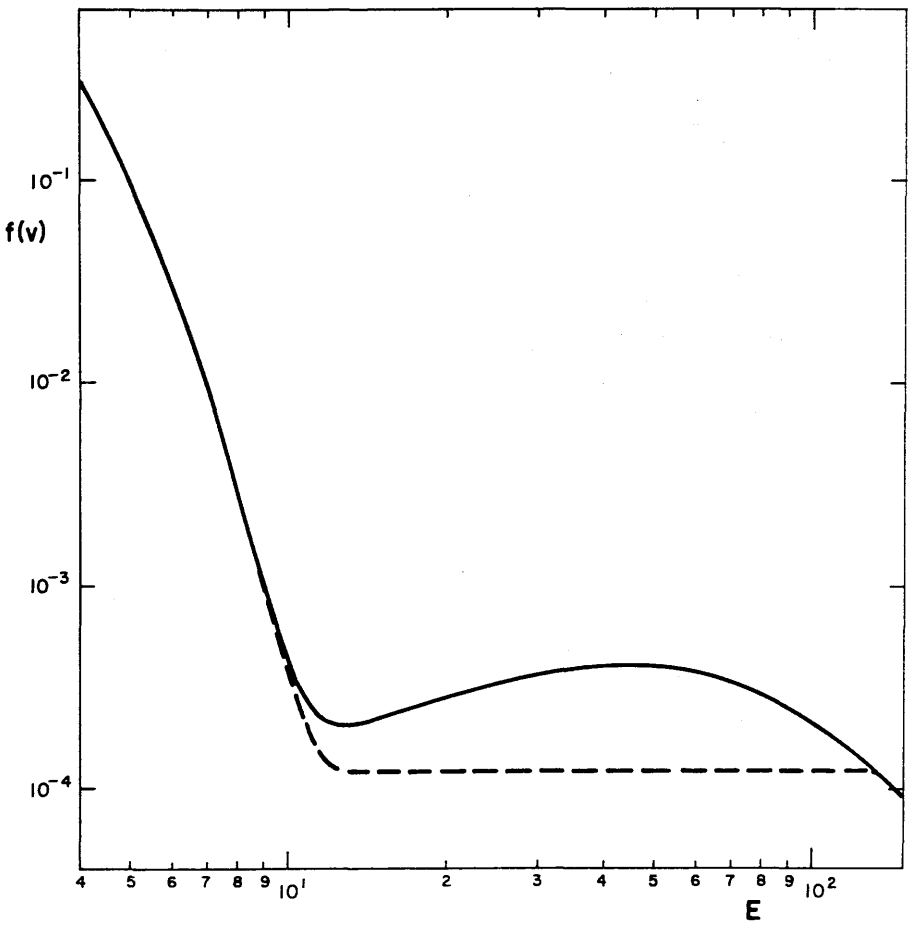

Figure 4.3(b) As Figure 4.3(a) except at a column depth of 10^{21} cm^{-2}.

obtained by Hamilton and Petrosian (1986). These authors showed that (4.28) and (4.29) can be integrated over coordinate space to give

$$\tilde{W}(v) = \frac{2Kn}{m\ \gamma_c\ v} \left[\tilde{f}_{coll}(v) - \tilde{f}(v) \right] \qquad (4.51)$$

where a tilda denotes a quantity integrated from 0 to ∞ with respect to x, and $f_{coll}(v)$ is the collisionally evolved solution. The requirement that $\tilde{W}(v) \geq 0$ implies that $\tilde{f}_{coll}(v) \geq \tilde{f}(v)$, for all v. It is not clear whether or not the distributions shown in Figures 4.2 and 4.3 will satisfy this condition, since it does not necessarily preclude $f_{coll}(v) < f(v)$ at a single point in space. There does appear to be a discrepancy between (4.51) and Figures 4.2a and 4.3a, in which $f_{coll}(v) < f(v)$ at the lower edge of the plateau: this may be due to the fact that (4.51) is only valid for a cold plasma, and does not take into account the complicated interaction of the beam with the Maxwellian background.

(4.51) can be used to obtain an upper limit on the spatially integrated wavelevel, since $f_{coll}(v)$ can be easily evaluated from the injected flux distribution. Assuming $f_{coll}(v) >> f(v)$, Hamilton and Petrosian show that

$$\frac{\tilde{W}_p}{n\ k_B\ T} \approx \frac{E_o^2}{Kn} \left(\frac{n_o}{n}\right) \left(\frac{v_e}{v_o}\right) \qquad (4.52)$$

where $\frac{1}{2} mv_0^2 = E_0$ and n_0 is the beam density at the point of injection. If we assume that the length of the electron stream is of the order of the collisional stopping distance E_0^2/Kn, then

(4.52) implies a spatially averaged wavelevel comparable to that given by (4.34). It should be noted, however, that (4.51) is only valid if the beam is stopped collisionally in the corona, which will not be the case if the coronal column depth is less than about 10^{20} cm^{-2}. Furthermore, Figures 4.2 and 4.3 show that f(v) is not negligible compared with $f_{coll}(v)$, and therefore the assumption $\tilde{f}_{coll}(v) >> \tilde{f}(v)$ is probably not justified. Finally, it should be emphasized that the beam density n_b at the point where wave generation starts is considerably less than the injected beam density n_0, due to collisions having removed most of the low energy electrons.

4.5 Discussion

In this chapter we have constructed a one dimensional model of beam relaxation in a collision-dominated plasma, and progressed as far as possible using analytical techniques. The crude treatment of quasi-linear relaxation described in the previous section was essentially heuristic, based on physically plausible assumptions: we do not attempt to justify it rigorously. The results appear to make reasonable sense, and can be used via (4.33) to obtain an order of magnitude estimate of the thick target wavelevel. In order to determine W_p accurately, however, and to incorporate quasi-linear dynamics into the evolution of the electron beam in a rigorous way, a purely numerical approach is essential. One might criticize, for example, the assumption in Section 4.4 that quasi-linear interactions are neglected entirely when f(v) is stable, and 'switched on' abruptly at the onset of instability. Indeed,

Hoyng et al. (1979) claim that quasi-linear interactions maintain the stability of the distribution, and that consequently the wave energy density is never more than a few times the thermal level. This conclusion is based, however, on the assumption that the electron and wave distributions are never highly anisotropic, and may therefore be incorrect in the case of a highly collimated beam. Nevertheless it is desirable to solve numerically the full one dimensional quasi-linear equations (4.21) and (4.22), in order to assess the possible stabilizing influence of Langmuir waves on the particle distribution. The numerical approach also enables us to incorporate additional processes, such as reverse current energy losses, which cannot be handled analytically.

The relaxed electron distributions shown in Figures 4.2 and 4.3 are sufficiently different from the collisionally evolved distributions to suggest that they might produce substantially different bremsstrahlung spectra, particularly if the quasi-linear plateau extends into the tens of keV range. We will assess quantitatively the effect of quasi-linear interactions on the hard X-ray spectrum in Chapter 5. We will also consider the effect of relaxation on the rate of collisional energy deposition.

CHAPTER 5

THE QUASI-LINEAR RELAXATION OF THICK TARGET ELECTRON BEAMS - NUMERICAL MODEL

5.1 Introduction

In this chapter we present numerical computations of the steady state thick target electron distribution and the Langmuir wavelevel, based on a finite difference computer code which is described in detail in Appendix B. In Section 5.4 we compute the energy deposition rate and hard X-ray signature of a relaxed beam, and compare the results with those obtained from a purely collisional model of beam relaxation. In Section 5.5 we discuss the extent to which the wavelevel is reduced by reverse current Ohmic losses. Using idealized assumptions, we estimate in Section 5.6 the flux of 2nd harmonic radiation produced by a Langmuir unstable thick target beam, and consider whether reverse drift microwave bursts might be consistent with a plasma radiation interpretation.

5.2 The Equations

It is convenient to introduce the dimensionless variables

$$\tilde{dx} = \frac{1}{2\, n\, \lambda_D^4}\, dx \qquad (5.1)$$

$$\tilde{v} = v/v_e \qquad (5.2)$$

$$\tilde{f} = 2\pi\, v_e\, \lambda_D^3\, f \qquad (5.3)$$

$$\tilde{W} = \frac{2\pi \lambda_D^3}{k_B T} v_e W \qquad (5.4)$$

In a steady state, (4.21) and (4.22) then become (omitting tildas from dimensionless quantities)

$$v \frac{\partial f}{\partial x} = \frac{\partial}{\partial v}\left[\frac{\ell n\, v}{2\pi v^2} f + vW\frac{\partial f}{\partial v} + \frac{\ell n\, \Lambda}{2\pi v^2}\left(f + \frac{1}{v}\frac{\partial f}{\partial v}\right)\right] \qquad (5.5)$$

$$\frac{3}{v}\frac{\partial W}{\partial x} = \frac{\ell n\, v}{2\pi v} f + v^2 W \frac{\partial f}{\partial v} - \left(\frac{2}{9\pi}\right)^{\frac{1}{2}} \frac{\ell n\, \Lambda_o}{2\pi} W \qquad (5.6)$$

where we have assumed that the background plasma is homogeneous, i.e. T and n are independent of x. It is essential to include the collisional diffusion term in (5.5), so that f retains a Maxwellian form as $v \to 0$ (as far as the numerical code is concerned, the distribution function is a single entity: there is no distinction between the beam and the background). A simplification of (5.6) can be made if we assume that the waves are in local equilibrium with the electrons unless instability develops. That is, we set $\partial W/\partial x = 0$ in (5.6) unless $\partial f/\partial v > 0$. W is then given by

$$W(x,v) = \frac{\frac{\ell n\, v}{2\pi v} f(x,v)}{\left(\frac{2}{9\pi}\right)^{\frac{1}{2}} \frac{\ell n \Lambda_o}{2\pi} - v^2 \frac{\partial f}{\partial v}(x,v)} \qquad (5.7)$$

If the electron distribution is stable, spontaneous emission of waves almost exactly balances Landau damping (collisional damping is negligible unless there is instability), and the wave distribution evolves only slowly with depth. Mathematically, it

is consistent to neglect $\partial W/\partial x$ in (5.6) while retaining $\partial f/\partial x$ in (5.5) for the reason given in Section 4.3, namely that the Langmuir waves propagate at a group velocity which is typically an order of magnitude less than the beam velocity. At the onset of instability, the wave distribution grows to a significant level in a relatively short distance and the full equation (5.6) must therefore be solved (cf. Hoyng et al. 1979). In order to acheive numerical stability, it is in fact convenient to retain $\partial W/\partial x$ in (5.6) whenever the electron distribution is unstable.

To obtain a numerical solution we require boundary conditions in coordinate space and velocity space. The electron distribution at x=0 is given by

$$f(o,v) = f_o(v) + f_b(o,v) \qquad (5.8)$$

where, as before, f_0 is the distribution function of the background plasma. In our dimensionless units,

$$f_o(v) = (2\pi)^{\frac{1}{2}} \; n \; \lambda_D^3 \; e^{-v^2/2} \qquad (5.9)$$

$f_b(0,v)$ is determined by the injected electron flux spectrum, which, once again, we assume to be a modified power law of the type invoked in Chapters 3 and 4. Using the relation

$$v\, f_b(o,v)\, dv = F(E)dE$$

we obtain, in dimensionless units,

$$f_b(o,v) = 2\pi \; v_e \; \lambda_D^3 \; m(\delta-1) \; F_o \; E_o^{\delta-1} \; (E_o + E)^{-\delta} \qquad (5.10)$$

The boundary condition at x=0 for the wave spectrum is

determined by the requirement that the waves are initially in equilibrium (since the particle distribution is stable). W(0,v) is therefore given by (5.7) with x=0.

The boundary conditions in velocity space are determined by the physical requirements that f(x,v) should tend to a Maxwellian distribution as $v \to 0$ (so that the beam merges with the background) and that $f \to 0$ as $v \to \infty$ (so that f is normalizable, has finite energy, and so on). In practice it is convenient to take v=1 (in units of v_e) as the lower boundary in velocity space, and an upper boundary $v=v_{max}$ such that the electron distribution is stable for all x at that velocity. The value of v_{max} is arbitrary provided it is sufficiently large that the distribution function is not significantly affected by collisional losses at that velocity (the results presented ih this chapter were obtained with $v_{max} \gtrsim 20$). The simplest boundary condition to take at v=1 is that f is constant. This is acceptable provided the plasma density is constant and the beam density is much less than the plasma density (cf. comments in Section 4.4). If we further prescribe $f(x,v_{max})=0$ it follows from (5.7) that $W(x,1)=W(x,v_{max})=0$. This provides a complete set of boundary conditions which enable a numerical solution to be determined. A description of the numerical method is given in Appendix B.

In order to obtain a quantitative comparison with the standard collisional thick target model, it is also necessary to solve the one dimensional Fokker-Planck equation

$$v \frac{\partial f}{\partial x} = \frac{\ell n \Lambda}{2\pi} \cdot \frac{\partial}{\partial v} \left(\frac{f}{v^2} + \frac{1}{v^3} \cdot \frac{\partial f}{\partial v} \right) \qquad (5.11)$$

subject to the same boundary conditions as the full quasi-linear equations. A trivial modification of the numerical method is required to obtain the solution (see Appendix B).

5.3 The Electron and Langmuir Wave Distributions

The results presented in this section were obtained with the following model parameters: $T = 10^7$K, $n = 10^{10} - 10^{11}$ cm^{-3}, $F_0 = 10^{18} - 10^{19}$ electrons cm^{-2} s^{-1}, $E_0 = 20$keV, $\delta = 4$. The loop length was taken to be 10^{10}cm: this is about a factor of 3 greater than the maximum observed length of a flaring coronal loop, and was chosen to illustrate the effects of quasi-linear relaxation on collisional energy deposition and bremsstrahlung emission under the most extreme conditions.

Figures 5.1a and b show isometric plots of the solution of the Fokker-Planck equation (5.11) with $n = 10^{10}$ cm^{-3} and $n = 10^{11}$ cm^{-3} respectively. In each case, the injected electron flux was taken to be 10^{19} electrons cm^{-2} s^{-1}. The formation of a positive slope in f(v) as x increases is clearly apparent. The results can be verified analytically in the limit of large v: for v>>1 (the cold target approximation) (5.11) reduces to

$$v \frac{\partial f}{\partial x} = \frac{\ell n \Lambda}{2\pi} \frac{\partial}{\partial v} \left(\frac{f}{v^2}\right) \qquad (5.12)$$

which has general solution

$$f(x,v) = v^2 H \left[\left(v^4 + \frac{2 \ell n \Lambda}{\pi} x\right)^{\frac{1}{4}}\right] \qquad (5.13)$$

where the function H is determined by the injected beam distribution. From (5.10) it follows that

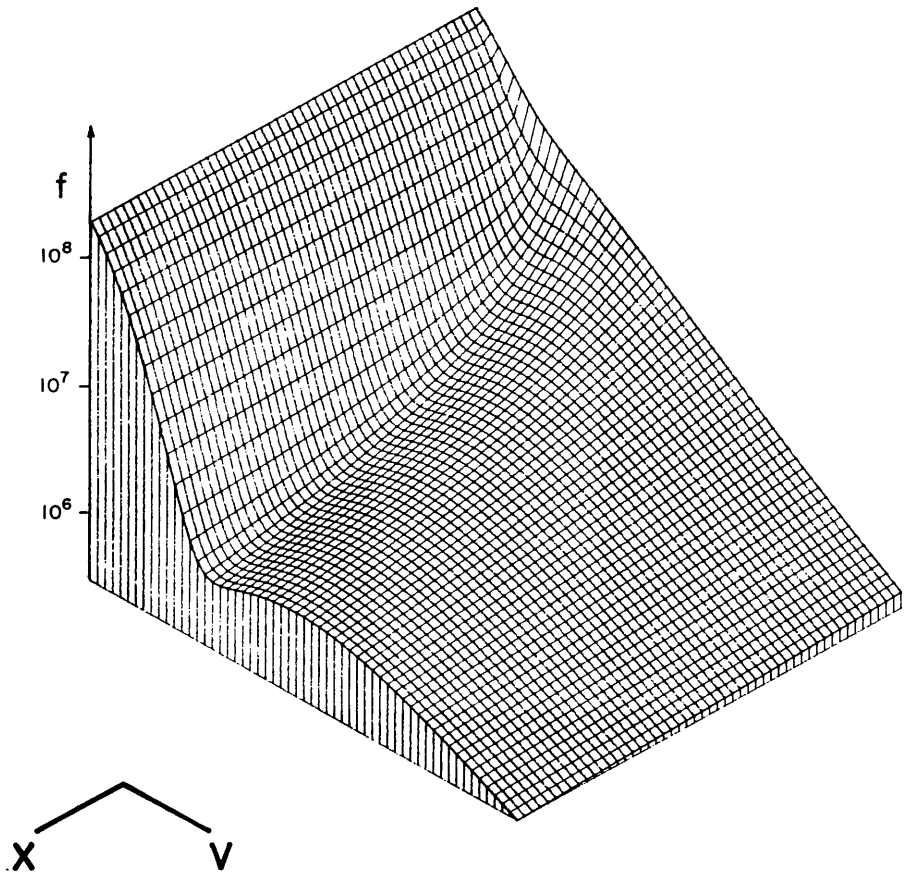

Figure 5.1(a) The solution of the Fokker-Planck equation (5.11) with $n = 10^{10}$ cm^{-3}. In dimensionless units, x runs from 0 up to 220.5 and v runs from 1 up to 12.

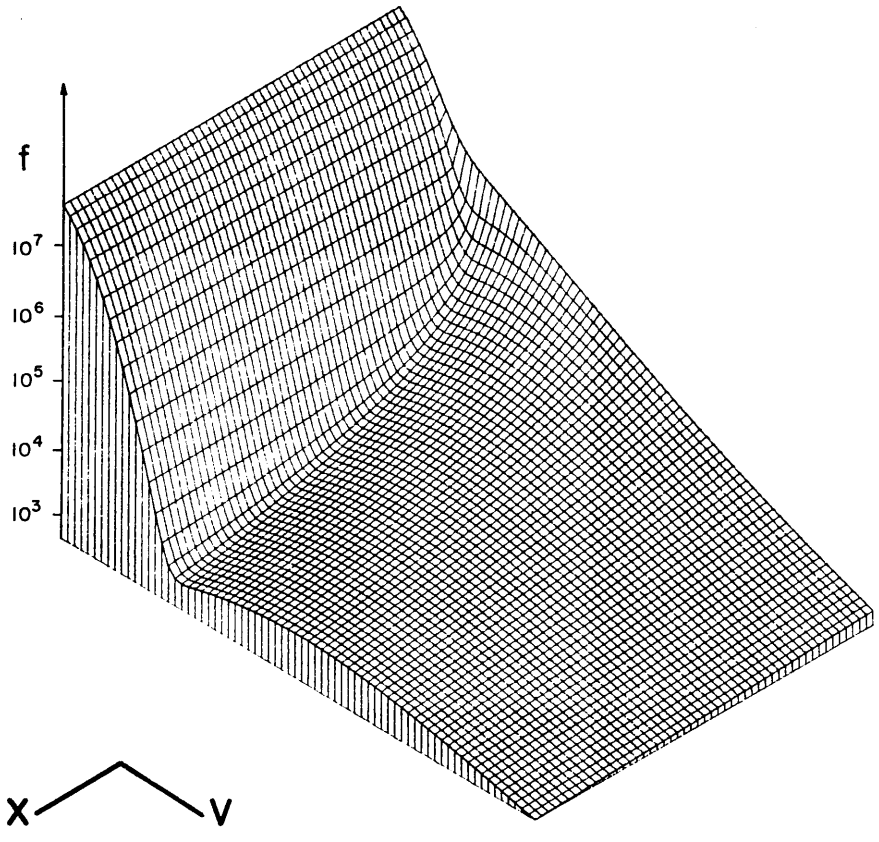

Figure 5.1(b) As Figure 5.1(a) except with $n = 10^{11}$ cm^{-3}. x runs from 0 up to 2205 and v runs from 1 up to 20.

$$f(x,v) = A \frac{v^2}{(v^4 + \frac{2\ell n\, \Lambda}{\pi} x)^{\frac{1}{2}}} \left[v_o^2 + (v^4 + \frac{2\ell n\, \Lambda}{\pi} x)^{\frac{1}{2}} \right]^{-\delta} \quad (5.14)$$

where $A = 2\pi v_e \lambda_D^3 m(\delta-1) F_o E_o^{\delta-1} (2/mv_e^2)^{\delta}$ and $\frac{1}{2} m(v_o v_e)^2 = E_0$. The numerical solutions are found to be in almost exact agreement with (5.14) for large v: the discrepancy is of order $1/v^2$, as implied by the diffusion term in (5.11).

Figures 5.2 and 5.3 show the solutions of the quasi-linear equations (5.5) and (5.6). As we would expect, the regions of positive slope in Figure 5.1 have been replaced with plateaux in Figure 5.2 (cf. (4.32)). As x increases, the plateau height falls and the region in velocity space of unstable wave growth becomes wider. Outside the plateaux, Figures 5.1 and 5.2 are almost identical, showing that quasi-linear interactions have a completely negligible influence on the particle distribution except when instability occurs. Our results are in contrast with those of Hoyng et al. (1979), who found a quite negligible enhancement of the wave energy density above the thermal level (Hoyng et al. assumed model parameters and boundary conditions similar to those used in this chapter). In our case, the wave distribution is amplified by a factor of around 10^8 in Figure 5.3a, and around 10^6 in Figure 5.3b. In the case of a one dimensional beam, we may therefore conclude that wave-particle interactions do <u>not</u> maintain the stability of the particle distribution. The probable reason for the discrepancy between our results and those of Hoyng et al. has been discussed in Chapter 4. Figures 5.1 and 5.2 are in good agreement with Figures 4.2 and 4.3, and thus vindicate the method used to infer

(a) $n = 10^{10}\ cm^{-3}$

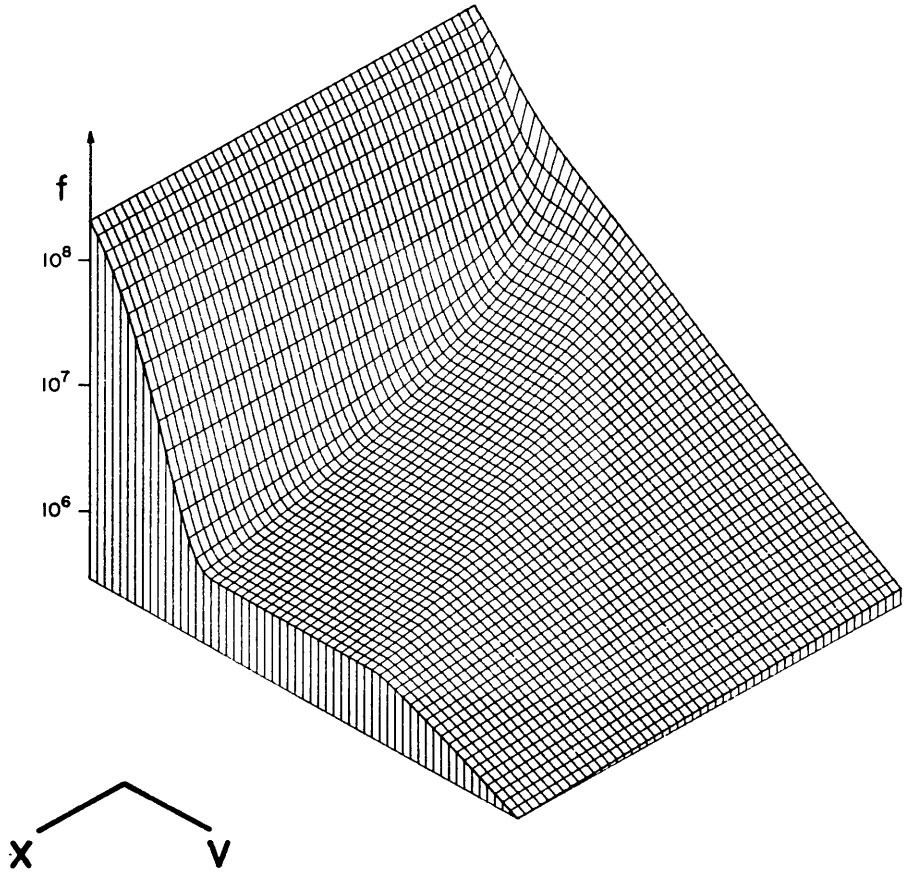

Figure 5.2 Electron distribution functions, allowing for quasi-linear interactions. Except in the regions of the plateaux, the solutions are almost identical to those shown in Figure 5.1.

(b) $n = 10^{11}\ cm^{-3}$

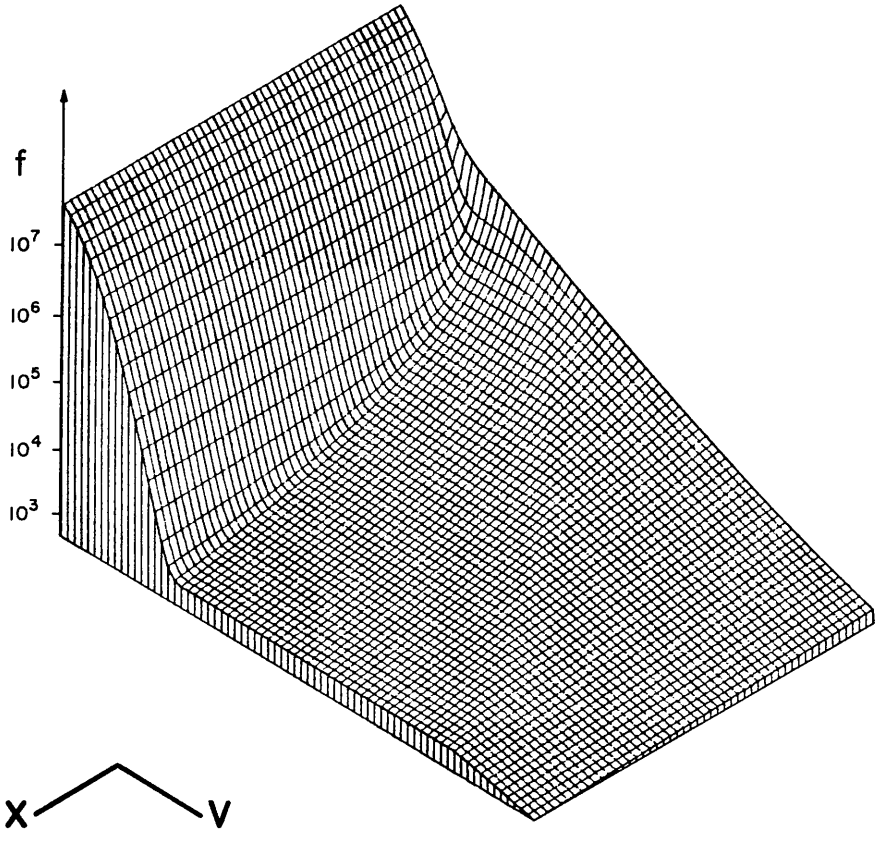

(a) $n = 10^{10}\ cm^{-3}$

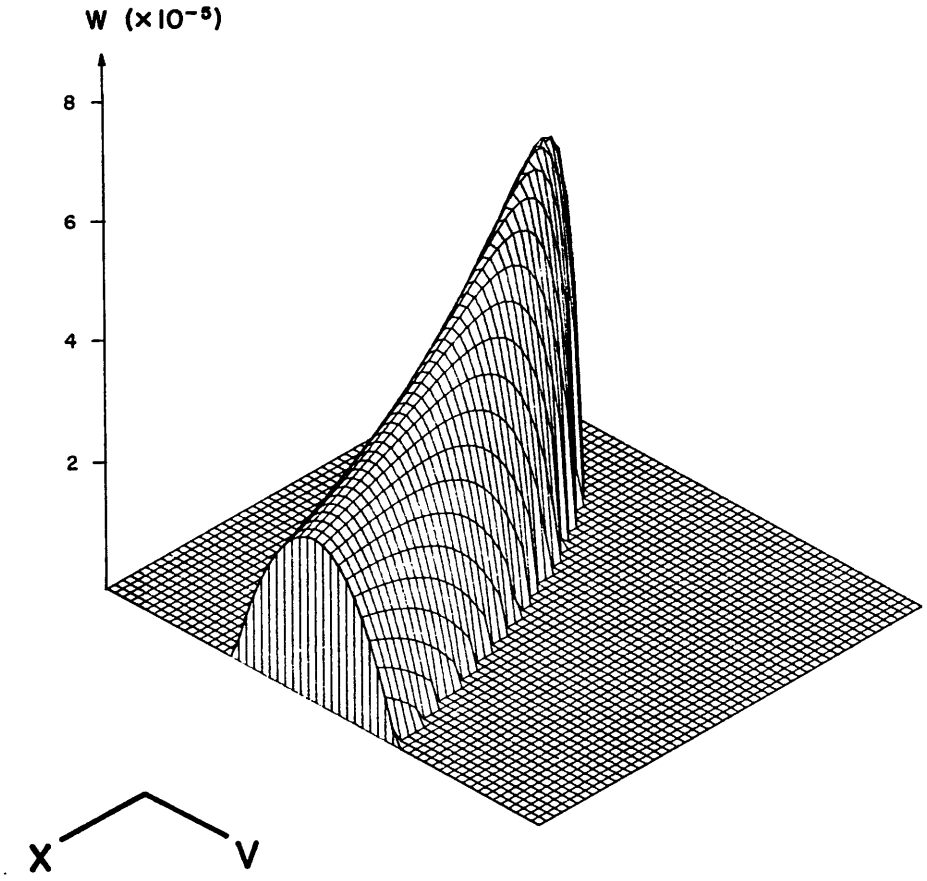

Figure 5.3 The Langmuir wave distributions corresponding to the particle distributions shown in Figure 5.2. The (x,v) grids are identical to those in Figures 5.1 and 5.2.

(b) $n = 10^{11}\ cm^{-3}$

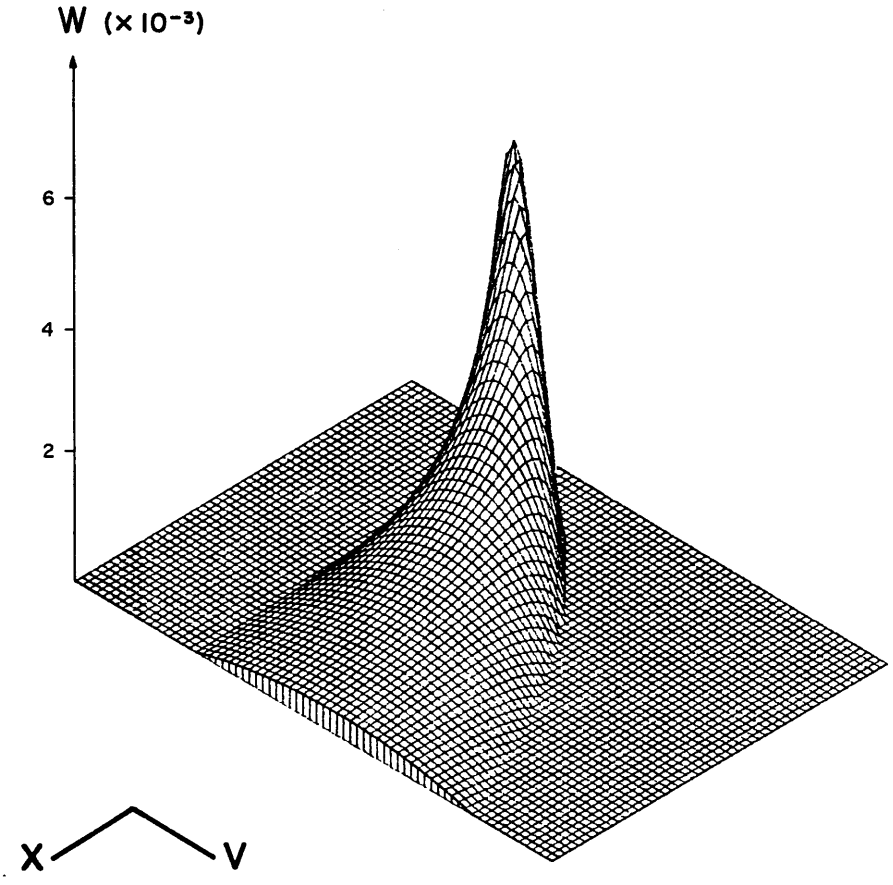

the relaxed state of the particle distribution which was described in Section 4.4.

The normalized wavelevel is given in terms of the dimensionless wave spectrum by

$$\frac{W_p}{n\, k_B\, T} = \frac{1}{2\pi\, n\, \lambda_D^3} \int_1^\infty W(v)dv \qquad (5.15)$$

The integral can be easily evaluated numerically for each space point from the results shown in Figure 5.3. Figures 5.4a and b show W_p/nk_BT as a function of x. In each case, the wavelevel increases very rapidly at the onset of instability to a maximum value, and then falls off much more gradually. Substituting in (4.33) the numerically determined values of f_p, v_1 and v_2, we find that (4.33) overestimates the wavelevel by a factor of between 3 and 10. This rather large discrepancy indicates the necessity of performing a numerical calculation, if the wavelevel is to be determined with acceptable accuracy.

It would be useful to establish a scaling law between the wavelevel and the injected electron flux. Unfortunately, the range of unstable wavenumbers depends on several other parameters, notably the plasma temperature and density, in a nontrivial way, and therfore no simple scaling law exists. It appears, however, that the maximum wavelevel rises faster than linearly as the injected flux is increased. For example, if we prescribe the same parameters as those used to obtain Figure 5.4a except that $F_0 = 10^{18}$ cm^{-2} s^{-1}, we find that $W_p/nk_BT \lesssim 4\times10^{-5}$. Note that a high beam flux implies a high steady state temperature (cf. Section 4.4), which tends to inhibit wave

(a) $n = 10^{10}\ cm^{-3}$

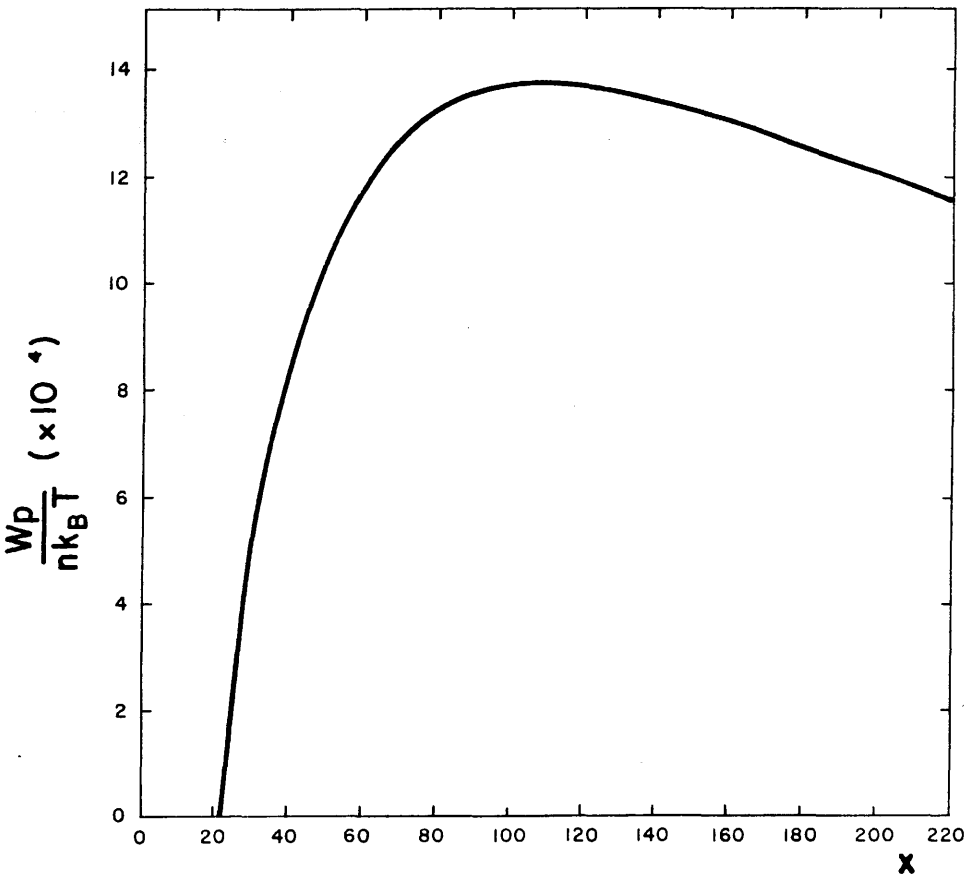

Figure 5.4 Normalized wavelevel as a function of x, obtained by integrating over the wave spectra shown in Figure 5.3. Note how rapidly the wavelevel rises at the onset of instability.

(b) $n = 10^{11}\ cm^{-3}$

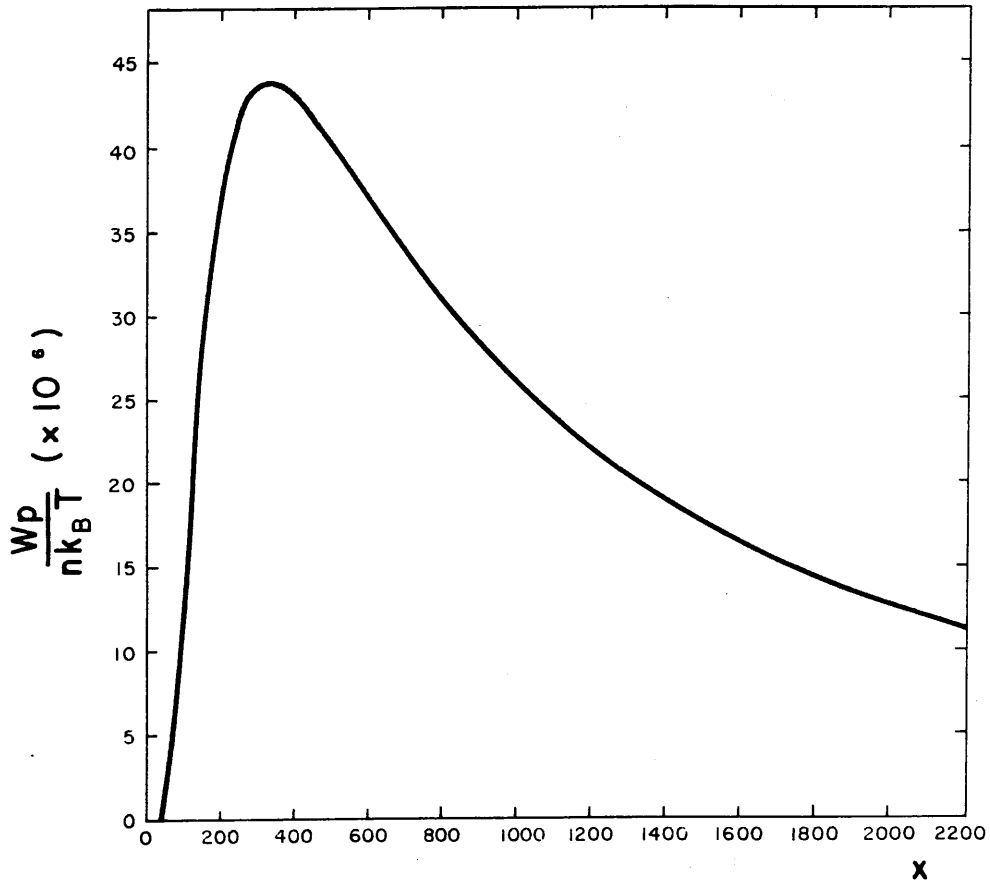
$\frac{W_p}{nk_BT}$ (x 10^6)
45
40
35
30
25
20
15
10
5
0
0
200
400
600
800
1000
1200
1400
1600
1800
2000
2200
X

generation. It appears unlikely that, for any set of realistic and consistent parameters, the wavelevel produced by a steady state beam is much greater than that shown in Figure 5.4a.

5.4 Energy Deposition and Bremsstrahlung Emission

The energy deposited by the beam in the plasma (ergs cm^{-3} s^{-1}) due to collisional losses is given by (4.36). It is appropriate to use the expression (4.44) for the collisional energy loss rate: (4.36) can then be written in the form

$$I_B = \frac{K n}{\pi m \lambda_D^2 v_e^2} \omega_p \int_{y_o}^{\infty} \frac{\psi(y)}{y} f_b(x, \sqrt{2}y) \qquad (5.16)$$

where $y_0 \simeq 1$ is the value of y at which $\psi = 0$ and f_b is the (dimensionless) beam component of f(v). There is clearly a problem in determining f_b, since only the total distribution function is known a priori. Our numerical results show that f(v) relaxes very quickly to a Maxwellian distribution in the vicinity of $v=v_e$, at the same temperature but a higher density than the background plasma at the point of injection. This rapid relaxation may be attributed to the v^{-3} dependence of the collision frequency. By fitting a Maxwellian to the first few solution points ($v \gtrsim v_e$), and extrapolating this fit to the rest of the distribution, the beam component of f(v) can be determined empirically.

Figures 5.5a and b show the total energy deposition rates I_T corresponding to the distribution functions shown in Figure 5.1 (broken line) and Figure 5.2 (solid line), the latter including the contribution of collisional wave damping, $I_W = \gamma_c W_p$ (cf.

(a) $n = 10^{10}$ cm^{-3}

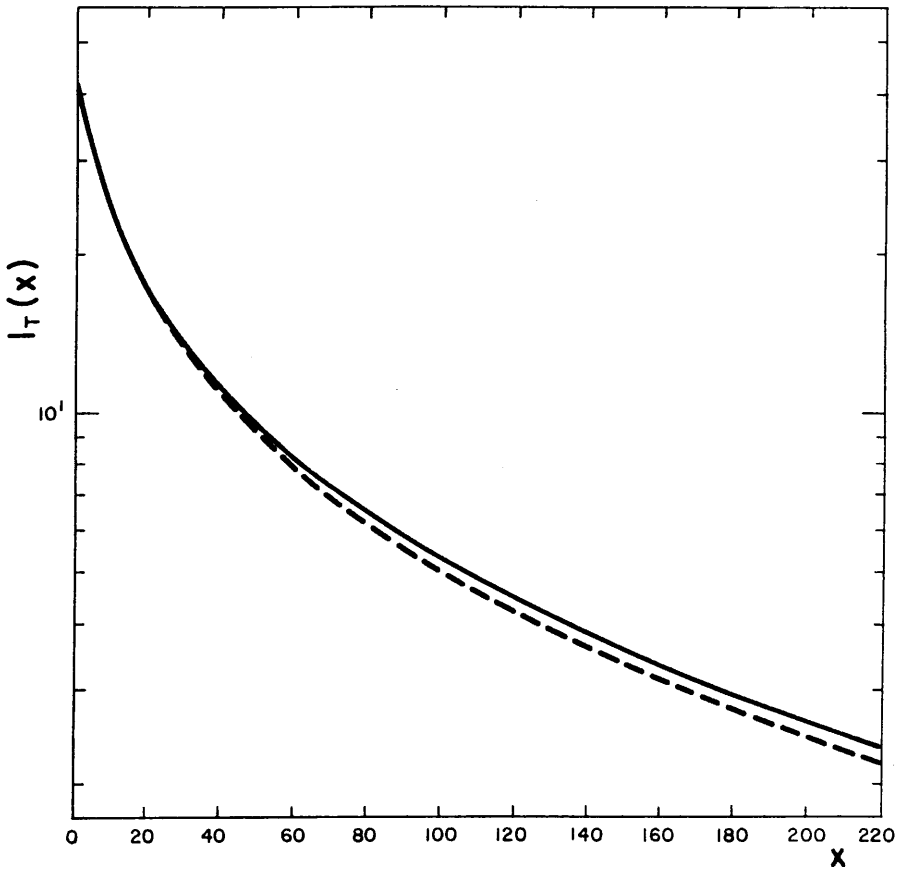

Figure 5.5 Energy deposition rates corresponding to the distribution functions shown in Figure 5.1 (broken lines) and Figure 5.2 (solid lines). The latter include the contribution of collisional wave damping, $\gamma_c W_p$ (I_T is measured in ergs cm^{-3} s^{-1}).

(b) $n = 10^{11}\ cm^{-3}$

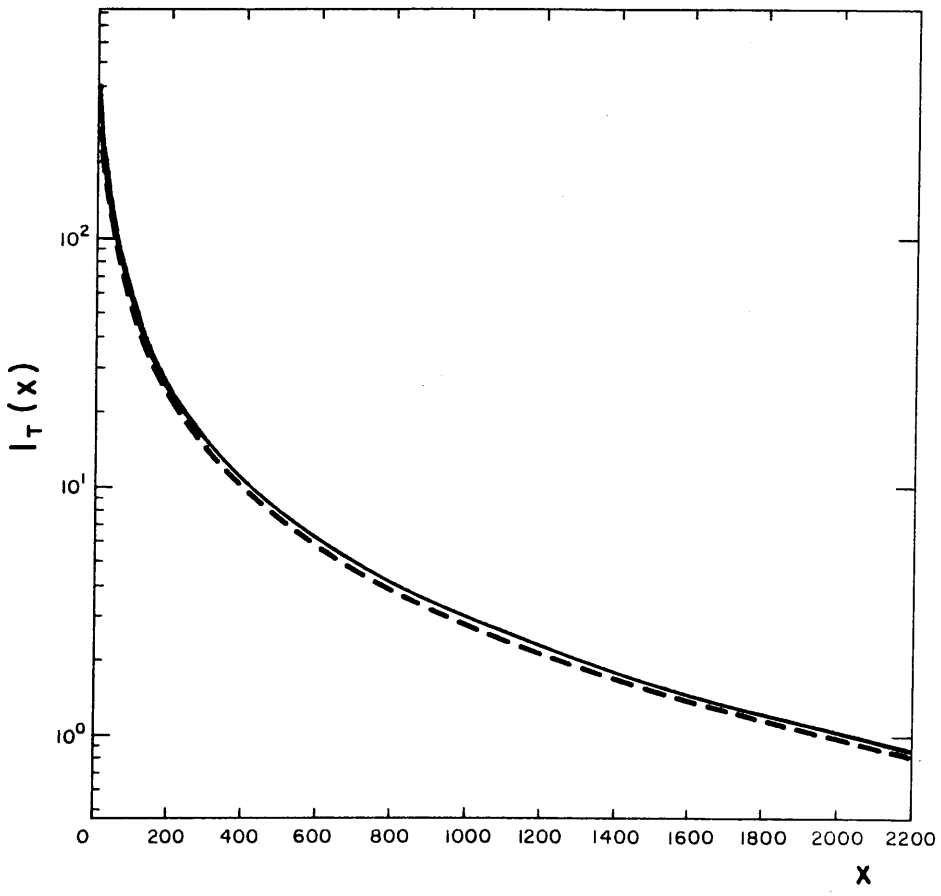
$I_T(x)$
10^2
10^1
10^0
0
200
400
600
800
1000
1200
1400
1600
1800
2000
2200
X

Section 4.3). It can be seen that Langmuir wave generation makes very little difference to the total heating rate: in each case, I_T is enhanced by no more than 8%. I_B is slightly reduced as the result of quasi-linear relaxation, but this is more than offset by collisional wave damping. After the onset of instability, we find that I_W is a substantial fraction of the total heating rate: this is consistent with the approximate analytical results obtained in Section 4.3.

The collisionless quasi-linear equations satisfy the second law of thermodynamics, in the sense that the entropy of the particle-wave system is a monotonic increasing function of time (Harris 1969). It is therefore not surprising that the plasma should relax towards thermal equilibrium more rapidly when quasi-linear interactions are taken into account. What <u>is</u> perhaps surprising is that the presence of Langmuir waves should bring about such a small increase in the total heating rate. In view of the sensitive temperature dependence of the conductive flux ($F \sim T^{7/2}$), we may conclude that the effect of Langmuir wave generation on the mean steady state temperature is completely negligible.

We now consider the X-ray signature of a relaxed thick target beam. Neglecting directivity effects, the volume integrated bremsstrahlung flux observed at the earth (photons cm^{-2} s^{-1} keV^{-1}) is given by

$$I(\varepsilon) = \frac{A}{4\pi d^2}\int_0^L dx \int_\varepsilon^\infty nQ(\varepsilon,E)\, G(x,E)dE \qquad (5.17)$$

where, as in Section 4.4, G(x,E) denotes the electron flux spectrum, Q(ε,E) is the bremsstrahlung cross-section differential in photon energy, ε is photon energy, A is the area of the (plane parallel) beam and L is the length of the coronal loop. d denotes the astronomical unit. Following Brown (1971) we adopt the nonrelativistic Bethe-Heitler formula (Heitler 1954)

$$Q(\varepsilon,E) = \frac{8}{3}\,\alpha\, r_e^2\, \frac{m\,c^2}{\varepsilon\,E}\, \ell n \left[\frac{1+\sqrt{1-\varepsilon/E}}{1-\sqrt{1-\varepsilon/E}}\right] \qquad (5.18)$$

where α is the fine structure constant and r_e is the classical electron radius. Putting $y=E/\varepsilon$, (5.17) may then be written in a form convenient for numerical computation:

$$I(\varepsilon) = \frac{Q_o\, c^2}{4\pi^2 d^2}\, \frac{n^2 A}{\omega_p \varepsilon} \int_o^{\ell} dx \int_1^{\infty} dy\; \ell n \left[\frac{1+\sqrt{1-1/y}}{1-\sqrt{1-1/y}}\right] \frac{f(x,\sqrt{2}y)}{y} \qquad (5.19)$$

where $Q_0 = \frac{8}{3}\alpha r_e^2$ and ℓ is now the dimensionless length of the loop. If f(x,v) were determined by Coulomb collisions alone, (5.19) could be inverted analytically in the limit $\ell\to\infty$ to yield the injected electron flux in terms of $I(\varepsilon)$ (cf. Section 2.4 and Brown 1971).

The X-ray spectra corresponding to the distribution functions shown in Figure 5.1 (broken line) and Figure 5.2 (solid line) are shown in Figures 5.6a and b. In each case the beam area was taken to be 3×10^{17} cm^2: combined with $F_0 = 10^{19}$ electrons cm^{-2} s^{-1}, this gives a total injected flux of 3×10^{36} electrons s^{-1}, which is a typical thick target value (e.g. Brown 1976). The bremsstrahlung flux is reduced by quasi-linear interactions in

(a) $n = 10^{10}$ cm^{-3}

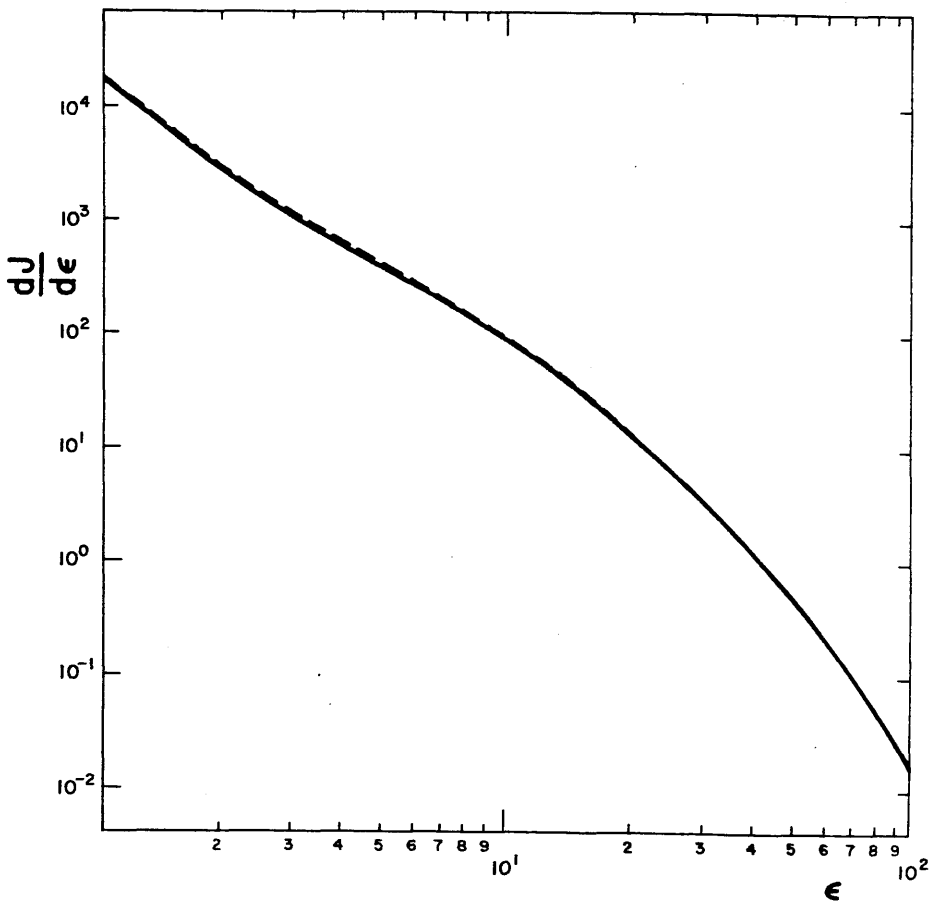

Figure 5.6 Volume integrated bremsstrahlung spectra corresponding to the distribution functions shown in Figure 5.1 (broken lines) and Figure 5.2 (solid lines) ($dJ/d\varepsilon$ is measured in photons cm^{-2} s^{-1} keV^{-1} and ε is measured in keV).

(b) $n = 10^{11}\ cm^{-3}$

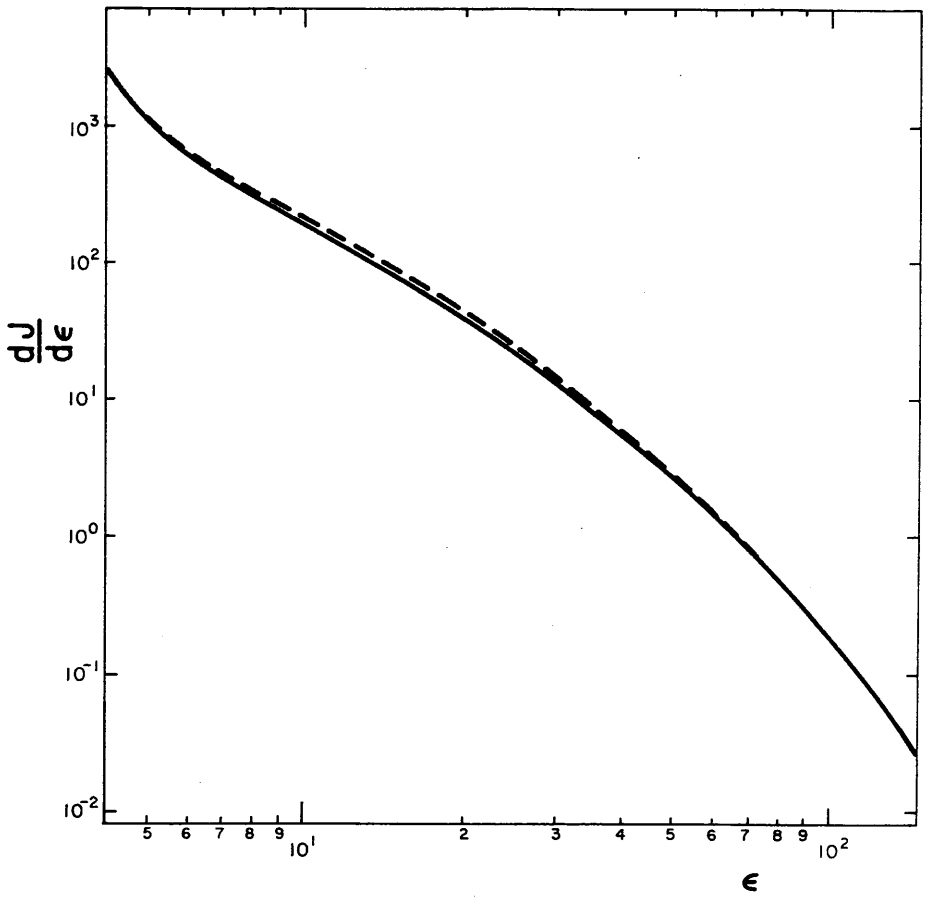
10^3
10^2
10^1
10^0
10^{-1}
10^{-2}
$\frac{dJ}{d\epsilon}$
5 6 7 8 9 10^1 2 3 4 5 6 7 8 9 10^2
ϵ

an energy range corresponding roughly to the velocity plateau in the electron distribution, but the reduction is never more than about 4% in the case of $n = 10^{10}$ cm^{-3}, and $\lesssim$12% in the case of $n = 10^{11}$ cm^{-3}. It may therefore be inferred that wave-particle interactions have an observationally negligible effect on the X-ray spectrum. The fact that qualitatively different electron distributions can produce almost identical photon spectra may be attributed to the well-known 'filtering' property of the Bethe-Heitler cross-section, which also means that the solution f of the integral equation (5.19) is extremely sensitive to small perturbations in the function $I(\varepsilon)$ (Brown 1975; Craig 1979).

5.5 Reverse Current Losses

Reverse currents can be incorporated into the kinetic treatment of beam relaxation by writing (4.1) in the form

$$\underline{v}.\frac{\partial f}{\partial \underline{x}} - \frac{e}{m}\underline{E}.\frac{\partial f}{\partial \underline{v}} = \left(\frac{\partial f}{\partial t}\right)_w + \left(\frac{\partial f}{\partial t}\right)_c \qquad (5.20)$$

Assuming that current neutralization has taken place (cf. Brown and Bingham 1984), the steady state form of Ohm's law can be written in the form

$$\underline{E} = \eta \underline{J}_R = -\eta \underline{J}_b = -\eta\left[-e\int f_b(\underline{v})\underline{v}\, d^3\underline{v}\right] \qquad (5.21)$$

where $\underline{J}_b$ is the current carried by the beam, $\underline{J}_R$ is the reverse current and η is the plasma resistivity. As before, $f_b(\underline{v})$ is the beam component of $f(\underline{v})$. Repeating the procedure described in Section 4.2, (5.20) can be reduced to the one dimensional form

$$v \frac{\partial f}{\partial x} - \frac{e^2 \eta}{m} \int_o^\infty f_b(v')v' \, dv' \cdot \frac{\partial f}{\partial v} = \left(\frac{\partial f}{\partial t}\right)_w + \left(\frac{\partial f}{\partial t}\right)_c \qquad (5.22)$$

The effect of the reverse current term in (5.22) is to reduce the energy of every beam electron by an amount

$$\Delta E = e \int_o^x |\underline{E}(x')| \, dx'$$

i.e.

$$\Delta E = e^2 \int_o^x \eta(x')dx' \int_o^\infty f_b(x',v')v' \, dv' \qquad (5.23)$$

This tends to suppress Langmuir wave generation, because it results in a more rapid thermalization of the beam distribution. The fact that ΔE is independent of velocity means that, unlike collisional losses, reverse current Ohmic losses cannot produce a positive slope in f(v).

We assume the classical expression for the resistivity of a fully ionized hydrogen plasma (Spitzer 1962)

$$\eta = \frac{\pi^{3/2} m^{1/2} e^2 \ell n \, \Lambda_o}{2(2k_B T)^{3/2}} \qquad (5.24)$$

This is valid provided the beam is sufficiently dilute (cf. (4.14)-(4.16)), and provided the plasma is stable to the generation of ion-acoustic waves: the presence of ion-acoustic turbulence enhances the effective collision frequency, leading to an anomalous resistivity which may exceed the classical value by a large factor. However, ion-acoustic instability can only occur when the electron temperature is much greater than the ion

temperature (e.g. Melrose 1986). Our assumed steady state requires the electron and ion temperatures to be equal (cf. Section 4.4), and under those conditions ion-acoustic waves are strongly Landau damped. We are therefore justified in assuming the resistivity to be classical (Langmuir waves do not significantly affect the resistivity of the plasma, because they have a suprathermal phase velocity and therefore can only interact with electrons in the tail of the distribution).

The appropriate dimensionless form of (5.22) is

$$v\frac{\partial f}{\partial x} - a\int_0^\infty f_b(v')dv'\frac{\partial f}{\partial v}$$

$$= \frac{\partial}{\partial v}\left[\frac{\ell n\, v}{2\pi\, v^2} + v\, W\frac{\partial f}{\partial v} + \frac{\ell n\Lambda}{2\pi\, v^2}\left(f + \frac{1}{v}\cdot\frac{\partial f}{\partial v}\right)\right] \qquad (5.25)$$

where $a = n^{\frac{1}{2}}\, e^3/(2^{7/2}(k_B T)^{3/2})\ell n\Lambda_o$. To obtain a numerical solution of (5.25) we impose the same velocity space boundary conditions as before, i.e. f is prescribed to be constant at v=1 and equal to zero at $v=v_{max}$. Strictly speaking, this is incorrect, since the requirement of current neutrality means that the Maxwellian component of f has a drift velocity given by

$$v_d = \frac{n_b}{n} v_b \qquad (5.26)$$

in the notation of Section 4.3. The fact that both v_b and n_b vary with depth means that the numerical code cannot be easily modified to allow for the finite drift velocity of the background plasma, which tends to favour Langmuir wave generation by increasing the range of velocities over which f(v) has a positive slope. We believe, however, that this is a

secondary effect which may be neglected. It was pointed out in Section 4.4 that the beam density at the onset of instability is a small fraction of the injected beam density, and in practice we find that v_d is invariably much less than v_e when wave generation takes place.

$f_b(v)$ in (5.25) can be determined for each space point using the method described in Section 5.4. It is then quite straightforward to generalize the numerical method to include the reverse current term (see Appendix B).

Figures 5.7a and b show the normalized wavelevel, for the two cases considered earlier, when reverse current energy losses are taken into account. The broken lines indicate the wavelevel when reverse currents are neglected. As expected, the most significant difference occurs in the low density case $n=10^{10}$ cm^{-3}, the peak wavelevel being reduced by about 40%. In the case of $n=10^{11}$ cm^{-3}, the wavelevel is reduced by no more than 10%. We have seen that the Langmuir wavelevel is maximized when a relatively high flux of electrons is injected into a relatively low density plasma. However, this is also the regime in which reverse current losses are most important, and reverse currents therefore play an important role in limiting the maximum wavelevel which can be produced by a thick target beam.

5.6 2nd Harmonic Plasma Radiation

There are several possible mechanisms for generating fundamental and 2nd harmonic plasma radiation. The process considered by Emslie and Smith (1984) is

$$\ell + \ell' \rightarrow \gamma \qquad (5.27)$$

(a) $n = 10^{10}\ cm^{-3}$

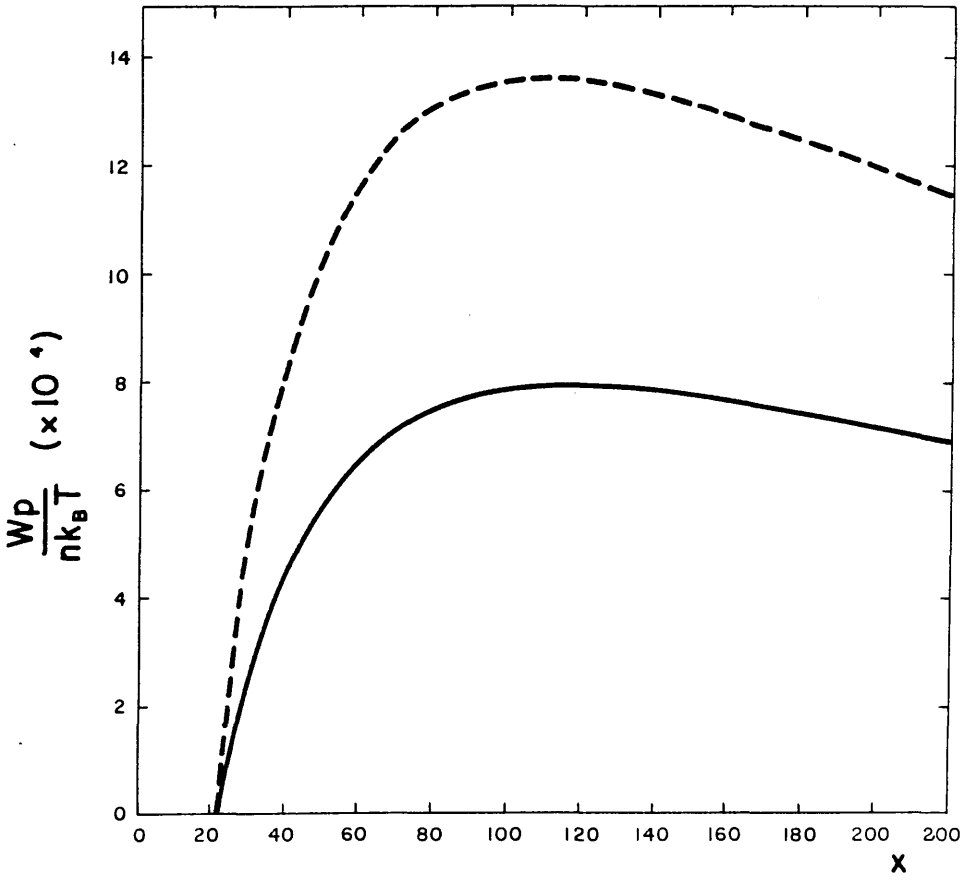

Figure 5.7 Normalized wavelevel as a function of x, allowing for reverse current energy losses (solid lines). For comparison, the curves in Figure 5.4 are also shown (broken lines).

(b) $n = 10^{11}\ cm^{-3}$

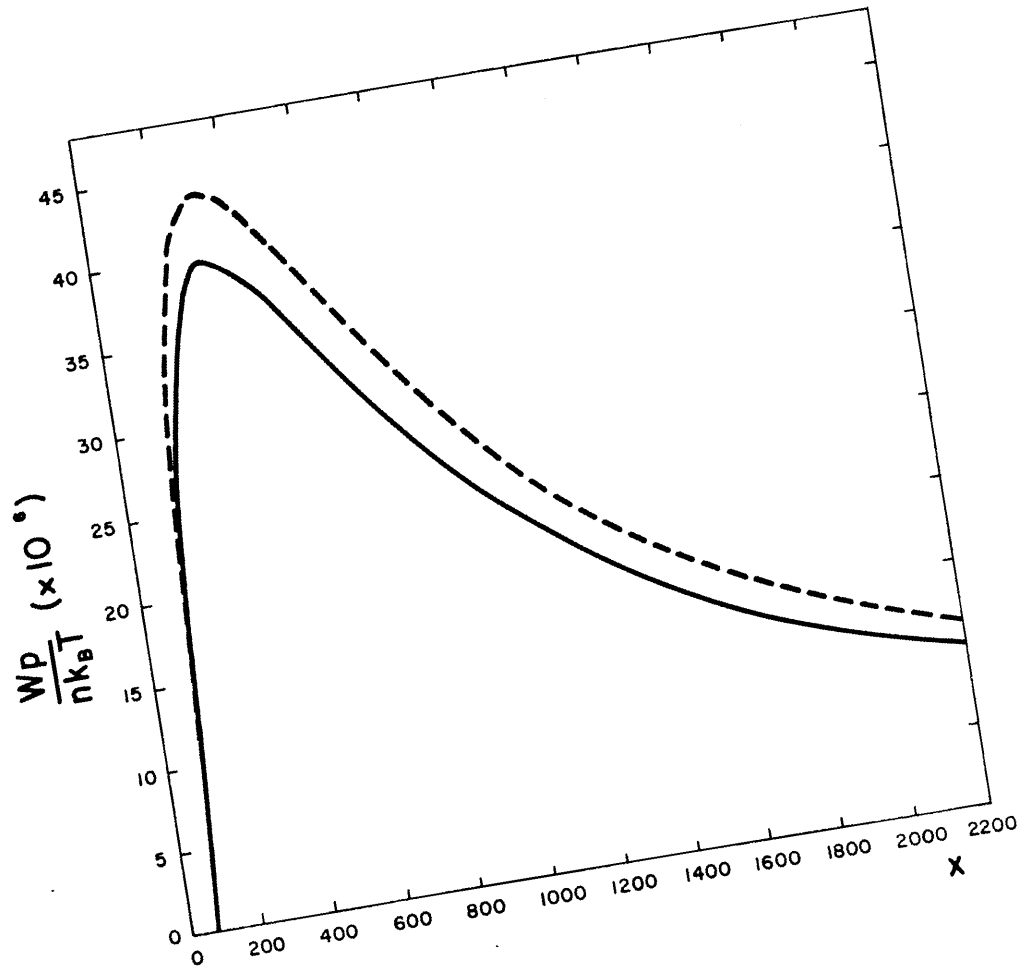
$\frac{W_p}{nk_BT}$ (x10^6)
45
40
35
30
25
20
15
10
5
0
0
200
400
600
800
1000
1200
1400
1600
1800
2000
2200
X

where ℓ , ℓ' denote Langmuir wave quanta and γ denotes a photon with a frequency (required by energy conservation) of about $2\omega_p$. If it is assumed that the Langmuir waves are distributed isotropically, a simple analytical expression for the microwave flux density due to this process may be obtained in terms of the wave energy density W_p. If we further assume that the radiation is optically thick, the width of the spectrum being determined by the finite spread in the Langmuir wave spectrum rather than by density inhomogeneities, then it can be shown that the appropriate expression for the flux density at the earth (ergs cm^{-2} Hz^{-1} s^{-1}) is

$$S_\nu = 2 \times 10^{-3} \frac{A}{d^2} \frac{v_1^4}{v_e c^2 \omega_p} W_p e^{-\tau} \qquad (5.28)$$

(Emslie and Smith 1984) where τ is the optical depth resulting from absorption by overlying material and v_1 is the minimum phase velocity in the Langmuir wave spectrum. Now at the peak of the solid curve in Figure 5.7a we have $W_p \simeq 10^{-2}$ ergs cm^{-3} and $v_1 \simeq 4v_e$. Taking $A = 3 \times 10^{17}$ cm^2 as before and $\tau \simeq 0.5$ (assuming that only free-free absorption occurs), we find that

$$S_\nu \simeq 15000 \text{ s.f.u.} \qquad (5.29)$$

at $\nu \simeq 2\nu_p \simeq 2$GHz. This compares with a typical observed flux at this frequency of less than 1000 s.f.u. in large events (Wiehl et al. 1985). The flux density predicted by (5.28) is not strongly model-dependent: for example, in the case of $n = 10^{11}$ cm^{-3}, we find that $S_\nu \simeq 6000$ s.f.u. when the other parameters are held constant. If, on the other hand, we prescribe the same

total injection rate of electrons (3×10^{36} s^{-1}) over an area of 3×10^{18} cm^2 and $n = 10^{10}$ cm^{-3}, we obtain $S_\nu \simeq 7000$ s.f.u.. These estimates of the microwave flux density are comparable to those found by Emslie and Smith (1984).

Can the reverse drift decimetric and microwave bursts of Benz et al. (1983) and Stähli and Benz (1987) be interpreted in terms of the mechanism described above? One of the events recorded by Benz et al. (their Figure 3) has a peak flux density of about 3000 s.f.u., and shows a discernible drift towards higher frequency with time. The bandwidth $\Delta\omega/\omega$, however, is around 0.01, whereas the predicted bandwidth of second harmonic emission is given by (e.g. Melrose 1980b)

$$\frac{\Delta\omega}{\omega} = \frac{6\ v_e^2}{v_1^2}\ \frac{\Delta k}{k} \simeq \frac{6\ v_e^2}{v_1^2} \sim 0.2 \qquad (5.30)$$

where Δk is the spread of wave numbers in the Langmuir wave spectrum, k is a typical wave number, and we have assumed $\Delta k \simeq k$. It therefore appears unlikely that this particular event can be interpreted in terms of the coalescence mechanism (5.27), unless $\Delta k \ll k$. The average bandwidth of the decimetric blips recorded by Benz et al. is around 0.03, which is still too narrow.

Stähli and Benz (1987) give only upper and lower limits for the bandwidth of the microwave bursts they describe: they find that $\Delta\omega/\omega$ may lie anywhere in the range 0.05–0.5, which is certainly consistent with (5.30). It was pointed out, however, in Section 2.5, that the typical flux density of the events recorded by Stähli and Benz is very much less than that predicted by Emslie and Smith. There are several possible

reasons for this. In the first place, there is no evidence that the drifting microwave bursts coincided with significant fluxes of hard X-ray emission. The injected electron fluxes producing these events may therefore have been much less than the 3×10^{36} s^{-1} assumed in this chapter. Secondly, the 2nd harmonic microwaves may be significantly attenuated because of gyroresonance absorption. For this to be effective, it is necessary for a harmonic of the gyrofrequency to be approximately equal to $2\omega_p$ over a distance which is much less than the gyroresonance absorption length corresponding to that harmonic (Emslie and Smith 1984; Hamilton and Petrosian 1987). In practice this requires coronal magnetic fields to be in excess of about 300G. Although field strengths of this order have been inferred from microwave observations (cf. Section 2.5), it is not yet possible to gauge accurately the effectiveness of gyroresonance absorption since there are no direct methods of deducing the structure of the magnetic field in a flaring coronal loop (cf. comments in Section 2.1).

It was pointed out earlier that (5.28) is only valid if the Langmuir wave spectrum is isotropic. Streaming instabilities produce Langmuir waves which are collimated in the direction of the beam, the degree of collimation depending on the ratio of gyro to plasma frequency (cf. Chapter 3). The requirement of momentum conservation means that the coalescence of two Langmuir waves can only occur if they are propagating in almost opposite directions, and therefore the primary spectrum of waves excited by an unstable beam cannot produce a significant flux of plasma radiation. The second harmonic emission observed in type III

bursts is usually explained by invoking either a secondary population of Langmuir waves (propagating in the counterstreaming direction) or soliton collapse (Goldman et al. 1980). The latter process requires the Langmuir waves to be strongly turbulent: we will discuss the question of whether this condition is likely to be satisfied in Chapter 6. An initially highly collimated distribution of Langmuir waves may be isotropized because of induced scattering on ions (also known as 'nonlinear Landau damping' - see, e.g., Melrose 1986). This is the mechanism invoked by Emslie and Smith (1984) to justify their assumption of isotropic Langmuir waves (see also Smith 1977). They show that, under certain idealized conditions (e.g. a monochromatic primary wave spectrum), the growth rate for waves in the anti-parallel direction can exceed the collisional damping rate by several orders of magnitude. They claim that isotropization would then rapidly occur (in about 20 e-folds), without quantitatively justifying this statement. In Chapter 7 we discuss how induced scattering on ions might be included in the one dimensional model of beam relaxation, in the realistic case of an extended primary wave spectrum.

CHAPTER 6

TIME DEPENDENT EFFECTS

6.1 Introduction

In Chapters 4 and 5 we treated the problem of Langmuir wave generation by a steady state thick target beam. We now relax the assumption of a steady state and consider the collisional and quasi-linear evolution of a time dependent beam. There are essentially two reasons for such a generalization. In the first place, there is no guarantee that, in the absence of nonlinear saturation mechanisms, a steady state wavelevel can ever be reached from physically realistic initial conditions. Indeed, Wentzel (1984) and LaRosa (1987) have proposed a model for the propagation of type III beams which requires nonlinear saturation to occur in a narrow region at the head of the beam. LaRosa claims that, without such saturation, the Langmuir waves would grow indefinitely. The proposed reason for this (LaRosa, private communication) is that beam electrons can enter a region of Langmuir turbulence with a positive slope, without having been affected by the waves, which are consequently amplified to a higher level. This can occur because the wave group velocity is very much less than the beam velocity. It is widely believed that the quasi-linear theory alone cannot explain the observed stability of type III streams, which enables them to propagate out as far as the earth, and that nonlinear processes must therefore be responsible for beam stabilization (see, for example, the review by Goldman, 1983). In the case of a collisionless inhomogeneous beam, it thus appears that a

quasi-linear steady state may not exist. Although we have argued (in Section 4.3) that the collision-dominated case is fundamentally different, the failure of quasi-linear theory to fully account for the observed properties of type III streams leads us to question the validity of our steady state model.

The second reason for performing a time dependent calculation concerns the shortest timescales observed in hard X-ray light curves. It was pointed out in Section 1.6 that a significant fraction of hard X-ray bursts exhibit fluctuations on timescales of between 100ms and 1s, and that there is some evidence (although this is controversial) of individual spikes with e-folding times as short as 20ms. Such timescales are comparable to, or shorter than, the transit time of a fast electron along a coronal loop. In such circumstances, time-of-flight effects are important, and a positive slope in f(v) may arise because of the finite velocity dispersion of the fast electrons. If this 'overtaking instability' occurs on a collisionless timescale, we would expect a large fraction of the beam energy to be transferred to Langmuir waves (cf. Section 4.3), and the wavelevel produced by a given beam flux would therefore be much greater than that predicted by a steady state calculation.

In Section 6.2 we discuss the problem of solving numerically the time dependent quasi-linear equations. Computations of the normalized wavelevel under various conditions are presented in Section 6.3. In the light of these results, we discuss in Section 6.4 the validity of the quasi-linear theory as a means of describing the propagation of thick target electron beams.

6.2 The Time Dependent Quasi-Linear Equations

The equations requiring numerical solution are (4.21) and (4.22). As before, we assume the Langmuir waves to be in equilibrium with the particle distribution except when instability occurs. In the stable regime, W is therefore given by

$$W(x,v,t) = \frac{e^2\omega_p^2 \; \frac{\ell n\, v/v_e}{v} \; f\,(x,v,t)}{\gamma_c - \frac{\pi\,\omega_p}{n} v^2\, \partial f/\partial v} \qquad (6.1)$$

When $\partial f/\partial v>0$, both $\partial W/\partial t$ and $\partial W/\partial x$ are retained in (4.22). We also assume the plasma temperature and density to be constant in both time and space.

At $x=0$ we assume the beam component of f to be separable in velocity and time

$$f_b\,(o,v,t) = \xi(t)\,\phi(v) \qquad (6.2)$$

where ϕ is taken to be the modified power law assumed in previous chapters:

$$\phi(v) = m\,F_{oo}\,E_o^{\delta-1}\,(\delta-1)\,(E_o + E)^{-\delta} \qquad (6.3)$$

F_{00} is now the total (i.e. time integrated) number of electrons injected per unit area. For reasons which will become apparent, ξ must be a smoothly-varying (i.e. continuous) function of time. A suitable choice is a Gaussian profile of the form

$$\xi(t) = \frac{1}{\sqrt{\pi}\,\tau}\; e^{-t^2/\tau^2} \qquad (6.4)$$

where τ is the injection timescale, and the normalization factor

is chosen such that

$$\int_{-\infty}^{+\infty} dt \int_{o}^{\infty} dv\, f_b(o,v,t)\, v = F_{oo} \qquad (6.5)$$

The wave distribution is given at the boundary by (6.1), with x=0.

The boundary condition (6.1) applies on a semi-infinite interval $t \in [t_0, \infty)$, where $t_0<0$. We assume that the system has evolved collisionally up to $t=t_0$: this dictates our choice of initial condition. Retaining only the collisional friction term on the right hand side of (4.21), we obtain

$$\left(\frac{\partial}{\partial t} + v \frac{\partial}{\partial x}\right) f = \frac{2Kn}{m^2} \frac{\partial}{\partial v} \left(\frac{f}{v^2}\right) \qquad (6.6)$$

the general solution of which may be written in the form

$$f_b(x,v,t) = \frac{v^2}{v'^2} H(v',t') \qquad (6.7)$$

where

$$v' = \left(v^4 + \frac{8\, Kn\, x}{m^2}\right)^{\frac{1}{4}} \qquad (6.8)$$

$$t' = t - \frac{m^2}{6Kn}\left[\left(v^4 + \frac{8Kn\, x}{m^2}\right)^{\frac{3}{4}} - v^3\right] \qquad (6.9)$$

(cf. Craig et al. 1985). H is determined by the requirement that (6.7) should be consistent with (6.2). This leads to the initial condition

$$f_b(x,v,t_o) = \frac{1}{\sqrt{\pi}\,\tau} \cdot \frac{E}{E'} e^{-t'^2/\tau^2}\, m\, F_{oo}\, E_o^{\delta-1} (E_o + E')^{-\delta} \qquad (6.10)$$

where $E' = 1/2mv'^2$ and t' is evaluated at $t=t_0$. t_0 is chosen to

be sufficiently large that the combined distribution function f(v) is stable for all $x \in [0,\infty)$ at $t=t_0$. The initial wave distribution is then given by (6.1) with $t=t_0$.

A few comments are appropriate regarding the choice of the injection profile, $\xi(t)$. One might attempt to model the impulsive injection of an electron beam by setting $\xi(t) = \delta(t)$. The velocity dependence of t', however, means that $\partial f/\partial v$ contains the derivative of ξ, and therefore such an injection profile would lead to an infinite growth or damping rate of Langmuir waves. This would also be true if $\xi(t)$ were set equal to a step function. In either case, a singularity would appear in the initial conditions, which would be impossible to handle numerically. When attempting to model microinstabilities such as Langmuir wave generation, it is therefore essential to prescribe an injection rate which is a smoothly varying function of time. If we crudely represent our injection profile by

$$f(o,v,t) = e^{-t^2/\tau^2} v^{-\alpha} \qquad (6.11)$$

then, neglecting both collisions and quasi-linear interactions,

$$f(x,v,t) = e^{-(t-x/v)^2/\tau^2} v^{-\alpha} \qquad (6.12)$$

and it can be easily shown that the condition for $\partial f/\partial v>0$ is that

$$t < \frac{x}{v} - \frac{1}{2}\alpha\tau^2\frac{v}{x} \qquad (6.13)$$

Now significant wave generation only occurs at a point in space and time where f is non-negligible. This will be the case if

$$-\tau \lesssim t - x/v \lesssim \tau \qquad (6.14)$$

Combining (6.13) with (6.14), and assuming $\alpha/2$ to be of order unity, it is clear that the overtaking instability will be important if $\tau \lesssim L/v$, where L is the length of the loop. Assuming $L=3\times10^9$cm and $v=c/3$, we may therefore predict significantly different results from the steady state case if the injection timescale is as short as 100ms (cf. Heyvaerts 1981).

Our numerical method is a straightforward generalization of that used in the steady state case (see Appendix B). The equations are solved as before in dimensionless form, with the dimensionless time variable defined to be

$$\tilde{t} = \frac{\omega_p}{2\, n\, \lambda_D^3}\, t \qquad (6.15)$$

A boundary value approach is used, the code stepping forward in space rather than time. The velocity space boundary conditions are the same as before, i.e. f is set equal to a constant (in space and time) at the thermal speed, and equal to zero at $v=v_{max}$. This creates a problem, in that the initial beam distribution given by (6.10) is clearly spatially dependent, and may therefore give rise to an unphysically large time derivative close to $v=v_e$ (see Appendix B). To ensure numerical stability, we introduce a modified beam distribution at the boundary and at $t=t_0$:

$$\begin{aligned} \tilde{f}_b &= 0 \qquad\qquad , \quad v \leqslant \beta \\ \tilde{f}_b &= e^{-\frac{\alpha}{v-\beta}} f_b \quad , \quad v > \beta \end{aligned} \qquad (6.16)$$

where $\beta>1$ (in units of v_e) and α determines the rate at which $\tilde{f}_b$ approaches f_b. α and β must be chosen such that the combined distribution remains stable (i.e. monotonic decreasing) at $x=0$ $\forall t$ and at $t=t_0$ $\forall x$. $\tilde{f}_b$ has the attractive property that it is differentiable to all orders in v, provided f_b is.

6.3 Numerical Results

The beam and plasma parameters were chosen in such a way that a direct comparison could be made with the results of the previous chapter. Thus, for example, the total beam flux F_{00} was set equal to a value which corresponds to a peak (instantaneous) injection rate of 10^{19} electrons cm^{-2} s^{-1}. Figures 6.1-6.3 show the normalized wavelevel as a function of space and time. In each case, $n = 10^{10}$ cm^{-3}, E_0 = 20keV and $\delta=4$. The loop length was taken to be $3x10^9$cm. It should be pointed out that the numerical results presented in this chapter are necessarily less accurate than those of Chapter 5: to maintain the same degree of accuracy with an extra (time) dimension is simply not possible with the available computing facilities. However, the numerical truncation error is quite acceptable when one considers the other approximations in the model (in particular the assumption of one dimensional geometry).

Figure 6.1 shows the wavelevel produced by a relatively long pulse of electrons (τ=1s). Such a pulse would produce a hard X-ray burst with an e-folding time approximately equal to the injection time (cf. Section 2.4). The temperature is 10^7K. At $x=3x10^9$cm, the Langmuir waves closely mimic the injection profile, rising and falling on a similar timescale. There is no

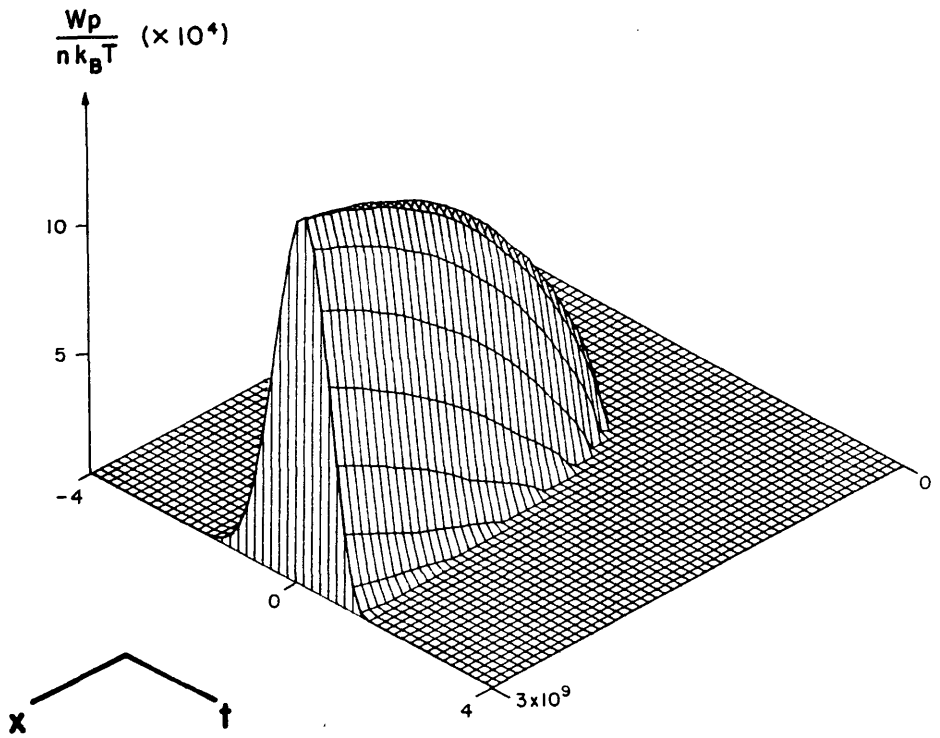

Figure 6.1 Normalized wavelevel as a function of space and time, with a peak (instantaneous) injected flux of 10^{19} electrons cm^{-2} s^{-1}, T = 10^7K and τ = 1s. The other beam and plasma parameters are given in the text (x is in cm and t is in seconds). The peak wavelevel is 1.5×10^{-3}.

discernible drift of the wavelevel with time. The maximum value of W_p/nk_BT is only slightly greater than that obtained in the steady state case (cf. Figure 5.4a): there is no indication of the wavelevel growing indefinitely with time, which LaRosa (1987) has claimed is an inevitable feature of the quasi-linear evolution of type III streams. The fact that the wavelevel remains well-behaved is presumably due to two factors. In the first place, the electron beam driving the instability is 'switched off' after a finite time, and the waves are then strongly Landau damped. Secondly, the injection time is sufficiently long that the overtaking instability is unlikely to be important, and the net growth rate remains small because of collisional damping. We may therefore conclude that a quasi-linear steady state does indeed exist, at least when the beam electrons are injected on a timescale of $\gtrsim$ 1s.

Figure 6.2 shows the wavelevel produced by a shorter pulse of electrons (τ=100ms). As before, T = 10^7K. In this case, W_p/nk_BT rapidly rises to a maximum value which is about a factor of 4 greater than the peak wavelevel in Figure 5.4a. At $x=3\times10^9$cm, the Langmuir wave 'burst' is noticeably smeared out in time, because of the velocity dispersion of the resonant electrons. The e-folding time is still of the order of 100ms, however. It can be clearly seen that the peak wavelevel drifts in the space-time plane. This could give rise to a reverse drift microwave burst of the type observed by Stahli and Benz (1987). The drift rate is given by

$$\frac{dx}{dt} \simeq 1.4 \times 10^{10} \text{cm s}^{-1} \qquad (6.17)$$

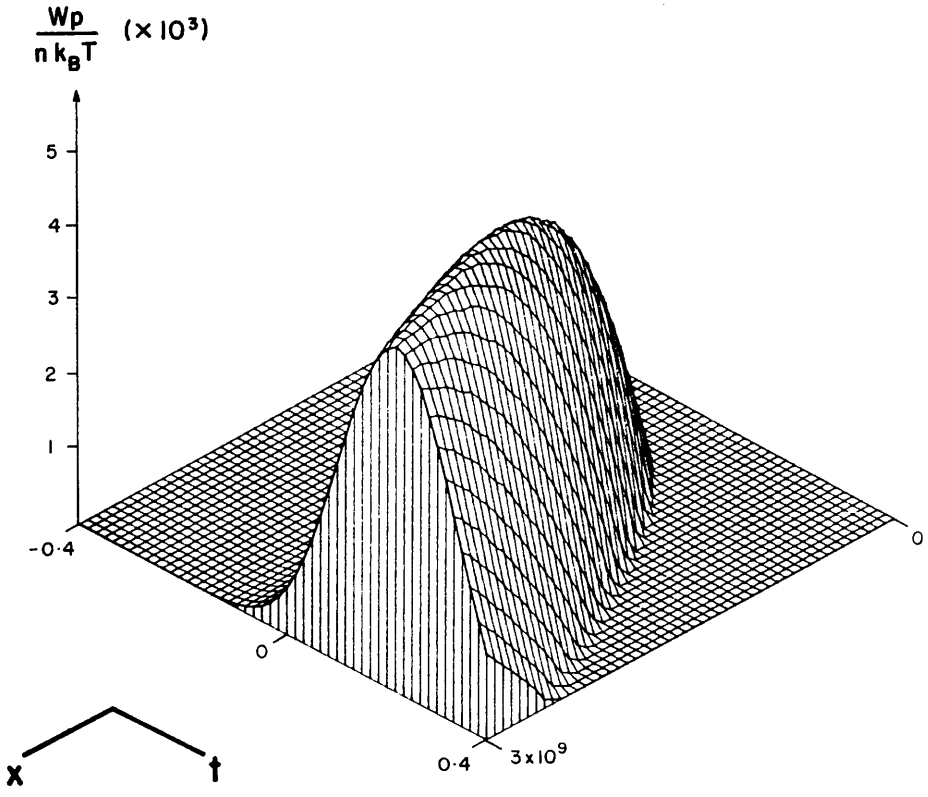

Figure 6.2 As Figure 6.1 except with τ = 0.1s. The peak wavelevel is 5.2×10^{-3}.

which corresponds to an electron energy of around 50keV.

Figure 6.3 shows the result of injecting the same pulse of electrons into a cooler plasma ($T=5\times10^6$K). The peak wavelevel is increased by another factor of 2, to 1.3×10^{-2}. This may be attributed to the fact that the Maxwellian part of the distribution falls off more rapidly with v, and therefore the range of unstable wave numbers is greater.

6.4 Discussion

We now consider the question of whether the Langmuir waves excited by a thick target electron beam are likely to be strongly turbulent. Langmuir waves give rise to an electrostatic pressure force, analogous to radiation pressure, which drives electrons away from regions of high wave turbulence. If this 'ponderomotive' force is strong enough, the wave energy density becomes increasingly localized and the plasma is then modulationally unstable. This is the meaning of the phrase 'strong turbulence'. It is frequently stated (e.g. Sudan 1984; LaRosa 1987) that the threshold wavelevel for strong turbulence is given by

$$\frac{W_p}{n\, k_B\, T} \gtrsim (\Delta k\, \lambda_D)^2 \simeq \frac{\Delta v^2}{v^4} \qquad (6.18)$$

where, as before, Δk is the spread of wave numbers in the spectrum, Δv is the corresponding spread in phase velocities, and v is an average resonant beam velocity (Δv and v are in units of v_e). (6.18) can be derived in a heuristic manner by equating the ponderomotive force to the pressure gradient force,

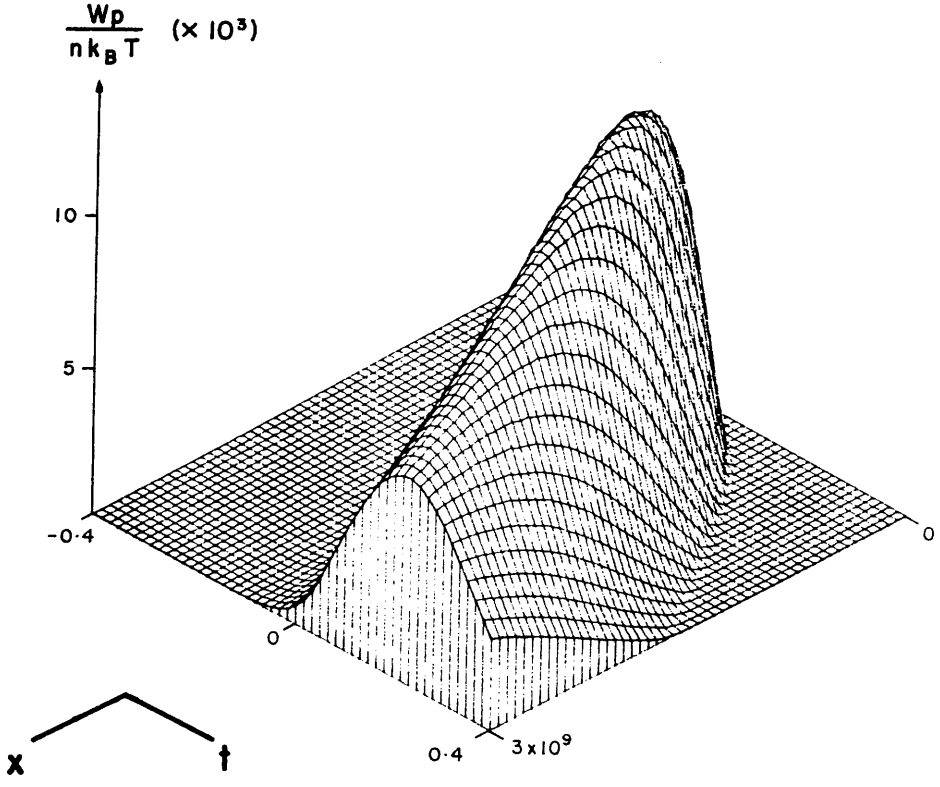

Figure 6.3 As Figure 6.2 except with T = 5×10^6K. The peak wavelevel is 1.3×10^{-2}.

and finding the wavelevel at which the dispersive properties of the plasma are affected by the presence of Langmuir turbulence (Sudan 1984). Implicit in this derivation is the assumption that the plasma is quasi-neutral, i.e. the ions respond to the electron density modulations in such a way as to maintain charge neutrality. If this condition is not satisfied (i.e. if the ion plasma period is comparable to or longer than the period of the modulation), then the modulational instability will only occur if the ponderomotive force can overcome both the electron pressure force and the electrostatic restoring force resulting from charge separation. (6.18) therefore represents a necessary, but possibly insufficient condition for strong turbulence.

It should be pointed out that strong turbulence criteria other than (6.18) have been derived by various authors. For example, Zakharov (1972) found that the modulational instability occurs if

$$\frac{W_p}{n k_B T} \gtrsim (k \lambda_D)^2 \qquad (6.19)$$

while Tsytovich (1970b) obtained the result

$$\frac{W_p}{n k_B T} \gtrsim 12 (k \lambda_D)^2 \qquad (6.20)$$

The exact threshold condition for strong turbulence remains controversial. It is clear, however, that (6.18) represents a minimal requirement: reversing the inequality yields a sufficient condition for the validity of the weak turbulence (i.e. quasi-linear) theory.

In the steady state problem, the weak turbulence condition is invariably satisfied. In the low density case ($n = 10^{10}$ cm^{-3}), we find that $\Delta v^2/v^4 \simeq 10^{-2}$ while $W_p/nk_BT \lesssim 8x10^{-4}$, when reverse current energy losses are taken into account (cf. Figure 5.7a). When $n = 10^{11}$ cm^{-3}, it turns out that $\Delta v^2/v^4 \simeq 8x10^{-3}$ while $W_p/nk_BT \lesssim 4x10^{-5}$. We may conclude that a thick target electron beam which is stable at the point of injection, and which is injected over a period $\tau \gtrsim 1s$, does not give rise to a modulational instability. In the case of a short injection time ($\tau = 0.1s$), the situation is less clear-cut. When $T=10^7K$, we find that $\Delta v^2/v^4 \simeq 8x10^{-3}$ at the time of maximum Langmuir turbulence, while $W_p/nk_BT \lesssim 5x10^{-3}$. The corresponding figures for $T=5x10^6K$ are $\Delta v^2/v^4 \simeq 5x10^{-3}$ and $W_p/nk_BT \lesssim 1.3x10^{-2}$. In the latter case it appears that the plasma may indeed be strongly turbulent. Several qualifying remarks are necessary, however. Our numerical results are such that the inequality (6.19) is never satisfied, and therefore the weak turbulence theory remains valid if the true threshold for modulational instability is given by (6.19) or (6.20) rather than (6.18). Furthermore, in our time dependent calculation we have neglected reverse current energy losses, which may reduce the wavelevel by as much as a factor of 2 (cf. Section 5.5). It is, in any case, not consistent to prescribe an instantaneous electron flux as high as 10^{19} electrons cm^{-2} s^{-1} and a steady state temperature as low as $5x10^6K$ (cf. remarks in Section 4.4). In practice the plasma would rapidly heat up to a temperature in excess of 10^7K, thus inhibiting wave growth. Finally, it should be emphasized that our use of a one dimensional model must inevitably result in an

overestimate of the wavelevel (cf. Chapter 3). On balance, it therefore seems reasonable to conclude that thick target electron beams are unlikely to be strongly turbulent, and that the propagation of such beams can be adequately described using the quasi-linear theory. Contrary to the claims of Vlahos and Papadopoulos (1979), it thus appears that nonlinear processes do not play any significant role in thick target beam evolution (cf. remarks in Section 4.3).

One consequence of the above conclusion is that the radiation mechanism proposed by Goldman et al. (1980) (i.e. soliton collapse) is unlikely to be relevant to our problem. However, even on the basis of the weak turbulence theory, the results of this chapter imply a flux of plasma microwave radiation which is as much as a factor of 10 greater than that given by (5.29). If the radiation calculation of Emslie and Smith (1984) is valid, there is thus a very large discrepancy between theory and observations (assuming gyroreonance absorption to be ineffective). We have already argued, however, that (5.28) may significantly overestimate the microwave flux because it is based on the unproved assumption of isotropic Langmuir waves. Although a quantitative prediction of the radiation flux density may be difficult, our numerical results do appear to be consistent with the timescales and frequency drift rates observed by Stähli and Benz (1987).

CHAPTER 7

FUTURE WORK

7.1 Introduction

In this thesis we have investigated the problem of Langmuir wave generation by thick target electron beams using an idealized mathematical model. We have shown that a sufficiently collimated electron beam, injected into the low corona, will become unstable because of collisional degradation. The resulting level of Langmuir turbulence, however, constitutes only a small fraction of the beam energy and has a quite negligible effect on both the thick target hard X-ray signature and the rate of energy deposition. Furthermore, the wavelevel is unlikely to be sufficiently high to excite the modulational instability. It may, however, produce an observable flux of 2nd harmonic plasma radiation, the detection of which could be used to establish useful constraints on beam parameters and flare models.

We now discuss two ways of extending the work described in previous chapters, relaxing the assumptions made so far. In Section 7.2 we consider the propagation of a thick target electron beam through an inhomogeneous plasma, using a simple steady state model of the corona. It was pointed out in Section 5.6 that the flux density of 2nd harmonic radiation produced by an electron beam depends crucially on the angular distribution of the Langmuir waves, and that scattering on thermal ions may produce a near-isotropic wave spectrum from an initially collimated one. In Section 7.3 we show how this process could be

incorporated into the one dimensional model developed in Chapters 4 and 5.

7.2 Density Inhomogeneities

Changes in the plasma density have the effect of shifting Langmuir waves out of resonance with the electrons which originally excited them. The waves are then Landau damped, and the particle distribution can develop a positive slope in velocity space without undergoing quasi-linear relaxation. Muschietti et al. (1985) have invoked such a stabilization mechanism to explain in situ observations of electron streams and Langmuir waves associated with type III bursts (Lin et al. 1981b). They proposed that stochastic large-scale density variations are responsible for removing Langmuir waves from resonance, and that this process can be represented by a pitch angle diffusion term in the evolution equation for the waves.

Density fluctuations of the kind envisaged by Muschietti et al. may well be present in the low corona, thus preventing Langmuir waves from reaching the levels predicted in Chapters 5 and 6. Suppose, on the other hand, that there is only a slow, hydrostatic density gradient. In this case, the waves evolve according to the equations of geometric optics, which are simply the characteristics of (4.2) in the absence of wave-particle interactions:

$$\dot{\underline{x}} = \frac{\partial \omega}{\partial \underline{k}} \qquad (7.1)$$

$$\dot{\underline{k}} = -\frac{\partial \omega}{\partial \underline{x}} \qquad (7.2)$$

(cf. Melrose, 1980a) where $\omega = (\omega_p^2 + 3k^2 v_e^2)^{\frac{1}{2}}$. In one dimension, we can write (7.2) in the form

$$\frac{dk}{dt} = -\frac{\partial}{\partial x}\left[(\omega_p^2 + 3k^2 v_e^2)^{\frac{1}{2}} \right]$$

$$\simeq -\frac{\omega_p}{2H} \qquad (7.3)$$

where $H = [d\ell n\, n/dx]^{-1}$ is the density scale height. A Langmuir wave quantum is therefore taken out of resonance ($\Delta k \sim k$) in a time

$$\Delta t \simeq \frac{2H\,k}{\omega_p} \simeq \frac{2H}{v} \qquad (7.4)$$

Quasi-linear relaxation will then be suppressed if

$$\Delta t\, \gamma \simeq \Delta t\, \gamma_c \lesssim 1 \qquad (7.5)$$

assuming that the wave growth rate is approximately equal to the collisional damping rate (cf. Section 4.3). From (4.15), (7.4) and (7.5) we obtain the inequality

$$E \gtrsim E_c \equiv 3 \times 10^{-16} \frac{(n\,H)^2}{T^3} \text{ keV} \qquad (7.6)$$

If the energy of the resonant particles is above this value Langmuir waves will be taken out of resonance before they can be amplified to an appreciable level.

To estimate H, we require an atmospheric model. Suppose the corona is in hydrostatic and thermal equilibrium: then, neglecting beam heating and radiative losses, we can write (e.g. Priest 1982)

$$\frac{dP}{dx} = - m_p n g \qquad (7.7)$$

$$\frac{d}{dx} (T^{5/2} \frac{dT}{dx}) = 0 \qquad (7.8)$$

where $P=2nk_BT$ is the pressure, m_p is the proton mass and g (assumed constant) is acceleration due to gravity. (7.8) is a simple energy equation, expressing conservation of thermal conductive flux. For simplicity, we assume the loop to be vertical. Using the boundary condition that T=0 at x=L (the bottom of the loop), we can easily show that (7.7) and (7.8) have solutions

$$T = T_o (1 - x/L)^{2/7} \qquad (7.9)$$

$$n = n_o (1 - x/L)^{-2/7} \exp [- \frac{7}{5} \cdot \frac{L}{H_g} \{(1 - x/L)^{5/7} - 1\}] \qquad (7.10)$$

where $H_g = 2k_B T_o / m_p g$ is the gravitational scale height at the top of the loop (the singularity in n can be avoided by allowing T to be nonzero at x=L). Putting $T_0 = 10^7$K gives $H_g = 6 \times 10^{10}$cm, which is more than an order of magnitude greater than the loop length L. It is clear from (7.10) that gravity is therefore unimportant, and to a good approximation the pressure is constant along the loop. Note that T and n have only a weak dependence on x except when $x \simeq L$, as we would expect in a realistic coronal model (cf. Priest 1982). From (7.10) we obtain

$$H^{-1} \equiv \frac{d \ln n}{dx} = \frac{1}{H_g} (1 - x/L)^{-2/7} + \frac{2}{7(L-x)} \simeq \frac{2}{7L} \qquad (7.11)$$

for $x \ll L$. Assuming $L \gtrsim 10^9$cm, $n \gtrsim 10^{10}$cm^{-3} and $T \lesssim 10^7$K, we find

that $E_c \gtrsim 30$keV.

In view of the results obtained in the time dependent case, it appears from this that the changes in density may indeed play a significant role in reducing the wavelevel. The above argument is rather crude, however, and a rigorous analysis, involving the solution of the full inhomogeneous quasi-linear equations, should be carried out. In dimensionless form, the appropriate steady state equations are

$$v\frac{\partial f}{\partial x} - v f \frac{d \ell n A}{dx} = \frac{\partial}{\partial v}\left[\frac{\ell n v}{2\pi v^2} f + v W \frac{\partial f}{\partial v} + \frac{\ell n \Lambda}{2\pi v^2}\left(f + \frac{1}{v}\cdot\frac{\partial f}{\partial v}\right)\right] \qquad (7.12)$$

$$\frac{3}{v}\left(\frac{\partial w}{\partial x} - W \frac{d \ell n B}{dx}\right) + \frac{1}{2}\frac{d \ell n n}{dx}\cdot\frac{\partial}{\partial v}(v^2 W) = \frac{\ell n v}{2\pi v} f + v^2 W \frac{\partial f}{\partial v} - \left(\frac{2}{9\pi}\right)^{\frac{1}{2}} \frac{\ell n \Lambda_o}{2\pi} W \qquad (7.13)$$

where $A = 2\pi v_e \lambda_D^3$ and $B = v_e \lambda_D^3 / k_B T$. Using a specific atmospheric model (such as the one described above), the numerical code could in principle be generalized to incorporate the additional terms in (7.12) and (7.13). There is an important qualitative difference, however, between (7.13) and (5.6) which complicates the problem of obtaining a numerical solution: the wave refraction term depends on $\partial W/\partial v$, and so there is an explicit coupling between adjacent values of W in the velocity grid. It can be seen from Figure 5.3 that W rises and falls rapidly in velocity space, and in fact when instability first appears we find that $|\partial W/\partial v|$ is extremely large at the edges of the quasi-linear plateau. The interface between the stable and

unstable regions of velocity space is rather analogous to a shock front in fluid mechanics, and it creates similar numerical problems (see, e.g., Richtmeyer and Morton, 1967). Attempts carried out so far by the present author to obtain a stable numerical solution of (7.12) and (7.13), using a simple finite difference algorithm, have failed whenever a realistic density gradient is prescribed. Specifically, it is found that rapidly growing oscillations appear in the wave spectrum shortly after the onset of instability, at which point the total wavelevel is only a small fraction of its value in the homogeneous case. This may be due simply to numerical instability, or it may perhaps indicate a real physical effect. Further work on this problem is clearly desirable, although in order to progress it may be necessary to resort to completely different numerical methods from those which were used successfully in the homogeneous case.

7.3 Induced and Spontaneous Scattering on Ions

The induced and spontaneous scattering of Langmuir waves on thermal ions can be represented by two additional terms in the evolution equation for the waves. It is convenient to separate the wave distribution into two components, W and W′, propagating in opposite directions: omitting electron-wave interaction terms, we can then write

$$\frac{\partial W}{\partial t} + \frac{3}{v} \cdot \frac{\partial W}{\partial x} = \alpha(W', W, v) + \gamma(W', v)W \qquad (7.14)$$

$$\frac{\partial W'}{\partial t} + \frac{3}{v'} \cdot \frac{\partial W'}{\partial x} = \alpha(W, W', v') + \gamma(W, v')W' \qquad (7.15)$$

where γ and α are the coefficients of induced and spontaneous scattering and $v'>0$ is the modulus of the phase velocity in the counterstreaming direction. Assuming equal electron and ion temperatures, the appropriate expressions for γ and α in one dimension are (Tsytovich and Shapiro 1965; Grognard 1985)

$$\gamma = \frac{1}{32}\left(\frac{18}{\pi}\right)^{\frac{1}{2}}\left(\frac{m_p}{m_e}\right)^{\frac{1}{2}}\int_1^{\infty} W'(v')\left(\frac{1}{v'}-\frac{1}{v}\right)\exp\left[-\frac{9}{8}\left(\frac{m_p}{m_e}\right)\left(\frac{1}{v'}-\frac{1}{v}\right)^2\right]dv' \tag{7.16}$$

$$\alpha = \frac{1}{16\pi}\left(\frac{1}{2\pi}\right)^{\frac{1}{2}}\left(\frac{m_p}{m_e}\right)^{\frac{1}{2}}\frac{1}{v^4}\int_1^{\infty}\frac{W'(v')-W(v)}{\frac{1}{v'}+\frac{1}{v}}\exp\left[-\frac{9}{8}\left(\frac{m_p}{m_e}\right)\left(\frac{1}{v'}-\frac{1}{v}\right)^2\right]dv' \tag{7.17}$$

where the electron mass is now denoted by m_e. The scattering rates in (7.15) can be obtained by interchanging the primed and unprimed quantities in (7.16) and (7.17).

It is clear that in general the interaction between the two populations of Langmuir waves is rather complicated, and that little progress can be made analytically. Note that γ can be a growth rate in some parts of the wave spectrum, and a damping rate in others. The counterstreaming Langmuir waves peak at a phase velocity which is displaced from that of the primary wave spectrum by an amount

$$\frac{\Delta v}{v} = \frac{2}{3}\left(\frac{m_e}{m_p}\right)^{\frac{1}{2}} v \simeq 1.6 \times 10^{-2}\, v \tag{7.18}$$

(Zheleznyakov and Zaitsev 1970). For typical beam velocities, this implies that $\Delta v/v \lesssim 0.1$, whereas the numerical results of Chapters 5 and 6 show that the waves have a bandwidth which is close to unity. The induced scattering growth rate used by

Emslie and Smith (1984) is based on the assumption of monochromatic Langmuir waves, which is only valid if the phase velocity shift $\Delta v/v$ is large compared with the bandwidth (Smith 1977). In our case, that condition is clearly not satisfied and the finite bandwidth of the primary wave spectrum must be taken into account.

In order to determine the extent to which Langmuir waves are scattered into the counterstreaming direction (thus satisfying the kinematic conditions required for 2nd harmonic radiation to be produced), the quasi-linear equations should be solved numerically as before, with the additional terms in (7.14) and (7.15) being taken into account. Collisional and Landau damping of counterstreaming waves should also be included in the calculation. Several authors (e.g Smith and Fung 1971; Grognard 1985) have carried out numerical simulations of induced and spontaneous scattering in the case of a homogeneous collisionless beam, and the results appear to indicate an asymptotic state in which the energy density of waves propagating in the backward direction is approximately equal to that of waves propagating in the forward direction. However, such calculations may be of little relevance to the realistic case of an inhomogeneous beam in a collision-dominated plasma (cf. Grognard 1985).

APPENDIX A

THE COLLISIONAL ENERGY LOSS RATE OF AN ELECTRON IN A WARM TARGET

Consider an electron propagating through a fully ionized plasma with velocity $\underline{v}$, undergoing a collision with a field electron. The field electrons have a Maxwellian distribution of velocities, density n and temperature T. The impact parameter giving a large deflection angle is much less than the mean separation of the field particles, so that only binary interactions need to be considered. Let $\Delta v_{\parallel}$ and $\Delta v_{\perp}$ be the changes in the parallel and perpendicular velocity components resulting from the collision (the parallel direction being defined by $\underline{v}$). Then the energy gained by the electron is given by

$$\Delta E = \frac{1}{2} m \left[(v + \Delta v_{\parallel})^2 + \Delta v_{\perp}^2 - v^2 \right]$$

$$= \frac{1}{2} m \left[\Delta v_{\parallel}^2 + \Delta v_{\perp}^2 + 2v \, \Delta v_{\parallel} \right] \qquad (A.1)$$

The energy loss rate associated with such collisions is therefore given by

$$\frac{dE}{dt} = \langle \Delta E \rangle = \frac{1}{2} m \left[\langle \Delta v_{\parallel}^2 \rangle + \langle \Delta v_{\perp}^2 \rangle + 2v \langle \Delta v_{\parallel} \rangle \right] \qquad (A.2)$$

where the brackets $\langle\rangle$ denote the average increase of a quantity per unit time. The diffusion coefficients $\langle \Delta v_{\parallel}^2 \rangle$, $\langle \Delta v_{\perp}^2 \rangle$ and $\langle \Delta v_{\parallel} \rangle$ were originally evaluated by Chandrasekhar (1942) in the context of stellar dynamics. Applying his results to the present problem yields

$$< \Delta v_{\parallel} > = - \frac{4K}{m\, k_B\, T} \quad n\, G(y) \qquad (A.3)$$

$$< \Delta v_{\parallel}^2 > = \frac{4K}{m^2\, v} \quad n\, G(y) \qquad (A.4)$$

$$< \Delta v_{\perp}^2 > = \frac{4K}{m^2\, v}\, n\, (\Phi(y) - G(y)) \qquad (A.5)$$

where $y=(E/k_BT)^{\frac{1}{2}}$,

$$\Phi(y) = \frac{2}{\sqrt{\pi}} \int_o^y e^{-t^2}\, dt \qquad (A.6)$$

is the error function and

$$G(y) = \frac{1}{2\, y^2} (\Phi(y) - y\, \Phi'(y)) \qquad (A.7)$$

Substituting (A.3), (A.4) and (A.5) into (A.2) yields

$$\frac{dE}{dt} = \frac{2Kn}{mv} (\Phi(y) - 4y^2\, G(y))$$

i.e.

$$\frac{dE}{dt} = - \frac{K}{E}\, n\, v\, [\ \Phi(y) - 2y\, \Phi'(y)\ ] \qquad (A.8)$$

APPENDIX B

NUMERICAL METHOD

Our numerical technique is closely based on that described by Grognard (1985). In order to write the discretised equations in a compact form, we introduce the finite difference operators ∂_j^+ and ∂_j^- such that

$$\partial_j^+ f_j = \frac{f_{j+1} - f_j}{\Delta v} \qquad (B.1)$$

$$\partial_j^- f_j = \frac{f_j - f_{j-1}}{\Delta v}$$

where $f_j = f(v_j)$, f being an arbitrary function of velocity, and Δv is the (constant) finite difference step in velocity space. A similar notation is used to denote finite differences in coordinate space and time.

B.1 The Steady State Problem

We consider first the steady state equations, (5.5) and (5.6). The evolution equation for the electrons can be discretised in the form

$$v_j \partial_i^+ f_j^i = \partial_j^- [(\alpha_{j+1} + \beta_{j+1}) f_{j+1}^i + (v_j W_j^i + \frac{\beta_j}{v_j}) \partial_j^+ f_{j+1}^{i+1}]$$

$$(2 \leq j \leq m-1 \; ; \quad 1 \leq i \leq n-1) \qquad (B.3)$$

where $\alpha_j = \ell n \, v_j / 2\pi v_j^2$ and $\beta_j = \ell n \Lambda / 2\pi v_j^2$. The phase space grid contains n coordinate points and m velocity points. f_j^1 is given by the boundary condition (5.10). (B.3) can be written in the tri-diagonal matrix form

$$-A_j f_{j-1}^{i+1} + (1 + A_j + B_j) f_j^{i+1} - B_j f_{j-1}^{i+1} = C_j \qquad (B.4)$$

where

$$A_j = \frac{\Delta x}{\Delta v^2 v_j} \left(v_{j-1} W_{j-1}^i + \frac{\beta_{j-1}}{v_{j-1}} \right) \qquad (B.5)$$

$$B_j = \frac{\Delta x}{\Delta v^2 v_j} \left(v_j W_j^i + \frac{\beta_j}{v_j} \right) \qquad (B.6)$$

$$C_j = f_j^i \left[1 - \frac{\Delta x}{\Delta v\, v_j} (\alpha_j + \beta_j) \right] + f_{j+1}^i \left[\frac{\Delta x}{\Delta v\, v_j} (\alpha_{j+1} + \beta_{j+1}) \right] \qquad (B.7)$$

Δx being the finite difference step in coordinate space. (B.4) is solved for f_j^{i+1} in terms of f_j^i, W_j^i by setting

$$f_j^{i+1} = E_j f_{j+1}^{i+1} + F_j \quad (1 \leq j \leq m-1) \qquad (B.8)$$

It can then be easily shown (Roache 1972, Appendix A) that, for $j \geq 2$,

$$E_j = \frac{B_j}{1 + B_j + A_j (1 - E_{j-1})} \qquad (B.9)$$

$$F_j = \frac{A_j F_{j-1} + C_j}{1 + B_j + A_j (1 - E_{j-1})} \qquad (B.10)$$

Using the lower velocity space boundary condition at v=1 ($f_1^{i+1} = f_1^i$), it can be seen from (B.8) with j=1 that $E_1=0$ and $F_1=f_1^i$. E_j and F_j for $j \geq 2$ are then given by (B.9) and (B.10). Finally, using the upper velocity space boundary condition

($f_m^{i+1} = f_m^i = 0$), f_j^{i+1} can be obtained from (B.8). The boundary conditions are such that a sufficient condition for f_j^{i+1} to be positive definite is that A_j, B_j and C_j are all positive. This requires that $f_j^i, W_j^i > 0$ and also that

$$\Delta x \leq \frac{\Delta v \; v_j}{\alpha_j + \beta_j}$$

i.e.

$$\Delta x \leq \frac{2\pi}{\ell n \, \Lambda} \Delta v \qquad (B.11)$$

In the stable regime ($\partial f/\partial v < 0$), the wavelevel is then given by the discretised form of (5.7):

$$W_j^{i+1} = \frac{v_j \alpha_j f_j^{i+1}}{\gamma_c - v_j^2 \partial_j^+ f_j^{i+1}} \quad (1 \leq j \leq m-1) \qquad (B.12)$$

where $\gamma_c = (2/9\pi)^{\frac{1}{2}} \ell n \, \Lambda_o / 2\pi$. W_j^1 is given by (B.12), with f_j^1 replacing f_j^{i+1}. In the unstable regime ($\partial f/\partial v > 0$), W_j^{i+1} is obtained from the finite difference equation

$$\frac{3}{v_j} \partial_i^+ W_j^i = \alpha_j v_j f_j^{i+1} + W_j^i (v_j^2 \partial_j^+ f_j^{i+1} - \gamma_c) \qquad (B.13)$$

i.e.

$$W_j^{i+1} = W_j^i \left(1 + \frac{v_j^3 \Delta x}{3} \partial_j^+ f_j^{i+1} - \frac{v_j \Delta x}{3} \gamma_c\right)$$

$$+ \frac{\alpha_j v_j^2 \Delta x}{3} f_j^{i+1} \quad (1 \leq j \leq m-1) \qquad (B.14)$$

W_m^{i+1} is prescribed to be zero.

(5.11) (the Fokker-Planck equation) can also be written in the form of (B.4). The coefficients are identical, except that $W_j^i = 0$ and $\alpha_j = 0$, and the same method of solution can be used. In this case, an analytical solution exists for large v, which

can be used to test the accuracy of the code (see Section 5.3).

B.2 Reverse Currents

The integral in (5.25) is evaluated for each space point using the quadrature approximation

$$b_i \equiv \int_0^\infty f_b\,(x_i,v')\,dv' \simeq \sum_{j=1}^{m} f_{b_j}^{\,i}\; w_j\;\Delta v \qquad (B.15)$$

where the weights w_j are those appropriate to Simpson's rule (note that in this case m should strictly be odd). (5.25) can then be approximated by the finite difference equation

$$v_j\;\partial_i^+ f_j^i \;-\; a\,b_i\;\partial_j^- f_{j+1}^i = \partial_j^-\left[(\alpha_{j+1}+\beta_{j+1})\,f_{j+1}^i + \left(v_j\,W_j^i + \frac{\beta_j}{v_j}\right)\partial_j^+ f_{j+1}^{i+1}\right] \qquad (B.16)$$

which can be solved for f_j^{i+1} by the same method as before, except that

$$C_j = f_j^i\left[1 - \frac{\Delta x}{\Delta v\;v_j}\,(\alpha_j+\beta_j+a\,b_i)\right] + f_{j+1}^i\left[\frac{\Delta x}{\Delta v\;v_j}\,(\alpha_{j+1}+\beta_{j+1}+a\,b_i)\right] \qquad (B.17)$$

The sufficient condition for f_j^{i+1} to be positive definite is now

$$\Delta x \;\lesssim\; \frac{2\pi\;\Delta v}{\ell n\;\Lambda + 2\pi\;a\;b_i} \qquad (B.18)$$

B.3 The Time Dependent Problem

The discrete form of the time dependent evolution equation for the electrons is

$$\partial_k^- f^i_{jk} + v_j \partial_i^+ f^i_{jk} = \partial_j^- \left[(\alpha_{j+1} + \beta_{j+1}) f^i_{j+1k} + (v_j W^i_{jk} + \frac{\beta_j}{v_j}) \partial_j^+ f^{i+1}_{j+1k} \right] \qquad (B.19)$$

$(2 \leq j \leq m-1 \; ; \quad 1 \leq i \leq n-1 \; ; \quad 2 \leq k \leq \ell \;)$

We use a boundary value approach, integrating forward in space rather than time. (B.19) can be written in the form

$$- A_j f^{i+1}_{j-1k} + (1 + A_j + B_j) f^{i+1}_{jk} - B_j f^{i+1}_{j+1k} = C_j \qquad (B.20)$$

where A_j and B_j are given by (B.5) and (B.6) (with W^i_{jk} replacing W^i_j), and C_j is now given by

$$C_j = f^i_{jk} \left[1 - \frac{\Delta x}{\Delta v \, v_j} (\alpha_j + \beta_j) \right] + f^i_{j+1k} \left[\frac{\Delta x}{\Delta v \, v_j} (\alpha_{j+1} + \beta_{j+1}) \right] - \frac{\Delta x}{v_j} \partial_k^- f^i_{jk} \qquad (B.21)$$

The system (B.20) can be solved for f^{i+1}_{jk} in terms of f^i_{jk}, W^i_{jk} $\forall k>1$, by the same method as that used in the steady state case. We again impose the velocity space boundary condition $f^{i+1}_{jk} = f^i_{jk}$. Close to the thermal speed, f relaxes rapidly to a Maxwellian distribution (cf. Section 5.4), and is thereafter maintained at an essentially constant level. The initial beam distribution given by (6.10), however, is spatially dependent: $f_b(x,v,t_o)$ becomes negligibly small at $v \simeq v_e$ for sufficiently large x. We therefore have the possibility of $f^i_{j2} >> f^i_{j1}$ for small j and i>>1. This would give rise to an unphysically large time derivative, $\partial_k^- f^i_{jk}$, which in turn may result in C_j becoming negative. To avoid the consequent risk of numerical instabilty,

we therefore introduce the modified beam distribution (6.16) at $t=t_0$. The boundary condition given by (6.2) is modified in a similar way, although this is not actually necessary for numerical stability.

In the stable regime, W_{jk}^{i+1} is given by

$$W_{jk}^{i+1} = \frac{v_j \alpha_j f_{jk}^{i+1}}{\gamma_c - v_j^2 \partial_j^+ f_{jk}^{i+1}} , \quad k \geq 1 \qquad (B.22)$$

which also defines the boundary and initial conditions for W. In the unstable regime,

$$W_{jk}^{i+1} = W_{jk}^{i} \left(1 + \frac{\Delta x}{3} v_j^3 \partial_j^+ f_{jk}^{i+1} - \frac{\Delta x}{3} v_j \gamma_c \right) + \frac{\alpha_j v_j^2 \Delta x}{3} f_{jk}^{i+1} - \frac{\Delta x v_j}{3} \partial_k^- W_{jk}^{i} \qquad (B.23)$$

REFERENCES

Achterberg, A.: 1981, Astron. Astrophys. 97, 259.

Acton, L.W., Canfield, R.C., Gunkler, T.A., Hudson, H.S., Kiplinger, A.L. and Leibacher, J.W.: 1982, Astrophys. J. 263, 409.

Antiochos, S.K. and Sturrock, P.A.: 1978, Astrophys. J. 220, 1137.

Antonucci, E. and Dennis, B.R.: 1983, Solar Phys., 86, 67.

Ayres, T.R. and Linsky, J.L.: 1976, Astrophys. J. 205, 874.

Bai, T.: 1982, Astrophys. J. 259, 341.

Bai, T. and Ramaty, R.: 1976, Solar Phys. 49, 343.

Barbosa, D.D.: 1979, Astrophys. J. 233, 383.

Benz, A.O.: 1986, Solar Phys. 104, 99.

Benz, A.O. and Kane, S.R.: 1986, Solar Phys. 104,179.

Benz, A.O., Bernold, T.E.X. and Dennis, B.R.: 1983, Astrophys. J. 271, 355.

Biskamp, D.: 1982, Phys. Lett. A 87, 357.

Biskamp, D.: 1986, Phys. Fluids 29, 1520.

Boldt, E. and Serlemitsos, P.: Astrophys. J. 157, 557.

Brown, J.C.: 1971, Solar Phys. 18, 489.

Brown, J.C.: 1972, Solar Phys. 26, 441.

Brown, J.C.: 1974, IAU Symp. 57, 395.

Brown, J.C.: 1975, IAU Symp. 68, 245.

Brown, J.C.: 1976, Phil. Trans. Roy. Soc. Lond. A281, 473.

Brown, J.C. and Bingham, R.: 1984, Astron. Astrophys. Letters 131, L11.

Brown, J.C. and Hayward, J.: 1982, Solar Phys. 80, 129.

Brown, J.C. and Hoyng, P.: 1975, Astrophys. J. 200, 734.

Brown, J.C. and McClymont, A.N.: 1974, Solar Phys. 41, 135.

Brown, J.C. and Smith, D.F.: 1980, Rep. Prog. Phys. 43, 125.

Brown, J.C., Craig, I.J.D. and Karpen, J.T.: 1980, Solar Phys. 67, 143.

Brown, J.C., Loran, J.M. and MacKinnon, A.L.: 1985, Astron. Astrophys. Letters 147, L10.

Brown, J.C., Melrose, D.B. and Spicer, D.S.: 1979, Astrophys. J. 228, 592.

Bruzek, A.: 1964, Astrophys. J. 140, 746.

Canfield, R.C. and Gunkler, T.A.: 1985, Astrophys. J. 288, 353.

Canfield, R.C., Gunkler, T.A. and Ricchiazzi, P.J.: 1984 Astrophys. J. 282, 296.

Canfield, R.C., Bely-Dubau, F., Brown, J.C., Dulk, G.A., Emslie, A.G., Enome, S., Gabriel, A.H., Kundu, M.R., Melrose, D.B., Neidig, D.F., Ohki, K., Petrosian, V., Poland, A.I., Rieger, E., Tanaka, K. and Zirin, H.: 1986, in M.R. Kundu and B. Woodgate (eds.), 'Energetic Phenomena on the Sun', NASA CP-2439.

Carrington, R.C.: 1859, Mon. Not. Roy. Astron. Soc. 20, 13.

Chandrasekhar, S.: 1942, 'Principles of Stellar Dynamics', University of Chicago Press.

Cheng, C.-C. and Widing, K.G.: 1975, Astrophys. J. 201, 735.

Chupp, E.L., Forrest, D.J., Higbie, P.R., Suri, A.N., Tsai, C. and Dunphy, P.P.: 1973, Nature 241, 333.

Chupp, E.L., Forrest, D.J., Ryan, J.M., Heslin, J., Reppin, C., Pinkau, K., Kanbach, G., Rieger, E. and Shore, G.H.: 1982, Astrophys. J. Letters 263, L95.

Cowley, S.W.H.: 1985,in E.R. Priest (ed.), 'Solar System Magnetic Fields', Dordrecht-Reidel.

Craig, I.J.D.: 1979, Astron. Astrophys. 79, 121.

Craig, I.J.D.: 1981, in E.R. Priest (ed.), 'Solar Flare Magnetohydrodynamics', Gordon and Breach.

Craig, I.J.D. and Brown, J.C.: 1976, Astron. Astrophys. 49, 239.

Craig, I.J.D. and Brown, J.C.: 1986, 'Inverse Problems in Astronomy', Adam Hilger.

Craig, I.J.D., MacKinnon, A.L. and Vilmer, N.: 1985, Astrophys. Space Sci. 116, 377.

Crannell, C.J., Frost, K.J., Matzler, C., Ohki, K. and Saba, J.L.: 1978, Astrophys. J. 223, 620.

Datlowe, D.W. and Lin, R.P.: 1973, Solar Phys. 32, 459.

Datlowe, D.W., O'Dell, S.L., Peterson, L.E. and Elcan, M.J.: 1977, Astrophys. J. 212, 561.

Davidson, R.C.: 1972, 'Methods in Nonlinear Plasma Theory', Academic Press.

Decker, R.B. and Vlahos, L.: 1986, Astrophys. J. 306, 710.

de Jager, C. and de Jonge, G.: 1978, Solar Phys. 58, 127.

Dennis, B.R.: 1985, Solar Phys. 100, 465.

Dennis, B.R., Chupp, E.L., Crannell, C.J., Doschek, G.A., Hudson, H.S., Hurford, G.J., Kane, S.R., Lin, R.P., Prince, T., Ramaty, R., Share, G. and Tandberg-Hanssen, E.A.: 1986, 'MAX'91', NASA publication.

Dermer, C.D. and Ramaty, R.: 1986, Astrophys. J. 301, 962.

Dietrich, W.F. and Simpson, J.A.: 1978, Astrophys. J. Letters 225, L41.

Duijveman, A., Hoyng, P. and Machado, M.E.: 1982, Solar Phys. 81, 137.

Dulk, G.A. and Marsh, K.A.: 1982, Astrophys. J. 259, 350.

Ellison, D.C. and Ramaty, R.: 1985, Astrophys. J. 298, 400.

Emslie, A.G.: 1980, Astrophys. J. 235, 1055.

Emslie, A.G.: 1981a, Astrophys. J. 245, 711.

Emslie, A.G.: 1981b, Astrophys. J. 249, 817.

Emslie, A.G.: 1983, Astrophys. J. 271, 367.

Emslie, A.G.: 1985, Solar Phys. 98, 281.

Emslie, A.G. and Brown, J.C.: 1985, Astrophys. J.295, 648.

Emslie, A.G. and Nagai, F.: 1985, Astrophys. J. 288, 779.

Emslie, A.G. and Smith, D.F.: 1984, Astrophys. J. 279, 882.

Emslie, A.G. and Vlahos, L.: 1980, Astrophys. J. 242, 359.

Emslie, A.G., Brown, J.C. and Donnelly, R.F.: 1978, Solar Phys. 57, 175.

Forbes, T.G. and Priest, E.R.: 1982, Solar Phys. 81, 303.

Forman, M.A., Ramaty, R. and Zweibel, E.G.: 1986, in P.A. Sturrock, T.E. Holzer, D.M. Mihalas and R.K. Ulrich (eds.), 'Physics of the Sun', Vol. 2, Dordrecht-Reidel.

Ginzburg, V.L.: 1961, 'Propagation of Electromagnetic Waves in Plasmas', Gordon and Breach.

Ginzburg, V.L. and Syrovatskii, S.I.: 1964, 'The Origin of Cosmic Rays', Pergamon Press.

Gold, T. and Hoyle, F.: 1960, Mon. Not. Roy. Astron. Soc. 120, 89.

Goldman, M.V.: 1983, Solar Phys. 89, 403.

Goldman, M.V., Reiter, G.F. and Nicholson, D.R.: 1980, Phys. Fluids 23, 388.

Gradshteyn, I.S. and Ryzhik, I.M.: 1980, 'Table of Integrals, Series and Products', Academic Press.

Green, R.M. and Sweet, P.A.: 1966, Astrophys. J. 147, 1153.

Grognard, R.J.-M.: 1975, Aust. J. Phys. 28, 731.

Grognard, R.J.-M.: 1985, in D.J. McLean and N.R. Labrum (eds.), 'Solar Radiophysics', Cambridge University Press., Ch. 11.

Hamilton, R.J. and Petrosian, V.: 1987, Astrophys. J. (in press).

Harris, E.G.: 1969, Adv. Plasma Phys. 3, 157.

Haug, E. and Elwert, G.: 1985, Solar Phys. 99, 219.

Heitler, W.: 1954, 'The Quantum Theory of Radiation', Oxford University Press.

Henoux, J.C.: 1975, Solar Phys. 42, 219.

Heyvaerts, J.: 1981, in E.R. Priest (ed.), 'Solar Flare Magnetohydrodynamics', Gordon and Breach.

Heyvaerts, J., Priest, E.R. and Rust, D.M.: 1977, Astrophys. J. 216, 123.

Hodgson, R.: 1859, Mon. Not. Roy. Astron. Soc. 20, 15.

Holman, G.D.: 1985, Astrophys. J. 293, 584.

Holman, G.D., Kundu, M.R. and Papadopoulos, K.: 1982, Astrophys. J. 257, 354.

Holt, S.S. and Cline, T.L.: 1968, Astrophys. J. 154, 1027.

Hoyng, P. and Melrose, D.B.: 1977, Astrophys. J. 218, 866.

Hoyng, P., Brown, J.C. and Van Beek, H.F.: 1976, Solar Phys. 48, 197.

Hoyng, P., Melrose, D.B. and Adams, J.C.: 1979, Astrophys. J. 230, 950.

Hudson, H.S.: 1972, Solar Phys. 24, 414.

Hudson, H.S.: 1985, Solar Phys. 100, 515.

Hudson, H.S. and Ohki, K.: 1972, Solar Phys. 23, 155.

Ichimoto, K. and Kurokawa, K.: 1984, Solar Phys. 93, 105.

Kahler, S.: 1971, Astrophys. J. 164, 365.

Kane, S.R.: 1983, Solar Phys. 86, 355.

Kane, S.R. and Anderson, R.A.: 1970, Astrophys. J. 162, 1003.

Kane, S.R., Fenimore, E.E., Klebesadel, R.W. and Laros, J.G.: 1982, Astrophys. J. Letters 254, L53.

Kane, S.R., Anderson, K.A., Evans, W.D., Klebesadel, R.W. and Laros, J.G.: 1979, Astrophys. J. Letters 233, L151.

Kaufmann, P., Strauss, F.M. and Schaal, R.E.: 1983, Solar Phys. 78, 389.

Kaufmann, P., Correia, E., Costa, J.E.R. and Zodi Vaz, A.M.: 1986, Astron. Astrophys. 157, 11.

Kaufmann, P., Correia, E., Costa, J.E.R. and Zodi Vaz, A.M.: 1985a, Nature 313, 380.

Kaufmann, P., Correia, E., Costa, J.E.R., Sawant, H.S. and Zodi Vaz, A.M.: 1985b, Solar Phys. 95, 155.

Kel'ner, S.R. and Skrynnikov, Yu.I.: 1985, Soviet Astron.-AJ 29, 445.

Kiplinger, A.L., Dennis, B.R., Emslie, A.G., Frost, K.J. and Orwig, L.E.: 1983a, Astrophys. J. Letters 265, L99.

Kiplinger, A.L., Dennis, B.R., Frost, K.J. and Orwig, L.E.: 1983b, Astrophys. J. 273, 783.

Klein, K.-L.: 1987, Astron. Astrophys. (submitted).

Klein, K.-L., Trottet, G. and Magun, A.: 1986, Solar Phys. 104, 243.

Knight, J.W. and Sturrock, P.A.: 1977, Astrophys. J. 218, 306.

Korchak, A.A.: 1967, Soviet Astron.-AJ 11, 258.

Korchak, A.A.: 1971, Solar Phys. 18, 284.

Krall, N.A. and Trivelpiece, A.W.: 1973, 'Principles of Plasma Physics', McGraw-Hill.

Kuijpers, J. and Melrose, D.B.: 1985, Astrophys. J. 294, 28.

Landau, L.D.: 1946, J. Phys. (USSR) 10, 25.

LaRosa, T.N.: 1987, Astrophys. J. (submitted).

Leach, J. and Petrosian, V.: 1981, Astrophys. J. 251, 781.

Leach, J. and Petrosian, V.: 1983, Astrophys. J. 269, 715.

Leach, J., Emslie, A.G. and Petrosian, V.: 1985, Solar Phys. 96, 331.

Lin, R.P.: 1974, Space Sci. Rev. 16, 189.

Lin, R.P.: 1985, Solar Phys. 100, 537.

Lin, R.P., Schwartz, R.A., Pelling, R.M. and Harley, K.C.: 1981a, Astrophys. J. Letters 251, L109.

Lin, R.P., Potter, D.W., Gurnett, D.A. and Scarf, F.L.: 1981b, Astrophys. J. 251, 369.

McClements, K.G.: 1987a, in preparation.

McClements, K.G.: 1987b, Solar Phys. (in press).

McClements, K.G.: 1987c, Astron. Astrophys. 175, 255.

McClements, K.G. and Brown, J.C.: 1986, Astron. Astrophys. 165, 235.

McClements, K.G., Brown, J.C. and Emslie, A.G.: 1986, in B.R. Dennis, L.E. Orwig and A.L. Kiplinger (eds.), 'Rapid Fluctuations in Solar Flares', NASA CP-2449.

Machado, M.E., Emslie, A.G. and Brown, J.C.: 1978, Solar Phys. 58, 363.

MacKinnon, A.L.: 1987, Astron. Astrophys. (submitted).

MacKinnon, A.L. and Brown, J.C.: 1984, Astron. Astrophys. 132, 229.

MacKinnon, A.L., Brown, J.C. and Hayward, J.: 1985, Solar Phys. 99, 231.

MacKinnon, A.L., Costa, J.E.R., Kaufmann, P. and Dennis, B.R.: 1986, Solar Phys. 104, 191.

McLean, D.J. and Labrum, N.R.: 1985, (eds.) 'Solar Radiophysics', Cambridge University Press.

McQuillan, P., Cromwell, D. and Brown, J.C.: 1987, Solar Phys. (submitted).

Mariska, J.T. and Poland, A.I.: 1985, Solar Phys. 96, 317.

Marsh, K.A. and Hurford, G.J.: 1980, Astrophys. J. Letters 240, L111.

Melrose, D.B.: 1980a, 'Plasma Astrophysics', Vol. 1, Gordon and Breach.

Melrose, D.B.: 1980b, 'Plasma Astrophysics', Vol. 2, Gordon and Breach.

Melrose, D.B.: 1985, in D.J. McLean and N.R. Labrum (eds.), 'Solar Radiophysics', Cambridge University Press, Ch. 8.

Melrose, D.B.: 1986, 'Instabilities in Space and Laboratory Plasmas', Cambridge University Press.

Melrose, D.B. and Brown, J.C.: 1976, Mon. Not. Roy. Astron. Soc. 176, 15.

Melrose, D.B. and Dulk, G.A.: 1982, Astrophys. J. 259, 844.

Melrose, D.B. and Dulk, G.A.: 1984, Astrophys. J. 282, 308.

Moghaddam-Taaheri, E., Vlahos, L., Rowland, H.L. and Papadopoulos, K.: 1985, Phys. Fluids 28, 3356.

Montgomery, D.C. and Tidman, D.A.: 1964, 'Plasma Kinetic Theory', McGraw-Hill.

Moore, R.O., McKenzie, D.L., Svestka, Z., Widing, K.G., Antiochos, S.K., Dere, K.P., Dodson-Prince, H.W., Hiei, E., Krall, K.R., Krieger, A.S., Mason, H.E., Petrasso, R.D., Pneuman, G.W., Silk, J.K., Vorpahl, J.A. and Withbroe, G.L.: 1980, in P.A. Sturrock (ed.), 'Solar Flares', Colorado Associated Univerisity Press.

Muschietti, L., Goldman, M.V. and Newman, D.: 1985, Solar Phys. 96, 181.

Nambu, M.: 1986, Astrophys. J. 303, 347.

Norman, C. and Smith, R.: 1978, Astron. Astrophys. 68, 145.

Orwig, L.E., Frost, K.J. and Dennis, B.R.: 1980, Solar Phys. 65, 25.

Parker, E.N.: 1963, Astrophys. J. Suppl. Ser. 8, 177.

Penrose, O.: 1960, Phys. Fluids 3, 258.

Peterson, L.E. and Winckler, J.R.: 1959, J. Geophys. Res. 64, 697.

Petrosian, V.: 1981, Astrophys. J. 251, 727.

Petschek, H.E.: 1964, in 'AAS-NASA Symp. on Solar Flares', NASA SP-50.

Poland, A.I., Machado, M.E., Wolfson, C.J., Frost, K.J., Woodgate, B.E., Shine, R.A., Kenny, P.J., Cheng, C.-C., Tandberg-Hanssen, E.A., Bruner, E.C. and Henze, W.: 1982, Solar Phys. 78, 201.

Priest, E.R.: 1982, 'Solar Magnetohydrodynamics', Dordrecht-Reidel.

Priest, E.R.: 1986, Solar Phys. 104, 1.

Priest, E.R., Cargill, P., Forbes, T.G., Hood, A.W. and Steinolfson, R.S.: 1986, in M.R. Kundu and B. Woodgate (eds.), 'Energetic Phenomena on the Sun', NASA CP-2439.

Ramaty, R.: 1969, Astrophys. J. 158, 753.

Ramaty, R.: 1986, in P.A. Sturrock, T.E. Holzer, D.M. Mihalas and R.K. Ulrich (eds.), 'Physics of the Sun', Vol. 2, Dordrecht-Reidel.

Ramaty, R. and Petrosian, V.: 1972, Astrophys. J. 178, 241.

Ramaty, R., Kozlovsky, B. and Lingenfelter, R.E.: 1975, Space Sci. Rev. 18, 341.

Ramaty, R., Murphy, R.J., Kozlovsky, B. and Lingenfelter, R.E.: 1983, Astrophys. J. Letters 273, L41.

Ramaty, R., Colgate, S.A., Dulk, G.A., Hoyng, P., Knight, J.W., Lin, R.P., Melrose, D.B., Orrall, F., Paizis, C., Shapiro, P.R., Smith, D.F. and Van Hollebeke, M.: 1980, in P.A. Sturrock (ed.), 'Solar Flares', Colorado Associated University Press.

Reames, D.V., Von Rosenvinge, T.T. and Lin, R.P.: 1985, Astrophys. J. 292, 716.

Richtmeyer, R.D. and Morton, K.W.: 1967, 'Difference Methods for Initial Value Problems', Interscience.

Rieger, E., Reppin, C. Kanbach, G., Forrest, D.J., Chupp, E.L. and Share, G.H.: 1983, 'Proc. 18th Int. Cosmic Ray Conf.', Bangalore, 1983.

Roache, P.J.: 1972, 'Computational Fluid Dynamics', Hermosa-Albuquerque.

Rowland, H.L. and Vlahos, L.: 1985, Astron. Astrophys. 142, 219.

Sakurai, T. and Uchida, Y.: 1977, Solar Phys. 52, 397.

Shapiro, V.D.: 1963, Soviet Phys.-JETP 17, 416.

Shimabukuro, F.I.: 1972, Solar Phys. 23, 169.

Simnett, G.M.: 1974, Space Sci. Rev. 16, 257.

Slottje, C.: 1978, Nature 275, 520.

Smith, D.F.: 1977, Astrophys. J. Letters 216, L53.

Smith, D.F.: 1980, Solar Phys. 66, 135.

Smith, D.F. and Brown, J.C.: 1980, Astrophys. J. 242, 799.

Smith, D.F. and Fung, P.C.W.: 1971, J. Plasma Phys. 5, 1.

Smith, D.F. and Lilliequist, C.G.: 1979, Astrophys. J. 232, 582.

Smith, D.F. and Spicer, D.S.: 1979, Solar Phys. 62, 359.

Soward, A.M. and Priest, E.R.: 1977, Phil. Trans. Roy. Soc. Lond. A284, 369.

Soward, A.M. and Priest, E.R.: 1982, J. Plasma Phys. 17, 337.

Spicer, D.S.: 1977, Solar Phys. 53, 305.

Spicer, D.S. and Sudan, R.N.: 1984, Astrophys. J. 280, 448.

Spitzer, L.: 1962, 'Physics of Fully Ionized Gases', Interscience.

Stähli, M. and Benz, A.O.: 1987, Astron. Astrophys. 175, 271.

Stähli, M. and Magun, A.: 1986, Solar Phys. 104, 117.

Steinolfson, R.S. and Van Hoven, G.: 1984a, Astrophys. J. 276, 391.

Steinolfson, R.S. and Van Hoven, G.: 1984b, Phys. Fluids 27, 1207.

Sturrock, P.A.: 1968, IAU Symp. 35, 471.

Sudan, R.N.: 1984, in M.N. Rosenbluth and R.Z. Sagdeev (eds.), 'Handbook of Plasma Physics', Vol. 2, Elsevier Science Publishers B.V..

Svestka, Z.: 1972, Ann. Rev. Astron. Astrophys. 10, 1.

Svestka, Z.: 1976, 'Solar Flares', Dordrecht-Reidel.

Svestka, Z.: 1981, in E.R. Priest (ed.), 'Solar Flare Magnetohydrodynamics', Gordon and Breach.

Sweet, P.A.: 1958, IAU Symp. 6, 123.

Takakura, T.: 1972, Solar Phys. 26, 151.

Takakura, T. and Kai, K.: 1966, Publ. Astron. Soc. Japan 18, 57.

Tanaka, K. and Nakagawa, Y.: 1973, Solar Phys. 33, 187.

Tindo, I.P., Shuryghin, A.I. and Steffen, W.: 1976, Solar Phys. 46, 219.

Tramiel, L.J., Chanan, G.A. and Novick, R.: 1984, Astrophys. J. 280, 440.

Trubnikov, B.A.: 1965, in M.A. Leontovich (ed.), 'Reviews of Plasma Physics', Vol. 1, Consultants Bureau.

Tsytovich, V.N.: 1970a, 'Nonlinear Effects in Plasma', Plenum.

Tsytovich, V.N.: 1970b, Soviet Phys.-JETP 30, 83.

Tsytovich, V.N. and Shapiro, V.D.: 1965, Nucl. Fusion 5, 228.

Tsytovich, V.N., Stenflo, J. and Wilhelmson, H.: 1975, Physica Scripta 11, 251.

Ugai, M. and Tsuda, T.: 1977, J. Plasma Phys. 17, 337.

Van Beek, H.F., Hoyng, P., Lafleur, B. and Simnett, G.M.: 1980, Solar Phys. 65, 39.

Van Hoven, G.: 1979, Astrophys. J. 232, 572.

Van Hoven, G., Steinolfson, R.S. and Tachi, T.: 1983, Astrophys. J. 268, 860.

Vlahos, L. and Papadopoulos, K.: 1979, Astrophys. J. 233, 717.

Vlahos, L. and Rowland, H.L.: 1984, Astron. Astrophys. 139, 263.

Vlahos, L. et al.: 1986, in M.R. Kundu and B. Woodgate (eds.), 'Energetic Phenomena on the Sun', NASA CP-2439.

Vorpahl, J.A., Gibson, E.G., Landecker, P.B., McKenzie, D.L. and Underwood, J.H.: 1975, Solar Phys. 45, 199.

Walters, G.M. and Harris, E.G.: 1968, Phys. Fluids 11, 112.

Wentzel, D.G.: 1976, Astrophys. J. 208, 595.

Wentzel, D.G.: 1984, Solar Phys. 90, 139.

Widing, K.G. and Cheng, C.-C.: 1974, Astrophys. J. Letters 144, L111.

Wiehl, H.J., Batchelor, D.A. Crannell, C.J., Dennis, B.R. and Price, P.N.: 1985, Solar Phys. 96, 339.

Winglee, R.M.: 1985, Astrophys. J. 291, 160.

Winglee, R.M. and Dulk, G.A.: 1986, Solar Phys. 104, 93.

Wolfson, C.J., Doyle, J.G., Leibacher, J.W. and Phillips, K.J.H.: 1983, Astrophys. J. 269, 319.

Woltjer, L.: 1958, Proc. Nat. Acad. Sci. 44, 489.

Woodgate, B.E., Tandberg-Hanssen, E.A., Bruner, E.C., Beckers, J.M., Brandt, J.C., Henze, W., Hyder, C.L., Kalet, M.W., Kenny, P.J., Knox, E.D., Michalitsianos, A.G., Rehse, R., Shine, R.A. and Tinsley, H.D.: 1980, Solar Phys. 65, 73.

Zaitsev, V.V. and Kaplan, S.A.: 1968, Astrophysics 2, 87.

Zakharov, V.E.: 1972, Soviet Phys.-JETP 35, 908.

Zheleznyakov, V.V. and Zaitsev, V.V.: 1970, Soviet Astron.-AJ 14, 47.

Zirin, H.: 1978, Solar Phys. 58, 95.

Zirin, H. and Tanaka, K.: 1973, Solar Phys. 32, 173.

Zweibel, E.G. and Hundhausen, A.J.: 1982, Solar Phys. 76, 261.